



UNIVERSIDAD DE GRANADA

PROGRAMA DE DOCTORADO EN QUÍMICA

DEPARTAMENTO DE QUÍMICA ORGÁNICA

PRODUCTION AND CHARACTERISATION OF PROTEIN CRYSTALS IN HYDROGELS TO SUPPORT INORGANIC PRECIPITATION IN CONFINED SPACES

MEMORIA DE TESIS DOCTORAL

presentada por

MARIIA SAVCHENKO

para optar al título de

DOCTORA EN QUÍMICA

dirigida por los doctores Luis Álvarez de Cienfuegos Rodríguez, José Antonio
Gavira Gallardo y Modesto Torcuato López López

Granada, 2022

Editor: Universidad de Granada. Tesis Doctorales
Autor: Mariia Savchenko
ISBN: 978-84-1117-613-2
URI: <https://hdl.handle.net/10481/79177>

La doctoranda / *The doctoral candidate* **Mariia Savchenko** y los directores de la tesis / *and the thesis supervisor/s*: **Luis Álvarez de Cienfuegos Rodríguez, José Antonio Gavira Gallardo y Modesto Torcuato López López**

Garantizamos, al firmar esta tesis doctoral, que el trabajo ha sido realizado por la doctoranda bajo la dirección de los directores de la tesis y hasta donde nuestro conocimiento alcanza, en la realización del trabajo, se han respetado los derechos de otros autores a ser citados, cuando se han utilizado sus resultados o publicaciones.

/

Guarantee, by signing this doctoral thesis, that the work has been done by the doctoral candidate under the direction of the thesis supervisor/s and, as far as our knowledge reaches, in the performance of the work, the rights of other authors to be cited (when their results or publications have been used) have been respected.

Lugar y fecha / *Place and date*:

Granada, 2022

Doctoranda / *Doctoral candidate*:

Mariia Savchenko

Director/es de la Tesis / *Thesis supervisor/s*:

Luis Álvarez de Cienfuegos Rodríguez

José Antonio Gavira Gallardo

Modesto Torcuato López López

AGRADECIMIENTOS

El trabajo recogido en esta memoria ha sido realizado en los grupos de investigación de la Universidad de Granada “Materiales Orgánicos Funcionales” (FQM-367) del Departamento de Química Orgánica, y “Física de Interfases y Sistemas Coloidales” (FQM-144) del Departamento de Física Aplicada, así como también en Laboratorio de Estudios Cristalograficos (RNM-143) del Consejo Superior de Investigaciones Científicas.

La presente Tesis Doctoral ha sido financiada por los proyectos científicos PID2020-118498GB-I00 “Magnetically programmable biocompatible hydrogel machines (MAFICMACH) y PID 2020-116261GB-100 “Biotechnological application of protein crystals”.

También quiero agradecer a la Escuela de Posgrado de la Universidad de Granada, al Vicerrectorado de Internacionalización, y personalmente a Wenceslao Martín Rosales, Antonio Garcia Casco, José Balderas Cejudo, Francisco Carrasco Marin, y María del Sol Ostos Rey, por la ayuda económica que me ha permitido finalizar esta tesis doctoral.

Mi gratitud a Encarnación Collado Cañas y Yolanda García Avilés del Vicerrectorado de Investigación y Transferencia así como a Mario Pardo Segovia del Vicerrectorado de Internacionalización por su inestimable ayuda y comprensión.

Mil gracias a mis directores de tesis Luis Álvarez de Cienfuegos Rodríguez, José Antonio Gavira Gallardo y Modesto Torcuato López López. Soy afortunada por haber sido vuestra doctoranda.

Luis, gracias por responder a un email de una chica ucraniana y después por contratarla dándole la oportunidad de ingresar en el mundo de la investigación. Tú has cambiado la vida de al menos una persona en este mundo. Estos años en Granada son los mejores de mi vida.

Gavi, ¿Por qué apareciste en mi vida antes? Lo que te dije hace 2 años cuando te conocí, lo mismo quiero decirte ahora: desearía que todos mis profesores en el grado en el máster hubiesen sido como tú. Gracias por enseñarme en estos 2 años un millón de cosas. Gracias por la inspiración y por las conversaciones sinceras.

Modesto, gracias por ser tan amable conmigo. Gracias por el contrato que me ha permitido vivir en Granada y hacer este trabajo. Gracias a esta oportunidad, a toda tu atención, y por tener siempre la puerta abierta.

A mis directores, una vez más, gracias por cristalizar las mentes de sus doctorandos: del caos a una estructura ordenada. Muchas gracias por vuestras ideas para este trabajo. Gracias a vuestra organización ha sido posible escribir esta tesis ahora. Un abrazo enorme a cada uno.

Gracias a mi ángel de la guarda, Mari Carmen. Mi tutora, mi amiga, mi salvadora, mi superheroe. Gracias por mi primera palabra española, por enseñarme todo desde el funcionamiento de una pipeta, hasta esta tesis. Si pudiera poner aquí todo lo que te agradezco, ocuparía más páginas que la parte científica de la esta tesis. No he podido ser más afortunada de descubrirte en el camino a Mundy. ¡Gracias a ti yo he sobrevivido! Te lo debo todo.

Gracias a mi Cristina. Gracias por enseñarme reología y Origin, así como por darme los dos consejos más importantes de la vida. Gracias por las recetas y el President Suite. Gracias por el vocabulario y consejos de colores. Gracias por compartir horas de decisiones difíciles en Jusk. Y mucho, mucho más. Dale un abrazo grande también a tus padres.

Gracias a mis mapaches Sandra y Miguel. Sandra, gracias por preguntarme mi número en el comedor hace 2 años y poco a poco adoptarme. No podía imaginar que encontrase una amiga así en mi vida. Inteligente, sincera e increíblemente amable. Siempre podré confiar en ti y tú en mí. Gracias por que existes. Miguel, hala Madrid. Te echamos mucho de menos. Gracias por las tardes de Champions y los días de comedores.

Gracias a Sara, mi amiga, mi ayuda, mi diccionario, mi fuente de humor. Gracias por las risas en el laboratorio. Gracias por ayudarme en cualquier momento y sobre cualquier cosa. Gracias por enseñarme tu corazón lleno del cariño que me has demostrado.

Gracias al niño Manuel, nuestro postdoc fuerte y favorito. Gracias por tu paciencia con nuestras bromas. Te queremos mucho, más que a la quiralidad.

My boys, Fede-aka-Carboncillo, Marcos y JuanPe, gracias por los desayunos de locura absoluta. Las mejores tostadas y conversaciones fueron allí, con vosotros en Mundy. Recordad comprar Paladuum.

Gracias a todos los compañeros de Química Orgánica: Raquel, Ana, Darío, Otilia, Rafa, Beatriz, Pablo, Ani, Lidia, Álvaro, Lucía, Arthur, Vicente, Jennifer, Jaime y Daniel. Gracias a los directores: JuanMa, Araceli, Víctor, Justi, Alba y Sara. He disfrutado mucho este tiempo. Gracias por vuestra ayuda en cualquier circunstancia y la atmosfera de amistad en el departamento.

Gracias Karina por tu amistad, consejos sabios, mi primera fería, y por los tacos con la salsa verde. Gracias por tu paciencia con mis primeras frases en español.

Gracias Rafa por ser mi ejemplo de científico. Gracias por enseñarme un montón de cosas. "Necesito ayuda con los geles y lo sé". Dr. Contreras, you rock.

A mi Física Aplicada, gracias por las mejores bromas de todo el mundo, por los viernes de tapas, por hospedarme en vuestros ordenadores, gracias porque os puedo torturar y amar. Gracias al despacho 13 por ser mi gabinete psicológico y mi enciclopedia. Vuestra ucraniana suelta siempre os tendrá en su corazón.

Gracias a todos mis compañeros del IACT por los almuerzos, el café, las tapas, la comida coreana, la nieve dentro de los zapatos y mucho más. Gracias a todos los compañeros del LEC, y personalmente a Raquel, Joaquín, Luis y Carmen, por toda vuestra ayuda, consejos y apoyo.

Especialmente gracias a Adriana Torres, mi mapache hippie soulmate. Gracias por tus pensamientos, palabras y acciones, por nuestras escaleras por la noche con empanadas argentinas y por hacer el lab 103 feliz. "If you are lucky, once in a lifetime you will meet a true mapache".

Gracias a mis colaboradores de ingeniería, Manuel Hurtado Estévez, Guillermo Rus y Juan Manuel Melchor Rodríguez por vuestro trabajo, ideas y apoyo. Gracias por enseñarme el mundo de la estadística, aplicaciones interesantes, y por la ayuda en logística.

Gracias a las colaboradoras de microbiología, Concepción Jiménez López, Ylenia Jabalera, Tamara Pozo y Francesca Oltolina, por su conocimiento y experiencia, ideas y procololos, y por abrirme la puerta (metafóricamente y literalmente también).

Спасибо папе за помощь в маленьких и больших делах. Спасибо за опору и все материальное и нематериальное, что у меня есть. Спасибо друг!

Дякую дідусю за недільні поїздки у "Дім Книги", за всі енциклопедії і допомогу у навчанні. Дякую за підтримку!

A la persona más querida en mi vida, mi mejor ingeniera y la mejor empleada de la embajada de Turquía, mi genio que me ha enseñado las dos alas de felicidad: la belleza y la utilidad. La persona más inteligente, valiente y libre. Mama, te quiero en todas las dimensiones, en todos los multiversos.

Байбачку

“Whether it’s a symphony or a coal mine, all work is an act of creating and comes from the same source: from an inviolate capacity to see through one’s own eyes — which means: the capacity to perform a rational identification — which means: the capacity to see, to connect and to make what had not been seen, connected and made before.

The man who produces an idea in any field of rational endeavor — the man who discovers new knowledge — is the permanent benefactor of humanity.”

Ayn Rand, “Atlas Shrugged”

SUMMARY

The present Doctoral Thesis manuscript is the result of the scientific work carried out by Mariia Savchenko during her doctoral studies. The thesis is focused on crystallization processes: from magnetite biomineralization to crystallization of protein macromolecules.

The thesis is organized in the following structure: a general introduction, two chapters and the general conclusions. Each chapter has a brief focus introduction, the main objectives, experimental section, results and discussion, and ends with the conclusions.

The *Introduction* contextualizes the work. It describes the fundamental of nucleation and crystal growth theories; factors that modify these processes: environment (gels and confinement media), external stimulus (ultrasonic waves); and briefly describes the substances used in the thesis.

In Chapter 1 entitled "*Lysozyme crystallisation in hydrogel media under ultrasound irradiation*" tells how ultrasonic waves affect the protein nucleation and growth in a hydrogel media. As first approach in this project, the specific set-up was designed, and the media that allow studying the effect without any interruptions were characterized. We showed that the application of ultrasound waves of selected energy affects the crystallization behaviour of lysozyme resulting in an induction of the nucleation and therefore affecting the final crystal size. These effect was observed in solution and in agarose if the concentration is below 0.100 (w/v) %. We propose this eco-friendly source of energy to control the production of protein crystals and to set desirable parameters.

In Chapter 2 entitled "*Protein crystals as a template for in situ formation of magnetite nanoparticles*", protein crystals were used as a reaction vessel to study the crystallization of another compound — magnetite, in confined spaces. The project was inspired by the magnetosomes of magnetotactic bacteria which produce magnetite with unusual morphologies, homogeneous size and superparamagnetic properties. In our case, the pores of the protein crystals control the formation of magnetite. We obtained homogeneous nanoparticles of 2 nm size regardless time, dimension of protein channel and crystalline/amorphous state. From the three model proteins used, maturation to magnetite nanoparticle was observed only in one case.

The manuscript ends with the scientific publications supporting the work.

CONTENTS

Introduction	17
1.1. Protein crystallisation: general approach and application.....	19
1.1.1. The protein's character.....	19
1.1.2. Introduction to protein crystallisation.....	21
1.1.3. Nucleation: conception of crystals.....	22
1.1.4. Crystal growth.....	28
1.1.5. Supersaturation.....	31
1.1.6. Protein crystallisation techniques.....	34
1.1.7. The necessity of protein crystallisation.....	36
1.2. Protein crystallisation in gel media.....	38
1.2.1. Gels nature & structure.....	38
1.2.2. Crystallogenesis in gels.....	40
1.2.3. Gels used for protein crystallization.....	41
1.3. Protein crystallization under ultrasound irradiation.....	47
1.3.1. Sonochemistry: application of ultrasound.....	47
1.3.2. Sonocrystallization.....	49
1.3.3. Sonocrystallization of proteins.....	50
1.4. Protein crystals as a template for <i>in situ</i> growth of inorganic materials.....	52
1.4.1. Crystallization in confinement.....	52
1.4.2. Protein crystals as a template for confinement growth.....	55
1.4.3. Nanoparticles of magnetite.....	58
Lysozyme crystallization in hydrogel media under ultrasound irradiation	65
2.1. Objectives of the study.....	68
2.2. Materials and methods.....	68

2.2.1.	Reagents and materials.....	68
2.2.2.	Design & set-up of the ultrasound equipment.....	68
2.2.3.	Characteristics of the materials.....	71
2.2.4.	Mechanical characterization of the gel media.....	74
2.2.5.	Crystallization set-up.....	74
2.2.6.	The experiment set-up.....	77
2.2.7.	Statistical analysis.....	79
2.3.	Results and discussion.....	80
2.3.1.	Lysozyme crystallization in solution under US.....	80
2.3.2.	Lysozyme crystallization in gel media under US.....	82
2.3.3.	Mechanical properties of the gel media.....	85
2.4.	Conclusions.....	85
	Magnetite crystallization in confined environments.....	89
3.1.	Objectives of the study.....	92
3.2.	Materials and methods.....	93
3.2.1.	Reagents and materials.....	93
3.2.2.	Preparation of cross-linked protein crystals.....	93
3.2.3.	<i>In situ</i> formation of magnetite.....	97
3.2.4.	Characterization of the nanoparticles.....	99
3.2.5.	Statistical analysis.....	100
3.3.	Results and discussion.....	101
3.3.1.	Precipitation of iron particles inside CLPCs.....	101
3.3.2.	Evolution of magnetite nanoparticles inside CLPCs.....	104
3.4.	Conclusions.....	113
	Annex.....	115

Introduction

1.1. Protein crystallisation: general approach and application

1.1.1. The protein's character

Proteins are ones of the most complex molecules in nature. Their structure (α -L amino acids residues united in a chain), are held together by peptide bonds form when the carboxyl group of one amino acid binds to the amino group of a second amino acid (*Figure 1.1*). The repetition of this reaction gives rise to the polypeptide chain. The sequence of the aminoacids in the chain is **primary structure** of a protein. Important fragments of this chain are conservative motifs (stable unchanged amino acid sequences.) that can be identified across species. Functions of unknown proteins and an extent of “kinship” between species of organisms are predicted by them.

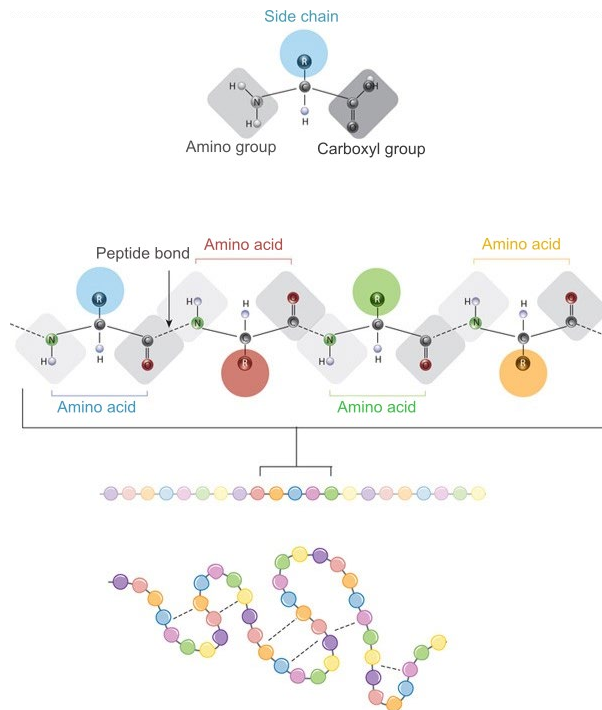


Figure 1.1. Peptide bond & liner chain (the primary structure) of protein formation. Adapted from Ref. 1.

¹ O'Connor, C. M. & Adams, J. U. *Essentials of Cell Biology*. Cambridge, MA: NPG Education, 2010.

Secondary structural elements (*Figure 1.2*) are formed by the interactions, mainly through hydrogen bonds of the main chain, arranged in two main structures: α -helices, when the chains are twisted around the axis of the molecule (including the π -helix and 3_{10} -helix variants), and β -sheets, when hydrogen bonds are formed between amino acids of the same chain that lays far apart from each other, or between different chains, connected by un-ordered amino acids forming loops.

The spatial fold of the secondary elements generates **tertiary structure**, typically responsible for proteins function and holds by covalent, ionic and, most importantly, hydrophobic interactions. Sometimes nature requires of a higher level of organization to be fully functional generating a fourth level of arrangement, **quaternary structure**, in which several polypeptide chain are grouped. It is formed by the same interactions as the tertiary structure.²

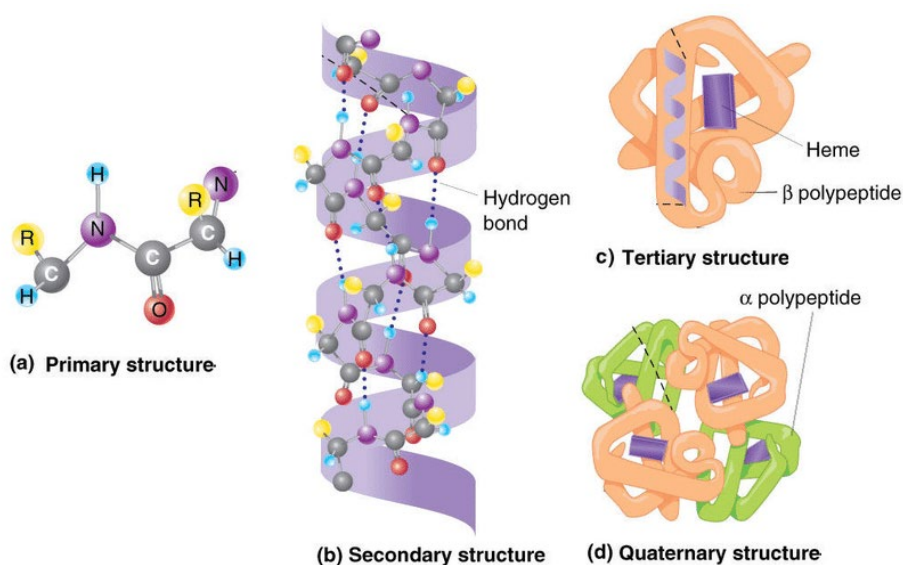


Figure 1.2. The four levels of protein structure. Reproduced from Ref. 3.

Proteins are very large molecules: the smallest protein called TRP-Cage from saliva of Gila monsters has just 20 amino acids;⁴ and sophisticated human proteins, for example Titin, that is responsible for muscle contraction, is greater

² C. I. Branden, J. Tooze, *Introduction to Protein Structure*, Garland Science, **2012**.

³ H. Hendy, W. Khalifa, M. Roushdy, A. B. Salem, *International Journal of Information Models and Analyses* **2015**, *4*.

⁴ R. Zhou, *Proc. Natl. Acad. Sci. U. S. A.* **2003**, *100*, 13280–13285.

than 1 μm in length and consists of 38.138 amino acids and weight approximately 3700 kDa.⁵

In addition to the large weight, proteins also have a complex character: they are amphoteric and amphiphilic. Their amphotericity results from the lateral carboxyl and nitrogen-containing groups, which can be ionised. Depending on the ratio of the groups (that in turns depends on which amino acids protein is formed), proteins are divided into acidic (which have more carboxyl groups and, accordingly, the isoelectric point located in the acidic region, for example, pepsin (enzyme of gastric juice) $\text{pI} \sim 1$; and the basic ones (which, on the contrary, have more nitrogen-containing groups), for example, salmin (salmon milt protein) with $\text{pI} \sim 12$.⁶

The structure of a protein also determines its behaviour in solutions. As shown in *Figure 1.3*, proteins also have both hydrophilic and hydrophobic regions.

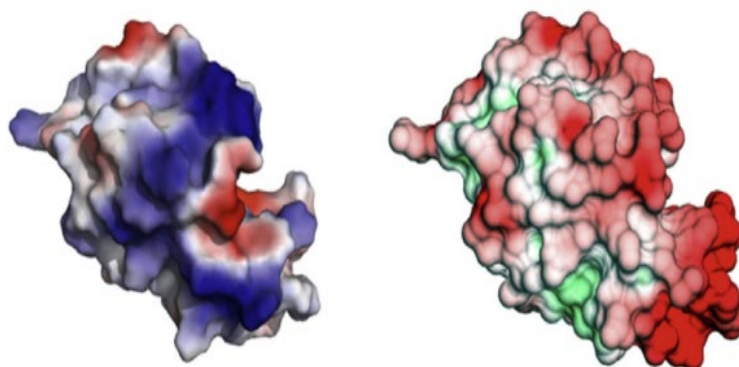


Figure 1.3. Representation of lysozyme electrostatic charge (blue – positive, red – negative, white – neutral charge) and hydrophobicity (green – hydrophobic, red – hydrophilic, white – amphiphilic character). Reproduced with permission from Ref. 7. Copyright © 2016, Elsevier Ltd.

1.1.2. Introduction to protein crystallisation

To crystallise proteins, which means to make these complex molecules self-organised in highly ordered microscopic solid-structure, is a challenge. That is why just 7% of all discovered proteins have being crystallised. Still, protein

⁵ H. L. Granzier, S. Labeit, *Circ. Res.* **2004**, 94, 284–295.

⁶ G. Meisenberg, W. H. Simmons, *Principles of Medical Biochemistry*, Elsevier, **2016**.

crystallisation is more empirical and lacks of any general theory to predict under which conditions a protein will crystallize.⁷

McPherson wrote, “*The problem of crystallisation is less approachable from a classical analytical standpoint, contains a substantial component of trial and error, and draws more from the collective experience of the past century. . . . It is much like prospecting for gold.*”⁸

The intrinsic peptide nature itself is not the only one limiting factor. The process of nucleation and growth of a crystal is influenced by many conditions, both physical and chemical. They are not always predictable and the modelling of the crystallisation process is sometimes comparable in complexity to the modelling of protein folding.⁷

1.1.3. Nucleation: conception of crystals

Basically, the crystallisation process involves two different processes: nucleation and crystal growth. Sometimes, authors distinguish a third one — cessation of growth.⁷

Namely, the nucleation determines polymorphs, the number of crystals, their size and size distribution.⁹

By definition nucleation is the reorganisation of atoms/molecules in the structure of a material, which leads to the formation of a new phase: from an unorganised phase with high free energy to an ordered phase with lower free energy.¹⁰ Gibbs was the first scientist who studied nucleation from a thermodynamic point of view as a density fluctuation of the parent phase.¹¹

Despite the fact that nucleation has been studied for more than a century, it is still poorly understood and is continuously under review in its general body-theory and with special emphasis also in the case of biological macromolecules — the nucleus is so small and fast that it is very difficult to observe and characterise

⁷ J. A. Gavira, *Arch. Biochem. Biophys.* **2016**, *602*, 3–11.

⁸ *Preparation and Analysis of Protein Crystals*, Krieger, **1982**.

⁹ H. Cölfen, *Crystals* **2020**, *10*, 61.

¹⁰ R. P. Sear, *CrystEngComm* **2014**, *16*, 6506–6522.

¹¹ J. W. Gibbs, **1879**.

experimentally. The question of *how exactly* nuclei appear in the system remains open.¹²

Today scientists consider several pathways of nucleation: classical and non-classical. For nucleation to begin, the system must overcome a certain energy barrier. In the Classical Nucleation Theory (CNT),¹³ the probability of nucleation is determined by the height of the energy barrier that in turn is determined by standard free energy of the critical nucleus. This critical nucleus is a transitional state between a metastable supersaturated solution and growing solid phase particles. In CNT the critical nucleus forms *as one monomer at a time* via atom-by-atom addition. The rate of nucleation depends on the size of the nucleus at the top of the energy barrier. If the nucleus passes this barrier, it stabilises and turns into a particle.¹⁴

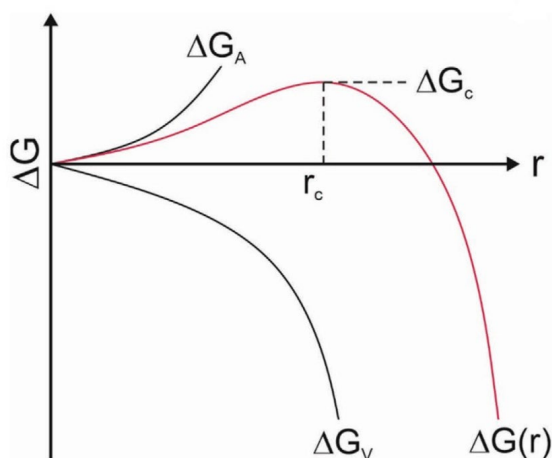


Figure 1.4. Graphic of the free energy (ΔG) of a growing crystal nucleus. There are two competing contributions to the free energy change: the favourable volume free energy (ΔG_V) that associated with of a spherical cluster formation with a volume $4\pi r^2$ and the surface free energy (ΔG_A) that describes energetically unfavourable new surface formation ($-n\Delta\mu$) when n numbers of particles turn from solution into solid state with difference in chemical potential between solute in solution and in solid state.

The maximum value (ΔG_c) corresponds to the critical nucleus with the lowest critical radius (r_c) that is capable to decrease its free energy with growing. Reproduced from Ref. 15.

¹² R. P. Sear, *J. Phys. Condens. Matter* **2007**, *19*, 033101.

¹³ M. Volmer, A. Weber, *Z. Phys. Chem.* **1926**, *119*, 277–301.

¹⁴ D. Gebauer, P. Raiteri, J. D. Gale, H. Cölfen, *Am. J. Sci.* **2018**, *318*, 969–988.

¹⁵ F. C. Meldrum, C. O’Shaughnessy, *Adv. Mater.* **2020**, *32*, e2001068.

From *Figure 1.4* according to CNT during the critical nucleus formation, the free energy (ΔG) decreases:

$$\Delta G = -n\Delta\mu + 4\pi r^2\gamma$$

Equation 1.1

where γ – the interfacial energy, r – the radius of the critical nucleus, n – the number of molecules the nucleus contains, $\Delta\mu$ – the chemical potential between solute in solution and in solid state

If a molecular volume (V_m) is known, the *Equation 1.1* can be written like:

$$\Delta G = -\frac{4}{3}\pi \frac{r^3}{V_m} \Delta\mu + 4\pi r^2\gamma$$

Equation 1.2

From *Equation 1.2*, the critical nucleus radius can derive to be:

$$r_c = \frac{2\gamma V_m}{\Delta\mu} = \frac{2\gamma V_m}{kT \ln S}$$

Equation 1.3¹⁵

where k – Boltzmann constant, T – temperature, S – supersaturation (see *Section 1.1.5*).

However, some parameters calculated theoretically according to CNT turned out to be much different from the ones obtained experimentally. Also, CNT was unsuitable for describing the nucleation of complex systems: one of the processes that could not be explained using CNT was the two-step protein nucleation mechanism, formulated by Galkin and Vekilov,¹⁶ its variations were considered by Rein ten Wolde and Daan Frenkel,¹⁷ and Gliko et al.¹⁸ (as dense liquid cluster precursors of metastable crystals respect to both the crystals and the low-concentration solution), and then experimentally proven by Maes et al.¹⁹ The

¹⁶ O. Galkin, P. G. Vekilov, *Proc. Natl. Acad. Sci. U. S. A.* **2000**, *97*, 6277–6281.

¹⁷ P. Wolde, D. Frenkel, *Science* **1997**, *277*, 1975–1978.

¹⁸ O. Gliko, N. Neumaier, W. Pan, I. Haase, M. Fischer, A. Bacher, S. Weinkauff, P. G. Vekilov, *J. Am. Chem. Soc.* **2005**, *127*, 3433–3438.

¹⁹ D. Maes, M. A. Vorontsova, M. A. C. Potenza, T. Sanvito, M. Sleutel, M. Giglio, P. G. Vekilov, *Acta Crystallogr. Sect. F Struct. Biol. Cryst. Commun.* **2015**, *71*, 815–822.

authors described amorphous mesoscopic-size metastable protein-rich clusters that appeared in supersaturated solutions of lysozyme and glucose isomerase. They *were* the places and precursors of protein crystals' genesis. More recently and following the colloidal theory for phase separation, scientists focused on creating multistep theories with several metastable intermediates.

According to Ostwald's rule of stages, when an unstable or metastable system becomes stable, the system passes through intermediate states, where each one has a free energy that is closest to the initial energy of the system.²⁰

Today non-classical theories of nucleation dominate. The difference between them is in the intermediate/s between the supersaturated solution and the solid phase. If in CNT this is one integral critical-sized nucleus, in non-classical theories these are alternative aggregates (*Figure 1.5*).

There is a "multistep nucleation theory" (MNT), originally developed only for proteins in which, intermediates act as liquidlike clusters that are stable respect to the parent liquid and metastable compared with the emerging crystalline phase.²¹ Gebauer and Cölfen²² proposed a similar mechanism for the pre-nucleation cluster (PNC) pathway. According to them, precursors to particles are thermodynamically stable clusters.

²⁰ J. Schmelzer, A. Abyzov, 03 **2017**, pp. 195–211.

²¹ M. Sleutel, A. E. S. Van Driessche, *Proc. Natl. Acad. Sci. U. S. A.* **2014**, *111*, E546–53.

²² D. Gebauer, H. Cölfen, *Nano Today* **2011**, *6*, 564–584.

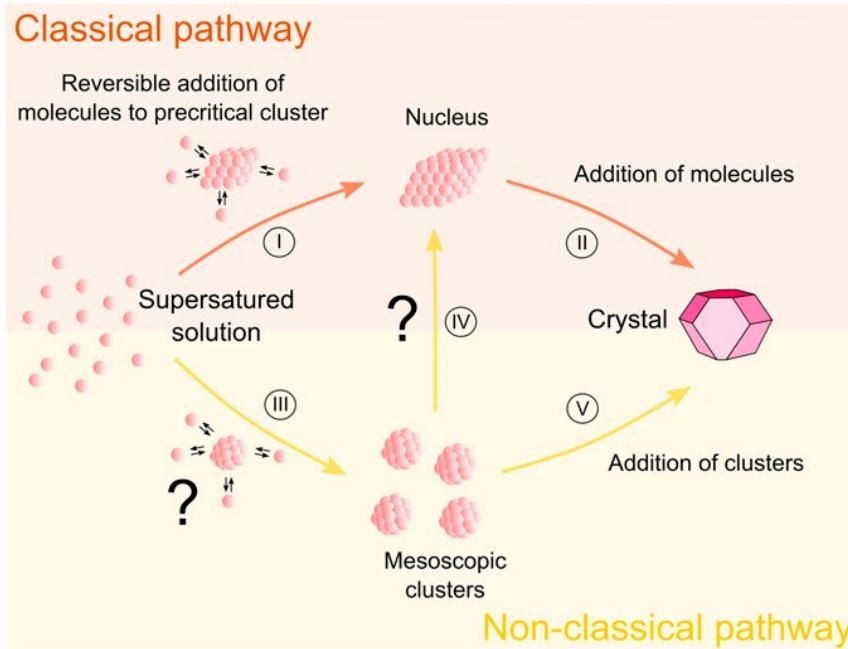


Figure 1.5. Comparison of classical (top) and nonclassical (bottom) pathways of crystallisation mechanism: simultaneously densification and increase in crystallinity (I); transient separation of cluster (III) and lattice (IV) formation; joining of clusters with the crystalline phase (V). Reproduced from Ref. 21.

Ou et al.²³ also describe nonclassical nucleation mechanisms as “aggregation of nuclei” (Figure 1.6), when two or more subcritical clusters merge to form a nucleus beyond the critical size. In this case, a certain part of the interfacial surface disappears, so the total free energy of the system decreases and the nucleus stabilises.

Another version is “stepwise nucleation”: due to the formation of an intermediate, the interfacial energy decreases and the energy threshold for nucleation simply decreases.

In addition, there is mixed nucleation, then the two nonclassical mechanisms take place simultaneously.

²³ X. Ou, J. Sietsma, M. J. Santofimia, *Acta Mater.* **2022**, 226, 117655.

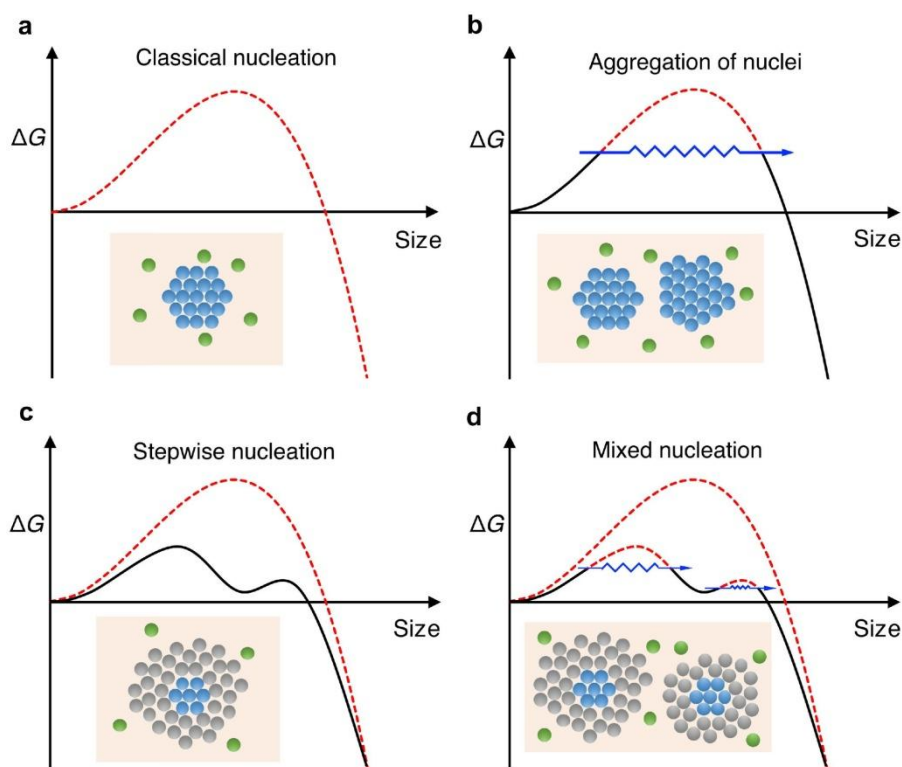


Figure 1.6. Schematic representation of the free-energy change due to nucleation G with the evolution of the nucleus by different pathways. Reproduced from Ref. 23.

Nevertheless, recently Baumgartner et al.²⁴ proposed a model that could be a bridge between CNT and non-classical theories (Figure 1.7). From CNT they keep the competition between the surface and volume free-energies and add an excess free energy for the primary particles. Depending on the sign of this excess free energy, nucleation will proceed directly by formation crystalline phase (if the excess free energy for the primary particles is negative, and they are stable) or by formation of amorphous precursors (when the excess free energy for the primary particles is positive and they are metastable).

²⁴ J. Baumgartner, A. Dey, P. H. H. Bomans, C. Le Coadou, P. Fratzl, N. A. J. M. Sommerdijk, D. Faivre, *Nat. Mater.* **2013**, *12*, 310–314.

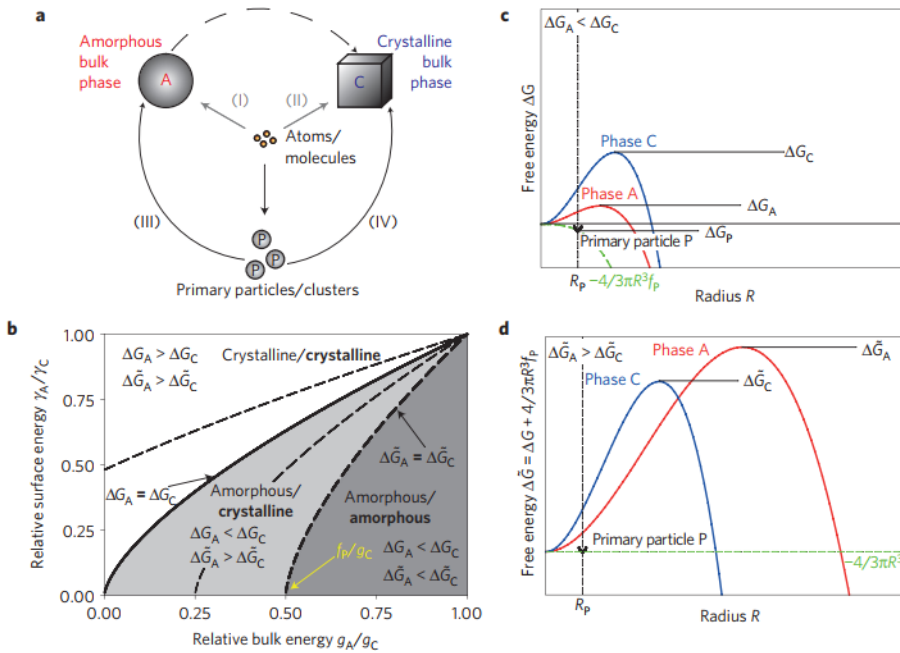


Figure 1.7. Illustration of the nucleation model proposed by Baumgartner et al.: a – scheme of the model; b – phase diagram describes on which scenario will go the nucleation depending on the excess free energy for the primary particles ($\Delta\bar{G}_A$ and $\Delta\bar{G}_C$). As previously, volume free energy is ΔG_V ; and the surface free energy is ΔG_A ; c – example of the system where the amorphous phase is forming; d – example with the direct formation of the crystalline phase. Reproduced with permission from Ref. 24. Copyright © 2013, Springer Nature.

1.1.4. Crystal growth

When, as a result of nucleation, the concentration of a substance decreases below the supersaturation level at which nucleation began, crystal growth starts.

Crystal growth is a non-equilibrium process, the main ideas of which were also laid down by Gibbs: *crystal growth will occur if the free energy of molecules in a crystal is less than in solution*. In this case, the molecules from the solution will may reach the surface of the crystal and be embedded in its crystal lattice kink site.²⁵

The process of crystal growth includes:

- Mass transport of the molecules from the bulk solution towards the

²⁵ J. W. Gibbs, 1928.

- crystal surface;
- Adsorption onto the crystal surface;
 - Migration of the molecules through the surface;
 - Incorporation into the lattice.²⁶

The classical model of crystal growth was formulated by Kossel and Stranski²⁷ in the Terrace-Ledge-Kink model (*Figure 1.8*): crystal growth units (atoms or molecules) are adsorbed on the crystal surface, diffuse along it to edges and kinks, where their incorporation is more advantageous. So the crystal grows layer by layer. This mechanism works a medium to high level of supersaturation but cannot explain the growth observed at low supersaturation level.

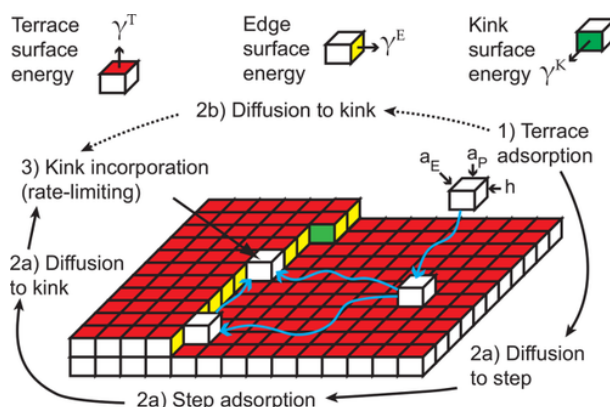


Figure 1.8. The surface structure of a crystal, showing sequential events of the incorporation mechanism. Reproduced with permission from Ref. 28. Copyright © 2017, John Wiley & Sons, Inc.

In this case the theory of Burton, Cabrera and Frank (BCF) explain that real solids are not perfectly crystalline and have defects such as screw dislocation. Thus, at the dislocation there is a kink site that will never be saturated and therefore, new molecules can be continually incorporated. This mechanism of growth is known as spiral-growth (*Figure 1.9*).²⁹

²⁶ V. K. Ivanov, P. P. Fedorov, A. Ye Baranchikov, V. V. Osiko, *Russ. Chem. Rev.* **2014**, *83*, 1204.

²⁷ N. Stranski, *Z Phys Chem-Stoch Ve* **1928**, 136.

²⁸ C. J. Tilbury, M. F. Doherty, *AIChE J.* **2017**, *63*, 1338–1352.

²⁹ W. K. Burton, N. Cabrera, F. C. Frank, N. F. Mott, *Philos. Trans. R. Soc. Lond. A* **1951**, *243*, 299–358.

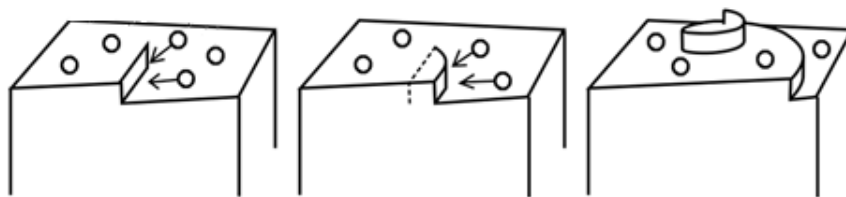
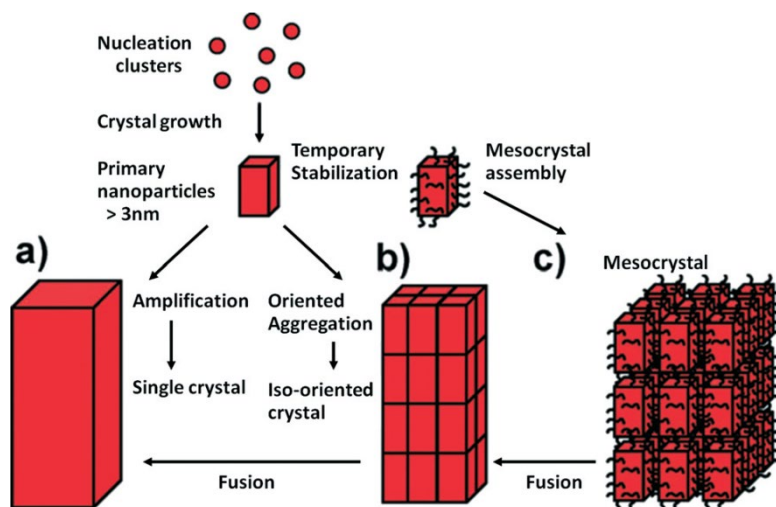


Figure 1.9. Mechanism of the spiral crystal growth. Reproduced with permission from Ref. 30. Copyright © 2018, American Chemical Society.

As in the case of nucleation, classical theories of crystal growth are unable to explain the formation of some structures such as functional materials including composite nanomaterials, hybrid organic-inorganic materials, multilevel hierarchical materials, etc. Thus, non-classical theories of crystal growth were developed (Figure 1.10). According to them, not individual atoms, molecules or ions, but whole blocks of the solid phase, amorphous or even liquid structure act as crystal units that are attached to the surface to promote the growth.³¹



³⁰ T. Ohtsuka, Y.-H. R. Tsai, Y. Giga, *Cryst. Growth Des.* **2018**, *18*, 1917–1929.

³¹ H. Cölfen, M. Antonietti, *Mesocrystals and Nonclassical Crystallization*, John Wiley & Sons, **2008**.

Figure 1.10. Classical (a) and l and non-classical crystallisation (b and c). Reproduced with permission from Ref. 32. Copyright © 2014, Royal Society of Chemistry.

1.1.5. Supersaturation

The driving force of crystallisation is the supersaturation of the solution. The supersaturation (S) is defined as the difference in chemical potential between solute in solution (μ_s) and in crystal (μ_c) phases:

$$\Delta\mu = \mu_s - \mu_c$$

Equation 1.4

$$\Delta\mu = kT \ln S$$

Equation 1.5¹⁴

Theoretically, nucleation occurs when the supersaturation (S) > 1 . However, Grossier et al.³³ studied the values of supersaturation for lysozyme crystallisation, and determined the lowest value on which the nucleation occurs $S = 1.998$ (*Figure 1.11*). Below this supersaturation value nucleation do not occur. It happens because the low concentration of protein (less molecules of protein) leads to higher depletion of the supersaturation during the formation of the nuclei until it reaches the size (critical nucleus) that corresponds to this supersaturation, but system cannot overcome this depletion of protein molecules at such low supersaturation and the critical nucleus dissolves. If the supersaturation is high enough, the critical nucleus is formed and protein in solution will still retain sufficient energy make it grows (*Figure 1.4*).

³² L. Bahrig, S. G. Hickey, A. Eychmüller, *CrystEngComm* **2014**.

³³ R. Grossier, S. Veessler, *Cryst. Growth Des.* **2009**, 9, 1917–1922.

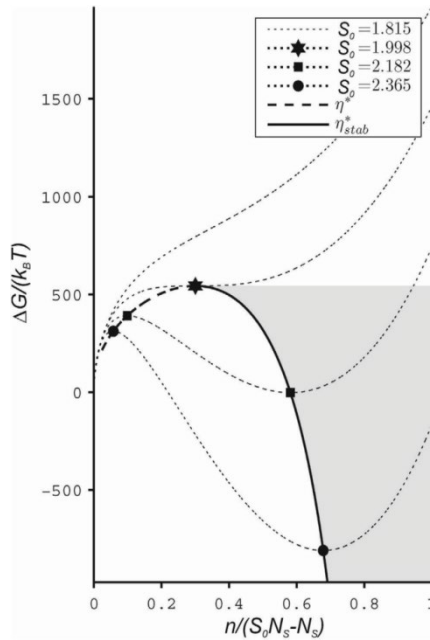


Figure 1.11. The free energy (ΔG) of the critical nuclei formation for different initial supersaturations of lysozyme (S_0). Reproduced with permission from Ref. 33. Copyright © 2009, American Chemical Society.

Meanwhile with the nuclei formation the free energy of the system decreases as:

$$\Delta G = -nk_B T \ln S_0 + An^{2/3}$$

Equation 1.6

where n – the number of molecules formed the nucleus, S_0 – the initial supersaturation, A – the prefactor which is determined from kinetic considerations and is determined as:

$$A = 4\pi\gamma \left(\frac{3V_m}{4\pi} \right)^{2/3}$$

Equation 1.7

where γ – the interfacial energy and V_m – the molecular volume.¹⁵

Therefore to induce nucleation it is necessary to drive the solution into a supersaturated state (Figure 1.12). Supersaturation is a non-equilibrium state there is an excess of energy and the system itself wants to get out of it to reach the equilibrium, the solubility curve. To do so the system will segregates a solid

phase, either the crystal nuclei which could growth or an amorphous phase if the saturation is too high.³⁴

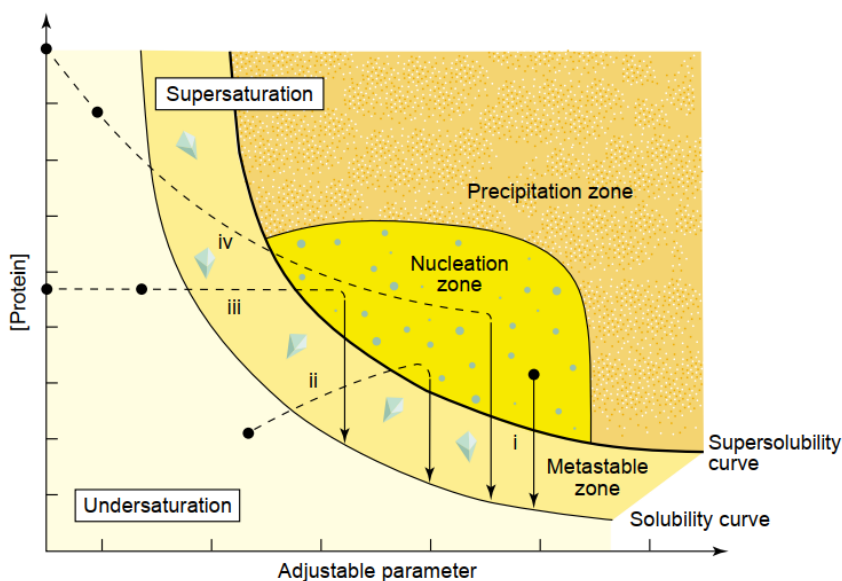


Figure 1.12. Phase diagram for a protein-precipitant couple with the solubility and metastability curves guides. Reproduced with permission from Ref. 35. Copyright © 2004, Elsevier Ltd.

Therefore, in order not to go too far and not get protein precipitation instead of crystals, we need to control the excess of energy gained (thermodynamic contribution) and the rate at which this excess of energy has been reached (kinetic contribution). This can be controlled using different crystallisation techniques.

To create a supersaturated solution, we can 1) decrease the solubility of the dissolved molecule (protein) or 2) decrease the solvent power of the solvent. Protein solubility depends on: temperature, pH, ionic strength, buffer types, additives, and precipitating agents.³⁶

Table 1.1 highlights to how exactly this can be done.

Direct mixing of protein and precipitant solutions to immediately create a

³⁴ A. McPherson, J. A. Gavira, *Acta Crystallogr. Sect. F Struct. Biol. Cryst. Commun.* **2014**, *70*, 2–20.

³⁵ N. E. Chayen, *Curr. Opin. Struct. Biol.* **2004**, *14*, 577–583.

supersaturated condition (batch method)

Alter the temperature

Add salt (increase ionic strength), salting out

Remove salt (decrease ionic strength), salting in

Alter pH through liquid or vapour phase

Add a ligand that changes the solubility of the macromolecule

Alteration the dielectric constant of the medium (by addition of organic solvents)

Evaporation

Addition of a polymer that produces volume exclusion

Addition of a cross-bridging agent that promotes lattice interactions

Concentration of the macromolecule by removal of water through a membrane

Removal of a solubilising agent (chaotrope)

Table 1.1 Methods for creating supersaturation. Reproduced with permission from Ref. 34. Copyright © 2014, International Union of Crystallography.

1.1.6. Protein crystallisation techniques

Based on the methods described on *Table 1.1*, there are principal techniques of protein crystallisation (*Figure 1.13*).

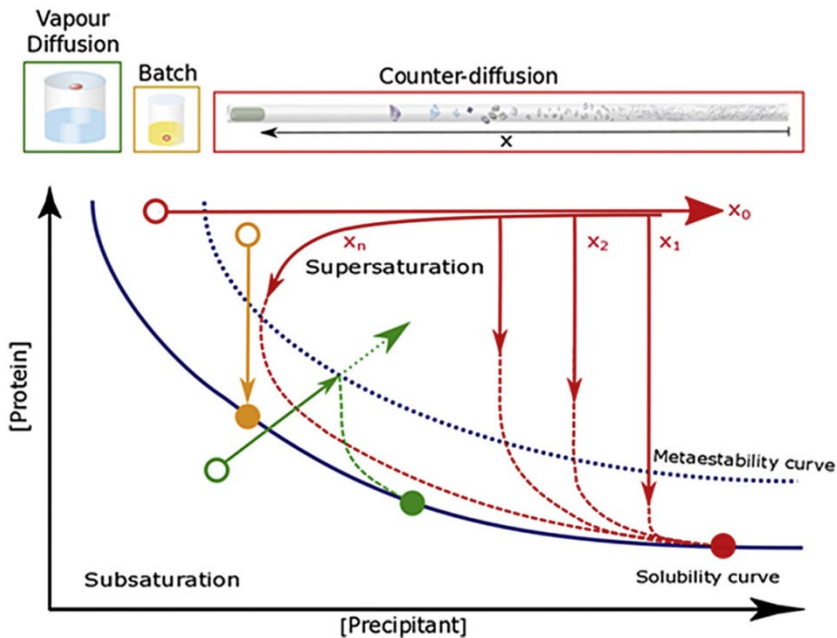


Figure 1.13. Phase diagram for a protein-precipitant couple for different protein crystallisation techniques with the solubility and metastability curves guides. Reproduced with permission from Ref. 7. Copyright © 2016, Elsevier Ltd.

Vapour diffusion, probably the most spread technique around the world, is a technique where a drop contains a protein, and a precipitant is equilibrated against a reservoir containing double concentration of the precipitant. Because in the reservoir the concentration of the precipitant is higher, water from the drop goes to the reservoir through the air, driving the protein/precipitant solution-mixture to a higher concentration state that may eventually enter the supersaturated region.

Batch crystallisation, very suitable for robotic manipulation, — is based in the direct mix of the protein with the precipitant cocktail. If initial conditions are far from equilibrium precipitation may occur. Because the system is not stable at this point, it goes to an equilibrium point.³⁶

In the counter-diffusion technique the system is strongly destabilised by driving it towards high supersaturation values at the beginning of the experiment. It is achieved by putting in contact two reservoirs: one containing the protein solution, and the second one with a precipitant solution. It is based on the absence of convection and the precipitant diffuses along the protein-reservoir driving the

system to high supersaturation at the point of contact and crossing the phase diagram at different values of supersaturation where the nucleation can occur.³⁶

1.1.7. The necessity of protein crystallisation

The lack of knowledge about the three-dimensional structure of a protein is the main obstacle hindering the drug design process as well as to understand any enzyme mechanism or protein function in general.³⁷

Although there are various methods for obtaining structural information of macromolecules (RMN, CryoEM, SAXS, etc.), the information about the exact arrangement of atoms in any macromolecule regardless the size or complexity is the X-ray crystallography since the probe used, the X-rays wavelength is in the order of magnitude of interatomic distance, Angströms.

This technique (*Figure 1.14*) requires high quality homogeneous crystals that will result in high quality diffraction data. The main reason why X-ray techniques require crystals: the signal from one protein molecule is extremely low and impossible for interpretation; and a crystal contains thousands of equal molecules organised in 3D (crystal lattice). In addition, the crystal of a protein is pure: it contains only the molecule and the solvent.³⁸

³⁶ F. Otálora, J. A. Gavira, J. D. Ng, J. M. García-Ruiz, *Prog. Biophys. Mol. Biol.* **2009**, *101*, 26–37.

³⁷ J. A. Gavira, F. Otálora, L. A. González-Ramírez, E. Melero, A. E. S. van Driessche, J. M. García-Ruiz, *Crystals* **2020**, *10*, 68.

³⁸ C. Mayer, *X-ray Scattering* **2017**.

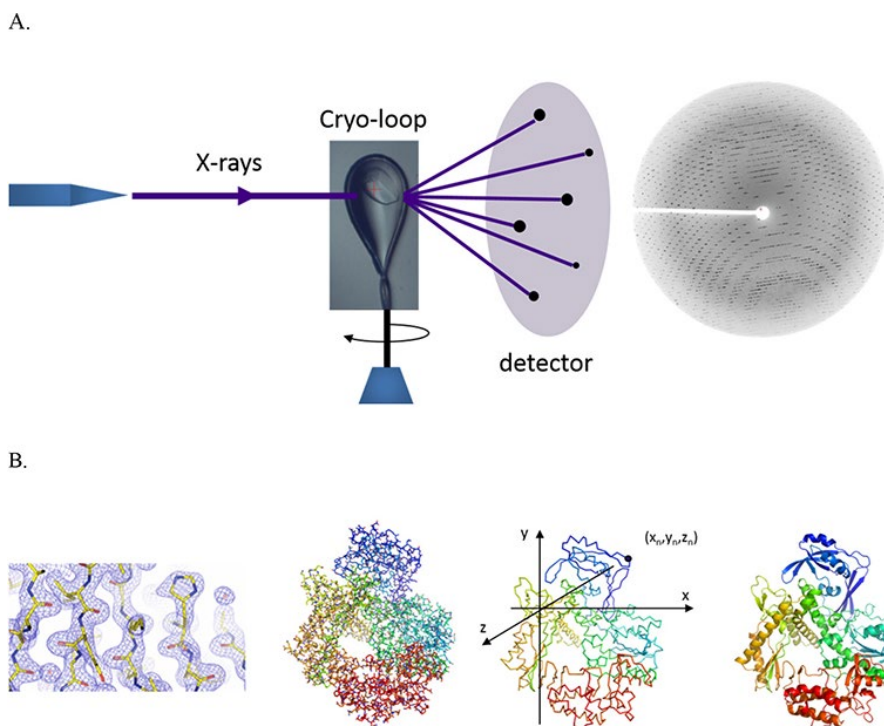


Figure 1.14. The algorithm of crystallographic determination of protein structure: A – X-ray bombardment of the frozen crystal for obtaining the diffraction of crystals electrons. B – electron density map transformed from the diffraction pattern and in turn converted into 3D structure of the protein. Reproduced from Ref. 38.

The jump started for the development of protein crystallisation (implementation of sophisticated protein crystallisation methods and enhancing data processing) was structural genomics. Since the beginning of the 1990s, large international consortiums started to work at first on the human genome project, and then on other organisms. Their goal is to decipher and create a library of macromolecules (DNA and its products — proteins).³⁹

The efforts of crystallographers are very justified: as of today (01/09/2022), 194820 determined molecules structures have already been put in the PDB (Protein Data Bank) — data bank of three-dimensional structures of proteins and nucleic acids.⁴⁰

³⁹ N. E. Chayen, E. Saridakis, *Nat. Methods* **2008**, 5, 147–153.

⁴⁰ PDB, <https://www.rcsb.org/>, **2022**.

Another application of protein crystals — protein purification. Historically, the aim of protein crystallisation in the 19th century was protein purification.

Although protein crystals frequently are unexplored material and most of all are used for structure determination, protein crystals could be used in biomedical space.

One of the main reasons — their total biocompatibility, that excludes cytotoxicity, unintended immune responses or genetic mutations.⁴¹

Compared to their soluble format, protein crystals have improved stability, higher concentration doses per volume and ease of handling. To increase protein stability and modifies the release profile, Contreras-Montoya et al.⁴² developed novel thermally stable insulin composite crystal formulations by crystallisation of human recombinant insulin in short-peptide hydrogels. The method does not change the chemical structure of the protein and demonstrates enhanced stability, slow-release profile *in vitro* and *in vivo*.

Beside it, the novel experimental field of using protein crystals for composite/hybrid materials was recently established. A summary of this can be found in *Section 1.4.2*.

1.2. Protein crystallisation in gel media

1.2.1. Gels nature & structure

Gels are structured systems consisting of a three-dimensional frame, formed by one solid component, and porous filled with another liquid component, which is held inside by surface tension effects.⁴³

Gels are soft and solid-like materials, which even though that most of their weight is liquid, have the properties of solids: the capacity to maintain shape, strength,

⁴¹ A. L. Margolin, M. A. Navia, *Angew. Chem. Int. Ed Engl.* **2001**, *40*, 2204–2222.

⁴² R. Contreras-Montoya, M. Arredondo-Amador, G. Escolano-Casado, M. C. Mañas-Torres, M. González, M. Conejero-Muriel, V. Bhatia, J. J. Díaz-Mochón, O. Martínez-Augustin, F. S. deMedina, M. T. Lopez-Lopez, F. Conejero-Lara, J. A. Gavira, L. Á. de Cienfuegos, *ACS Appl. Mater. Interfaces* **2021**, *13*, 11672–11682.

⁴³ C. Gila-Vilchez, M. C. Mañas-Torres, R. Contreras-Montoya, M. Alaminos, J. D. G. Duran, L. Á. de Cienfuegos, M. T. Lopez-Lopez, *Philos. Trans. A Math. Phys. Eng. Sci.* **2019**, *377*, 20180217.

ability to deformation (plasticity and elasticity), etc. Such mechanical properties are determined by a three-dimensional cross-linked network, formed by the component called gelator. The gelators can be inorganic (silicon dioxide, aluminium oxide), or organic substances (polyacrylamide,⁴⁴ alginate,⁴⁵ aromatic short-peptides,⁴⁶ etc.). The network can be formed by non-covalent bonds (physical gels) or covalent bonds (chemical gels). As a phase filling the pores, it can be water (hydrogels), organic solvents (organogels), or air (aerogels).⁴⁷

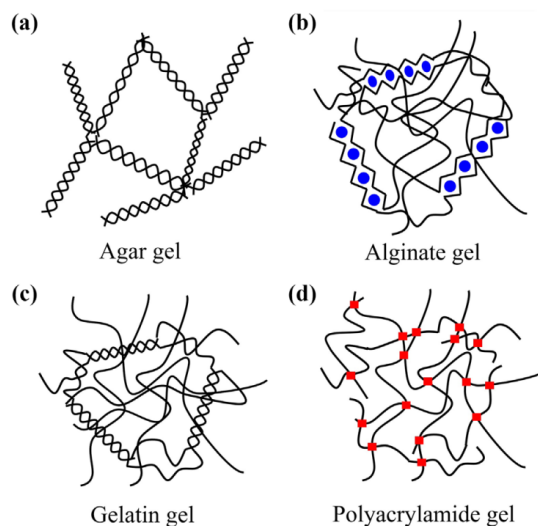


Figure 1.15. Structures and typical junction of the gels. Reproduced with permission from Ref. 48. Copyright © 2021, Springer Nature.

⁴⁴ M. C. Mañas-Torres, C. Gila-Vilchez, J. D. G. Durán, M. T. Lopez-Lopez, L. Álvarez de Cienfuegos, in *Magnetic Nanoparticle-Based Hybrid Materials* (Eds.: A. Ehrmann, T.A. Nguyen, M. Ahmadi, A. Farmani, P. Nguyen-Tri), Woodhead Publishing, **2021**, pp. 253–271.

⁴⁵ M. Barczak, P. Borowski, C. Gila-Vilchez, M. Alaminos, F. González-Caballero, M. T. López-López, *Carbohydr. Polym.* **2020**, *247*, 116747.

⁴⁶ M. C. Mañas-Torres, G. B. Ramírez-Rodríguez, J. I. García-Peiro, B. Parra-Torrejón, J. M. Cuerva, M. T. Lopez-Lopez, L. Álvarez de Cienfuegos, J. M. Delgado-López, *Inorg. Chem. Front.* **2022**, *9*, 743–752.

⁴⁷ K. Nayak, B. Das, in *Polymeric Gels* (Eds.: K. Pal, I. Banerjee), Woodhead Publishing, **2018**, pp. 3–27.

⁴⁸ M. R. Islam, M. L. Oyen, *Exp. Mech.* **2021**, *61*, 939–949.

1.2.2. Crystallogenesi in gels

Mass transport plays a very important role since it will control the incorporation of protein molecules into the crystal surface and the formation, or no, of a concentration depletion zone, which is replenished with the transfer of new molecules from the bulk solution.⁴⁹ With a constant mass transport rate, the depletion zone directly depends on the crystal growth rate. The diffusion, according to the first Fick's law, is directly proportional to the concentration gradient. Thus, the higher is the incorporation molecules into the crystal, the higher is the mass transport from the bulk solution to the crystal surface.

$$J = -D\nabla C$$

Equation 1.8

where D is the diffusion coefficient (the “-” sign indicates the flow direction from higher concentrations to lower ones). Therefore, with diffusion controlled mass transport regime, the supersaturation zone is stabilised and kinetically controlled.⁵⁰ Molecules from this zone can be stable and mildly move to the crystal, find the proper orientation and integrate into its lattice. However, in most protein crystallisation techniques mass transport is influenced by buoyant convective flows. In an environment with convection contribution (rapid fluid movement), the concentration depletion zone is thinner and the embedding of new molecules into the lattice with proper orientation is difficult producing crystals of lower quality.⁵¹

We can use the Grashhof number (Gr_n) to quantify the relative importance of buoyancy and viscous forces in a fluid system:

$$Gr_n = \frac{\text{buoyancy forces}}{\text{viscous drag forces}} = L^3 \alpha \Delta c g v^{-2}$$

Equation 1.9

⁴⁹ F. Otálora, M. L. Novella, J. A. Gavira, B. R. Thomas, J. M. García Ruiz, *Acta Crystallogr. D Biol. Crystallogr.* **2001**, *57*, 412–417.

⁵⁰ J. M. García-Ruiz, F. Otálora, A. García-Caballero, *Acta Crystallogr. Sect. F Struct. Biol. Cryst. Commun.* **2016**, *72*, 96–104.

⁵¹ F. Otálora, J. M. García-Ruiz, L. Carotenuto, D. Castagnolo, M. L. Novella, A. A. Chernov, *Acta Crystallogr. D Biol. Crystallogr.* **2002**, *58*, 1681–1689.

where Δc – the concentration difference, α – the solutal expansivity, ν – the kinematic viscosity, L – the length of a reactor, g – the acceleration due to gravity. The lower the Gr_n – the higher the reduction of the convection contribution. Besides microgravity experiment, on the Earth the simple way to reduce Gr_n is to increase the viscosity of the system or to use system with narrow characteristic length (L), which is the case of gel – the size of its pore.⁵²

Therefore, gels provide a medium in which the transport of molecules towards crystal nuclei and growing crystals is controlled by diffusion in a similar way than under microgravity conditions that have been proved to produce crystals of better quality.

Gavira et al. showed that crystals grown in the gel medium do not differ in quality from those crystals grown in microgravity conditions validating its use as the cheapest medium to grow good quality crystals.⁵³

The improvement in the quality of crystals grown in the gel environment has also been shown by Sauter et al. They carried out X-ray characterization of thaumatin crystals prepared in the agarose gel that diffracted to a previously unachieved resolution.⁵⁴

Besides the imposed control over the mass transport regime, gels also provide an impurity filter effects which can also explain the observed increase in quality.⁵⁵

In addition, crystals growth in gels helps to avoid sedimentation and fluid current associated to it⁵⁴ provides protection against mechanical influences during preparation for crystallographic analysis and transportation, without affecting the analysis, etc.⁵⁶

⁵² J. Garcia-Ruiz, M. L. Novella, R. Moreno, J. Gavira, *J. Cryst. Growth* **2001**, *232*, 165–172.

⁵³ J. A. Gavira, F. Otálora, L. A. González-Ramírez, E. Melero, A. E. S. van Driessche, J. M. García-Ruiz, *Crystals* **2020**, *10*.

⁵⁴ C. Sauter, B. Lorber, R. Giegé, *Proteins* **2002**, *48*, 146–150.

⁵⁵ A. A. Chernov, J. M. Garcia-Ruiz, B. R. Thomas, *J. Cryst. Growth* **2001**, *232*, 184–187.

⁵⁶ J. M. Garcia-Ruiz, L. A. Gonzalez-Ramirez, J. A. Gavira, F. Otálora, *Acta Crystallogr. D Biol. Crystallogr.* **2002**, *58*, 1638–1642.

1.2.3. Gels used for protein crystallisation

Since the growth of protein crystals in gels is the cheapest way to obtain high quality crystals, there are many successful examples of different proteins crystallisation in a gel media improving their quality (*Table 1.2*).

Protein	Gel type	Gel concentration % (w/v)	Crystallization system
Alliinase	Agarose	0.5	GCB
Anti-lysozyme camel antibody	Agarose	0.5	GCB
Apo ferritin	Agarose	0.3	Pasteur pipette
AP-Sm1 protein	Agarose	0.1-0.2	Glass capillary
Aspartyl tRNA synthetase-1	Agarose	0.1-0.2	Limbri plates
		0.08-0.3	
Bacteriophage T4 endonuclease VII	Agarose	0.1-0.2	Glass capillary
Canavalin	Agarose	0.2-0.6	Sitting-drop gel Microdialysis gel
Catalase	Agarose	0.5	GCB
Concanavalin A	Agarose	0.5	GCB
Cytochrome c	Agarose	0.5	GCB
Dehydroquinase (type II)	Agarose	0.5	GCB
Factor XIII	Agarose	0.5	GCB
Ferritin	Agarose	0.5	Glass tube GCB
Glucose isomerase	Agarose	0.5	GCB
Hfq protein	Agarose	0.1-0.2	Glass capillary
FBPase	Agarose	0.5	GCB
Insulin	Agarose	0.5	GCB
Lysozyme	Silica (TMS)	2-5% (v/v)	Glass tube
	Silica (TMS)	1.4% (v/v)	Glass capillary
	Agarose	0.2-0.6	Sitting-drop gel Microdialysis gel
	Agarose	0.5	GCB
	Agarose	0.2	Glass tube

	Agarose	1	Glass capillary
	Agarose	0.15-0.3	Lindemann glass capillary
	Agarose	0.5	Glass tube
	Gellan gum	0.25	Interferometric cell
Lumazine synthase	Agarose	0.5	GCB
(Pro-Pro-Gly) ₁₀	Agarose	0.5	GCB
Thaumatococcus	Agarose	0.5	Glass tube
	Agarose	0.15–0.3	Lindemann glass capillaries
	Agarose	0.15	APCF dialysis reactor
	Agarose	0.5	GCB
Tomato Bushy Stunt Virus	Agarose	0.1-0.2	Lindemann glass capillary
Triose phosphate isomerase	Agarose	0.5	GCB
Trypsin	Agarose	0.4	Glass tube
Xylanase	Agarose	0.5	GCB

Table 1.2. Protein crystals grown in gels. GCB - Granada Crystallisation Box, APCF - Advanced Protein Crystallization Facility Reproduced with permission from Ref. 57. Copyright © 2005, International Union of Crystallography.

Agarose gels

One of the most studied gels in which protein crystallisation was carried out is agarose gel. Agarose routinely extracted from some red algae Agarose gels consist of polysaccharide framework which is created by cooling down a sol below its gelling temperature (*Figure 1.16*). The interactions between the polysaccharide chains are formed with van der Waals or hydrogen bonds and its formation is reversible. Therefore, agarose gels are considered physical gels.⁵⁸

Agarose gels behave as a regular viscoelastic gel above its critical concentration of 0.12 % (w/v). Below this point they have characteristics of non-Newtonian fluids. At concentrations lower than 0.04 % (w/v) agarose gels get control over buoyancy and crystal sedimentation.⁵²

⁵⁷ R. Willaert, I. Zegers, L. Wyns, M. Sleutel, *Acta Crystallogr. D Biol. Crystallogr.* **2005**, *61*, 1280–1288

⁵⁸ M. Savchenko, M. Hurtado, M. T. Lopez-Lopez, G. Rus, L. Álvarez de Cienfuegos, J. Melchor, J. A. Gavira, *Ultrason. Sonochem.* **2022**, *88*, 106096.

The pores size in agarose gels is inversely proportional to its concentration: it decreases from 520 nm to 180 nm with increasing concentration from 0.7 to 5%.⁵⁹

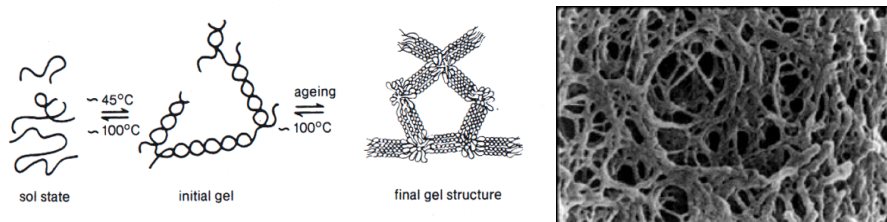


Figure 1.16. Formation and structure of agarose gel. Reproduced from Ref. 60.

In addition to obtaining high-quality crystals⁶¹ and successful crystallisation of proteins that could not be crystallised before in other media,⁶² a nucleation induction effect of agarose gels has also been observed. Artusio et al.⁶³ proved that there is the direct correlation between agarose concentration and increase in nucleation density (inversely correlated with crystal size) which is independent of the protein's nature, since the effect was observed for 5 different proteins.

Silica gels

For silica gel preparation (for protein crystallisation) sodium metasilicate, tetramethyl orthosilicate and tetraethyl orthosilicate have been tested. Unlike agarose gels, silica gels are formed by covalent bonds, that is, they are chemical gels (Figure 1.17). They are elastic, resistant to deformation, and as agarose gels, the pores size in silica gels is inversely proportional to its concentration: from 250 nm to 50 nm with increasing the concentration from 10% to 20%.⁶⁴

⁵⁹ M. Maaloum, N. Pernodet, B. Tinland, *Electrophoresis* **1998**, *19*, 1606–1610.

⁶⁰ P. Rutland. *Techniques in molecular biology — agarose gels (horizontal gel electrophoresis)* **2018**.

⁶¹ F. Artusio, A. Castellví, R. Pisano, J. A. Gavira, *Crystals* **2021**, *11*.

⁶² J. A. Gavira, W. de Jesus, A. Camara-Artigas, J. López-Garriga, J. M. García-Ruiz, *Acta Crystallogr. Sect. F Struct. Biol. Cryst. Commun.* **2006**, *62*, 196–199.

⁶³ F. Artusio, A. Castellví, A. Sacristán, R. Pisano, J. A. Gavira, *Cryst. Growth Des.* **2020**, *20*, 5564–5571.

⁶⁴ B. Lorber, C. Sauter, A. Théobald-Dietrich, A. Moreno, P. Schellenberger, M.-C. Robert, B. Capelle, S. Sanglier, N. Potier, R. Giegé, *Prog. Biophys. Mol. Biol.* **2009**, *101*, 13–25.

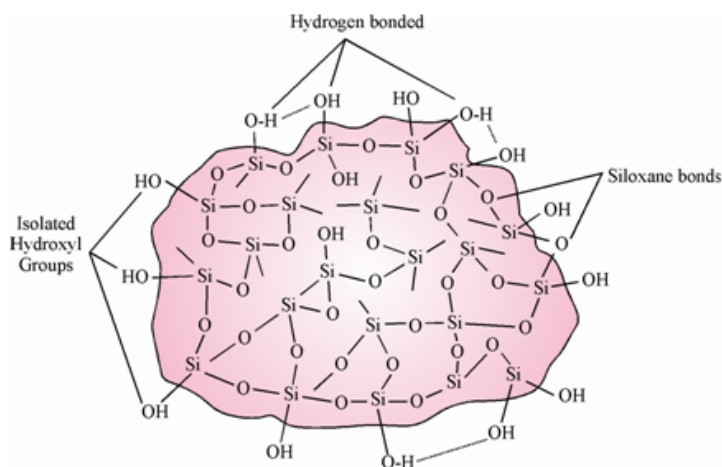


Figure 1.17. Structure of silica gel. Reproduced from Ref. 65.

Gavira et al. demonstrated that protein crystals could be grown in silica gels at concentration as high as 22% (v/v). They obtained protein crystals with incorporated silica fibres. The composite crystals maintained its short-range crystallographic order, were optically translucent and demonstrated high diffraction quality. Besides the clear impact on crystal shape as a function of silica concentration, the most relevant result was the inhibition of the nucleation which directly correlated with silica concentration.⁶⁶ Incorporation of silica into crystals can protect sensitive protein crystals from mechanical shocks, osmotic pressure, drying, etc. (that affects the diffraction quality) during manipulations.

Short-peptide supramolecular hydrogels

Short-peptide supramolecular hydrogels form their network by non-covalent bonds (mainly by hydrogen bonds and $\pi - \pi$ interactions). As biocompatible, biodegradable and produced at room temperature under mild conditions, these hydrogels are supposed to be a “green” alternative media for protein crystallisation.⁶⁷

⁶⁵ Adsorption Chromatography Assignment Help, can be found under <http://www.expertsmind.com/topic/packing-material-or-stationary-phase/adsorption-chromatography-913002.aspx>, 2022.

⁶⁶ J. A. Gavira, A. E. S. Van Driessche, J.-M. Garcia-Ruiz, *Cryst. Growth Des.* **2013**, *13*, 2522–2529.

⁶⁷ M. Conejero-Muriel, R. Contreras-Montoya, J. J. Díaz-Mochón, L. Álvarez de Cienfuegos, J. A. Gavira, *CrystEngComm.* **2015**, *17*, 8072–8078.

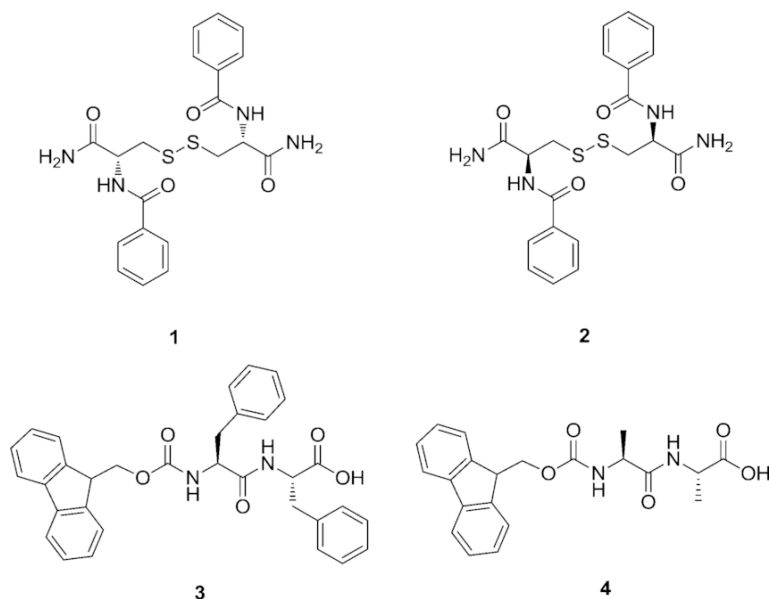


Figure 1.18. Short peptide derivatives that were used for supramolecular hydrogels formation. Reproduced from Ref. 67.

Conejero-Muriel et al.⁶⁸ for the first time carried out protein crystallization in short-peptide supramolecular hydrogels media. The authors successfully crystallised lysozyme, glucose isomerase and a formamidase in chiral hydrogels based on dimers of cysteine from L- and D-amino acids. They demonstrated the influence of the enantiomeric media on protein crystals quality and different polymorphs formation. In addition, by gel fibres incorporation into the crystals were obtained novel composite materials.

The research was continued by Contreras-Montoya et al.⁶⁹ who crystallized lysozyme in Fmoc-CF (fluorenylmethoxycarbonyl-cysteinylphenylalanine) hydrogels. Resulted composite crystals demonstrated resistance against local radiation damage by dipeptides' protection of crystals' sensitive groups.

Protein crystallization in short-peptide supramolecular hydrogels also allows obtaining composite materials for biotechnological applications. Thus, Contreras-

⁶⁸ M. Conejero-Muriel, J. A. Gavira, E. Pineda-Molina, A. Belsom, M. Bradley, M. Moral, J. García-López Durán, A. Luque González, J. J. Díaz-Mochón, R. Contreras-Montoya, A. Martínez-Peragón, J. M. Cuerva, L. Álvarez de Cienfuegos, *ChemCommun.* **2015**, 51, 3862.

⁶⁹ R. Contreras-Montoya, A. Castellvi, G. Escolano-Casado, J. Juanhuix, M. Conejero-Muriel, M. T. Lopez-Lopez, J. M. Cuerva, L. Álvarez de Cienfuegos, J. A. Gavira, *Cryst. Growth Des.* **2019**, 19, 4229–4233.

Montoya et al.⁷⁰ crystallized insulin in Fmoc-AA (fluorenylmethoxycarbonyl-dialanine) hydrogels. These crystals showed enhanced stability and slower dissolution rate than crystals grown in agarose. Because of the included hydrogel, insulin crystals in experiments *in vitro* and *in vivo* had slower release profile being therapeutically active.

1.3. Protein crystallisation under ultrasound irradiation

1.3.1. Sonochemistry: application of ultrasound

All chemical reactions need energy and matter. The source of energy has a great impact on the course of a chemical reaction. Ultrasonic irradiation is an unusual source due to its duration, extraordinary local heating and pressure that is caused by cavitation.⁷¹ That is why chemical effects after applications of ultrasound, have attracted the attention of scientists since 1927.⁷² The area that studies the effects of ultrasonic waves (20kHz–10MHz) on chemical reactions is called sonochemistry.⁷³

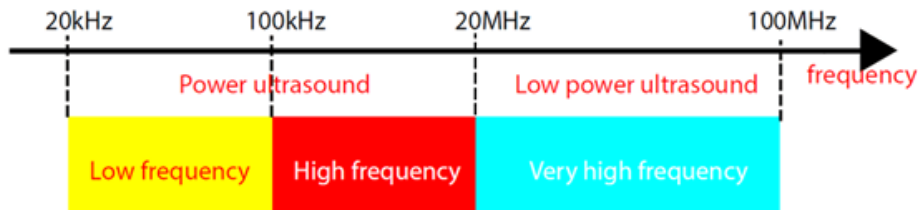


Figure 1.19. The diapason of ultrasound frequency. Reproduced from Ref. 74.

Because of large wavelengths, 10-100 cm, there is no direct intercalation between an ultrasonic wave and molecules.⁷⁵ Most of the effects are caused by acoustic

⁷⁰ R. Contreras-Montoya, M. Arredondo-Amador, G. Escolano-Casado, M. C. Mañas-Torres, M. González, M. Conejero-Muriel, V. Bhatia, J. J. Díaz-Mochón, O. Martínez-Augustin, F. S. de Medina, M. T. Lopez-Lopez, F. Conejero-Lara, J. A. Gavira, L. Á. de Cienfuegos, *ACS Appl. Mater. Interfaces* **2021**, *13*, 11672–11682.

⁷¹ K. S. Suslick, *Science* **1990**, *247*, 1439–1445.

⁷² W. T. Richards, A. L. Loomis, *J. Am. Chem. Soc.* **1927**, *49*, 3086–3100.

⁷³ P. D. Lickiss, *J. Chem. Technol. Biotechnol.* **1994**, *59*, 208–208.

⁷⁴ A. Franco, C. Bartoli, *J. Phys. Conf. Ser.* **2019**, *1224*, 012035.

cavitation; stable and transient ones (*Figure 1.20*). Stable cavitation, when a bubble oscillates many times around its equilibrium radius while transient cavitation, is when a bubble grows rapidly during a few acoustic cycles and subsequently collapse releasing the acquired energy provoking the formation of local hot spots with temperatures around 5000°C and pressures in the order of 1000 atm.⁷⁶

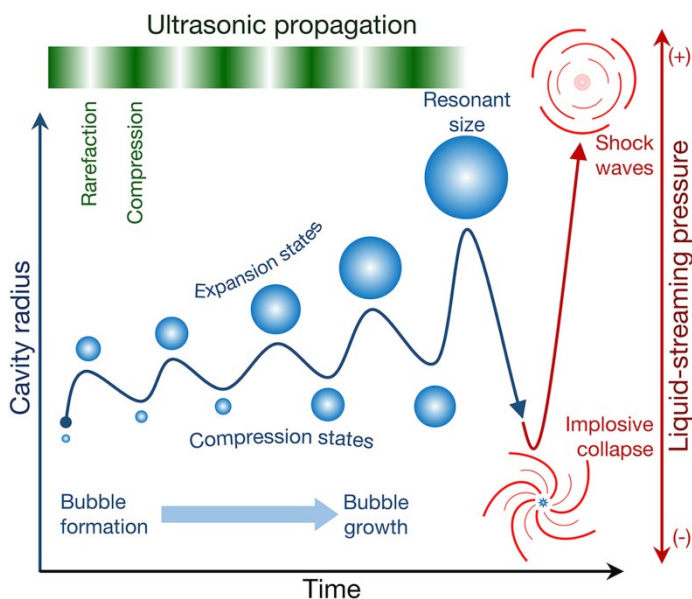


Figure 1.20. Illustrations of acoustic cavitation caused by ultrasound. Reproduced from Ref. 77.

Because of the bubbles' collapse, shock waves with velocities up to ~ 4000 m/s and high-pressure amplitudes of 106 kPa are generated. The shock waves can cause high-speed collisions between micron-sized solid particles (i.e., interparticle collisions) and directly interact with particles, causing destruction (i.e., sonofragmentation).⁷⁴

Due to the simplicity of producing ultrasound, the cheap price of the equipment, safety, waste prevention (reducing the amount of solvents, less pure reagents,

⁷⁵ A. B. P. Lever, in *Comprehensive Coordination Chemistry II* (Eds.: J.A. McCleverty, T.J. Meyer), Pergamon, Oxford, **2003**, p. xviii.

⁷⁶ A. Gedanken, **2001**, pp. 9450–9456.

⁷⁷ T. Q. Bui, H. T. M. Ngo, H. T. Tran, *Journal of Science: Advanced Materials and Devices* **2018**, *3*, 323–330.

increasing catalysis), sonochemistry could be an eco-friendly alternative source of energy.

Nowadays, ultrasound is effectively applied in analytical and organic chemistry, biotechnology, polymerization, and in an experimental way in crystallisation.⁷⁸

1.3.2. Sonocrystallization

Sonocrystallization is the crystallisation under the influence of ultrasound irradiation at any stage of the process. Although it has some distinguishing traits, concrete mechanisms of the effects of ultrasonic waves on the crystallisation process still are not established and have to be discussed.

The hypothetical mechanisms are associated with acoustic cavitation: cavitation accelerates micro-scale mixing and turbulence that leads to enhanced diffusion and uniform supersaturation which in turn decreases induction time (the time lapse between the moment of reaching a certain supersaturation and the appearance of crystals),⁷⁹ and therefore the width of the metastable zone (“the area between an equilibrium saturation curve and the experimentally observed supersaturation point at which nucleation occurs spontaneously”),⁸⁰ and increases nucleation rate, distribution of nuclei and rate of appearance of crystals.⁸¹ Also, due to enhanced velocity in solution, solute molecules have more chance to assemble and the formation of the nucleus requires less energy.⁸²

There are some studies that demonstrate that nucleation rate might be also increased by the impact of the presence of bubbles on the solvation: part of solute molecules contact with bubbles, not with solvent molecules, that decrease the critical excess free energy for nucleation,⁸³ and also the bubbles could behave as new nucleation sites.⁸⁴

⁷⁸ L. H. Thompson, L. K. Doraiswamy, *Ind. Eng. Chem. Res.* **1999**, *38*, 1215–1249.

⁷⁹ D. Kashchiev, D. Verdoes, A.G. Van Vermolen, *J. Cryst. Growth* **1991**, *110*, 373.

⁸⁰ *Org. Process Res. Dev.* **2002**, *6*, 201–202.

⁸¹ H. N. Kim, K. S. Suslick, *Crystals* **2018**, *8*, DOI 10.3390/cryst8070280.

⁸² G. Rucroft, D. Hipkiss, T. Ly, N. Maxted, P. W. Cains, *Org. Process Res. Dev.* **2005**, *9*, 923–932.

⁸³ Vekilov, P.G. Nucleation. *Cryst. Growth Des.* **2010**, *10*, 5007–5019

⁸⁴ M. Saclier, R. Peczkalski, J. Andrieu, *Ultrason. Sonochem.* **2010**, *17*, 98–105.

Another possible mechanism is driven by high local pressure, which appears after the collapse of bubbles, as it is mentioned in *Section 1.3.1*: the pressure increases supersaturation which in turn increases nucleation.

Practically, all the mechanisms described above should lead to increasing the amount of crystals because of enhanced nucleation (appears more nucleus that grows into crystals) and decreasing their sizes because of exhausting of the substance that was used to form the nucleus. Indeed, there are plenty of studies about crystallisation of inorganic/organic substances that agree with this prediction.^{85,86,87,88,89}

Nevertheless, there are some reports about obtaining bigger crystals after the ultrasound irradiation and correlation between a set-up of ultrasound and crystals size.⁹⁰ Also Delgado and Sun⁹¹ demonstrated the enhanced crystals growth with the ultrasound application associated with cavitation due to molecular addition from liquid to crystal lattice.

The impact of ultrasound on secondary nucleation is not yet well understood. Secondary nucleation is the process when new nuclei grow from already existing nuclei or from fragmented crystals. The reasons for crystals/nuclei fragmentation are shockwaves and cavitation generated by ultrasound. So, with an application of ultrasound, there should appear more new nucleation sites for secondary nucleation,⁹² but according to Li,⁹⁰ the excess of the substance would be used for crystals growth, not for new nucleation.

⁸⁵ H. Hatakka, H. Alatalo, M. Louhi-Kultanen, I. Lassila, E. Hægström, *Chem. Eng. Technol.* **2010**, *33*, 751–756.

⁸⁶ R. Jamshidi, D. Rossi, N. Saffari, A. Gavriilidis, L. Mazzei, *Cryst. Growth Des.* **2016**, *16*, 4607–4619.

⁸⁷ J. Lee, M. Ashokkumar, S. E. Kentish, *Ultrason. Sonochem.* **2014**, *21*, 60–68.

⁸⁸ K. A. Ramisetty, A. B. Pandit, P. R. Gogate, *Ind. Eng. Chem. Res.* **2013**, *52*, 17573–17582.

⁸⁹ C.-S. Su, C.-Y. Liao, W.-D. Jheng, *Chem. Eng. Technol.* **2015**, *38*, 181–186.

⁹⁰ H. Li, H. Li, Z. Guo, Y. Liu, *Ultrason. Sonochem.* **2006**, *13*, 359–363.

⁹¹ A. E. Delgado, D.-W. Sun, in *Ultrasound Technologies for Food and Bioprocessing* (Eds.: H. Feng, G. Barbosa-Canovas, J. Weiss), Springer New York, New York, NY, **2011**, pp. 495–509.

⁹² B. W. Zeiger, K. S. Suslick, *J. Am. Chem. Soc.* **2011**, *133*, 14530–14533.

1.3.3. Sonocrystallization of proteins

Studying the crystallisation of complex biological macromolecules, such as proteins, with the presence of ultrasound is a challenge due to spontaneous and stochastic nature of nucleation and lack of any general theory about the mechanism of ultrasound influence.

That is why despite the first report of ultrasounds on the crystallisation kinetics was published in 1967⁹³ only recently started to appear reports over ultrasound effect on protein crystallization.

Nanev et al.⁹⁴ pioneer this investigation and showed that the application of ultrasound redoubles the nucleation rate of lysozyme crystals. He associates the increasing of nucleation rates with breaking of the protein crystals.

Kakinouchi et al.⁹⁵ examined that brief irradiation immediately after starting the experiment promotes crystallisation. On the contrary, long irradiation decreases the nucleation time. The authors also connect the results with damage by the ultrasonic power.

Crespo et al.⁹⁶ also observed the nucleation-promoting effect of ultrasound. The effect could be seen with the protein crystals grown at lower supersaturation levels due to faster formation of crystals induced by ultrasonic irradiation.

Kitayama et al.⁹⁷ studied the impact of ultrasonic waves on the crystallisation of lysozyme and glucose isomerase. The study showed the acceleration of crystallisation and formation of small and homogeneous crystals with application of continuous ultrasound as the result of fragmentation of previously formed crystals.

⁹³ S. L. Hem, *Ultrasonics* **1967**, *5*, 202–207.

⁹⁴ C. N. Nanev, A. Penkova, *J. Cryst. Growth* **2001**, *232*, 285–293.

⁹⁵ K. Kakinouchi, H. Adachi, H. Matsumura, T. Inoue, S. Murakami, Y. Mori, Y. Koga, K. Takano, S. Kanaya, *J. Cryst. Growth* **2006**, *292*, 437–440.

⁹⁶ R. Crespo, P. M. Martins, L. Gales, F. Rocha, A. M. Damas, *J. Appl. Crystallogr.* **2010**, *43*, 1419–1425.

⁹⁷ H. Kitayama, Y. Yoshimura, M. So, K. Sakurai, H. Yagi, Y. Goto, *Biochim. Biophys. Acta* **2013**, *1834*, 2640–2646.

More recently Ferreira et al.⁹⁸ investigated the effect of ultrasonication on protein crystallisation within a droplet microfluidics device. The authors observed an increasing nucleation rate when applying low-powered ultrasound. They also demonstrated a correlation between applied power of ultrasound and nucleation rate: there exists a certain critical power of ultrasound that provokes assembling of protein molecules in solution, that leads to cluster formation; but after reaching of this power, ultrasound induces competition between cluster formation and breakage. They also reported a reduction of the induction time and crystal size.

Mao et al.⁹⁹ also observed the nucleation-promoting effect of ultrasound on lysozyme crystallisation, which was translated in decreasing the induction time and the metastable zone width. Applying different ultrasound modes (long time continuous ultrasound and ultrasonic-stop method) they obtained small uniform crystals. Comparing outcomes, authors suggested an ultrasonic-stop method for getting lysozyme crystals with better morphology and uniform size distribution.

Besides some pointed studies, a systematized research about the influence of ultrasounds parameters as source, power, time, direction and amplitude on protein crystallization is still needed.

1.4. Protein crystals as a template for *in situ* growth of inorganic materials

1.4.1. Crystallisation in confinement

In many real-world environments crystallisation processes occur not in bulk or on perfect surfaces, but in limited volumes like frost heave, biomineralization (bones and seashells), growth of salt and ice crystals in the pores of masonry, etc. Moreover, some features of crystallisation in confined spaces differ from the general crystallisation mechanisms described in *Sections 1.1.4 – 1.1.5*. Therefore, it is important to identify and study these features for understanding the mechanisms behind this crystallization process to be able to control and to reproduce them since the obtained materials are technologically relevances.

⁹⁸ J. Ferreira, J. Opsteyn, F. Rocha, F. Castro, S. Kuhn, *Chem. Eng. Res. Des.* **2020**, *162*, 249–257.

⁹⁹ Y. Mao, F. Li, T. Wang, X. Cheng, G. Li, D. Li, X. Zhang, H. Hao, *Ultrason. Sonochem.* **2020**, *63*, 104975.

According to Meldrum and O'Shaughnessy, "*confinement is an environment that changes the kinetics or thermodynamics of crystallization by restricting the dimensions of the system in one, two, or three directions*".

Structures that limit the crystallisation space has direct length and scales (the dimensions vary from atomic to centimetre), and geometries i.e. droplets (levitated and pendant ones, segmented-flow microfluidic systems, droplets in microcapillaries, droplets on surfaces), surfactant assemblies (microemulsions, vesicles), nanoscale cylindrical pores (carbon nanotubes, matrices with multiple cylindrical pores, wedge-shaped geometries, mesoporous solids (crossed cylinders apparatus, mica pockets), etc.¹⁵

The influence of confined spaces on crystallisation

Besides alerting some physical parameters such as melting and freezing points, enthalpies of fusion, etc., the confinement affects the essential crystallisation parameters, such as, nucleation and growth and thus, having an impact on crystal size, polymorphism, morphology and stability.

Reduction of the nucleation rate

A confined environment means that the crystallisation process takes place in a small volume. Since nucleation is a probabilistic phenomenon, the reduction of the volume has a direct impact on it:

$$P(t) = 1 - \exp(JV_{conf}N_{conf}t)$$

Equation 1.10

where J – the nucleation rate, V_{conf} – the volume of a confined space, N_{conf} – the number of confined spaces (for example, droplets), and t – the time.¹⁵

Therefore, the probability of nucleation in a confined space is much lower than in a bulk solution and decreases in direct proportion to the decrease in volume.¹⁰⁰

Also in confined spaces, the driving force of the crystallisation process supersaturation is constantly depleted during the formation of the nucleus: new molecules, that would replenish the lack of molecules used for the nucleus

¹⁰⁰ P. Laval, J. B. Salmon, M. Joanicot, *J. Cryst. Growth* **2007**, 303, 622.

formation, have nowhere to come from. The constant decrease in supersaturation is described by:

$$S(n) = \left(\frac{S_0 N_s - n}{N_s} \right)$$

Equation 1.11

where N_s – the number of solute molecules the small volume has at saturation (the equilibrium state).

The *Equation 1.6* from *Section 1.1.5*, which describes the decrease in total free energy during the formation of the nucleus, taking into account the constant decrease in supersaturation will look like:

$$\Delta G_{conf}(n) = -kT \int_0^n \left(\frac{S_0 N_s - n}{N_s} \right) dn + A_n^{2/3}$$

Equation 1.12

Accordingly, the same initial supersaturation, which allows the formation of nuclei in solution, may not lead to nucleation through depletion in a confined space.

In addition, in small volumes, there are no (or reduced amounts of) impurities that act as nucleation sites.¹⁵

Stabilisation of metastable polymorphs

Crystallisation in confinement can lead to the development of metastable polymorphs, new crystal structures and even formation of extraordinary non crystallographic forms. Different polymorphs have critical nuclei of different sizes, and accordingly the nucleus of which is able to be formed. In solution, these restrictions are not present, so some polymorphs in solution are difficult to obtain.¹⁵ Also, it may happen that due to reduction in the nucleation rate: some substances simply cannot form since their critical nuclei size is bigger than the available space and therefore form amorphous aggregates.

Obtaining different stable polymorphs depends on the size of the confinement. Ha et al.¹⁰¹ demonstrated that obtaining different polymorphs and their stability depend on the pore size of a template they used for the crystallisation. Thus,

¹⁰¹ J.-M. Ha, J. H. Wolf, M. A. Hillmyer and M. D. Ward, *J. Am. Chem. Soc.*, **2004**, *126*, 3382–3383

anthranilic acid crystallised in small pores (7.5 nm) had only one polymorph which is not thermodynamically stable in bulk. This polymorph had small critical nuclei size and was able to form in the confinement, meanwhile in bigger pores (24 and 55 nm) were able to form other polymorphs with bigger critical nuclei size.

The stability of polymorphs is of paramount importance in pharmacology. Different polymorphs have different physical properties (dissolution, solubility, ability to aggregation, etc.) that significantly affect the behaviour of crystals, which has consequences most of all in bioavailability of drugs. Polymorphic transitions can also create big problems for pharmacologists.¹⁰²

Morphology changing

During crystallisation in confinement, crystals can take a form that is not typical for them during crystallisation in a bulk: their shape depends on the shape of the confinement (the matrix in which they are grown), as well as on its chemical composition. Wucher et al. showed that the fictionalization of the matrix surface affects the crystallogenesis: negatively charged surfaces functionalized with carboxylic acid and sulfonic acid groups contribute to the formation of polycrystalline structures, while positively charged surfaces allowed to obtain monocrystalline ones.¹⁰³ However, Yue et al.¹⁰⁴ demonstrated that the chemical composition of the surface did not affect the morphology of the crystals.

1.4.2. Protein crystals as a template for confinement growth

From 25 to 90% of the protein crystal volume accounts for the solvent. The rest, from 10 to 75%, fall on the protein molecules themselves, ordered via salt bridges, hydrogen bonds, hydrophobic interactions, forming highly ordered frameworks (*Figure 1.21*). In addition to the solvent, other substances can diffuse into the crystal³⁴ and even enzymatic reactions can be performed within the crystals pores.¹⁰⁵

¹⁰² Q. Jiang, M. D. Ward, *Chem. Soc. Rev.* **2014**, *43*, 2066–2079.

¹⁰³ B. Wucher, W. B. Yue, A. N. Kulak, F. C. Meldrum, *Chem. Mater.* **2007**, *19*, 1111.

¹⁰⁴ W. B. Yue, A. N. Kulak, F. C. Meldrum, *J. Mater. Chem.* **2006**, *16*, 408.

¹⁰⁵ Y. Azuma, R. Zschoche, M. Tinzl, D. Hilvert, *Angew. Chem. Int. Ed.* **2016**, *55*, 1531.

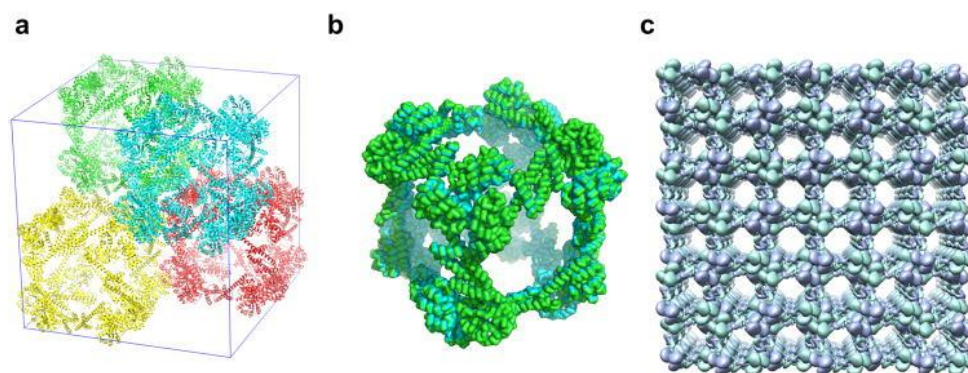
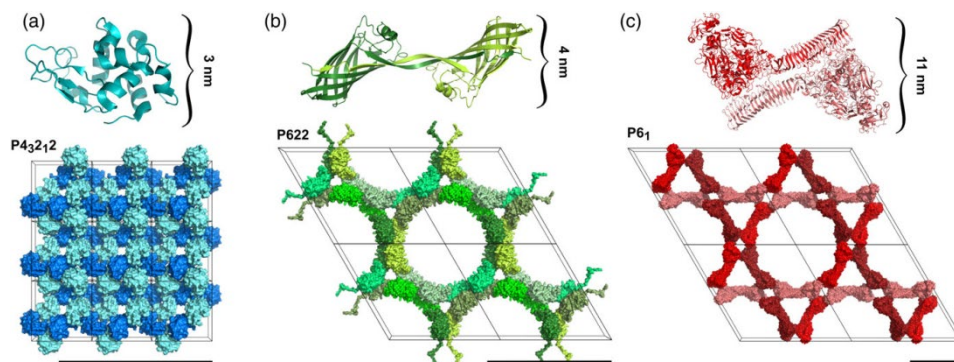


Figure 1.21. Crystal structure of the ATC-HL3 protein, represented highly porous protein lattice. Reproduced with permission from Ref. 106. Copyright © 2014, Springer Nature.

Protein crystals are biocompatible materials with well-ordered and defined porous network (Figure 1.22) with diameter from 0,3 to 10 nm,¹⁰⁷ and inner surface that can range from 800 to even 2000 m²·gr⁻¹.¹⁰⁸ Such nanostructure makes protein crystals an interesting tool for material design, especially for the creation of ordered solids of nanostructure materials.¹⁰⁹ Besides it, protein crystals consist of charged amino-acids that are periodically aligned within pores that can contribute to the accumulation of metal ions.³⁴



¹⁰⁶ Y.-T. Lai, E. Reading, G. L. Hura, K.-L. Tsai, A. Laganowsky, F. J. Asturias, J. A. Tainer, C. V. Robinson, T. O. Yeates, *Nat. Chem.* **2014**, *6*, 1065–1071.

¹⁰⁷ L. F. Hartje, C. D. Snow, *Wiley Interdiscip. Rev. Nanomed. Nanobiotechnol.* **2019**, *11*, e1547.

¹⁰⁸ L. L. Z. Vilenchik, J. P. Griffith, N. St. Clair, M. A. Navia, A. L. Margolin, *J. Am. Chem. Soc.* **1998**, *120*, 4290–4294.

¹⁰⁹ J. C. Falkner, M. E. Turner, J. K. Bosworth, T. J. Trentler, J. E. Johnson, T. Lin, V. L. Colvin, *J. Am. Chem. Soc.* **2005**, *127*, 5274–5275.

Figure 1.22. Crystal structure of the ATC-HL3 protein, represented highly porous protein lattice. Reproduced with permission from Ref. 107. Copyright © 2019, John Wiley & Sons, Inc.

At such, as in living organisms, protein residues coordinates metal ions for metal transport, catalysis of enzymatic reactions, and electron transfer. Protein crystals have also been exploited as a media to accumulate metallic nanoparticles of Ag¹¹⁰, Au¹¹¹, CoPt¹¹², CdS quantum dots¹¹³ in their inner cavities, or reinforced them with single-walled carbon nanotubes for obtaining composite materials with possibility to use these materials as 3D semiconducting materials.¹¹⁴

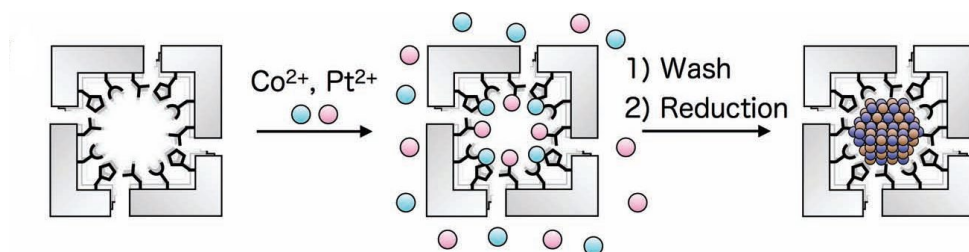


Figure 1.23. Schematic drawings describing the preparation of CoPt nanoparticles in a solvent channel of a lysozyme crystal. Adapted with permission from Ref. 112. Copyright © 2012, John Wiley & Sons, Inc.

¹¹⁰ M. Liang, L. Wang, R. Su, W. Qi, M. Wang, Y. Yu, Z. He, *Catalysis Science and Technology* **2013**, 3.

¹¹¹ H. Wei, Z. Wang, J. Zhang, S. House, Y. G. Gao, L. Yang, H. Robinson, L. H. Tan, H. Xing, C. Hou, I. M. Robertson, J. M. Zuo, Y. Lu, *Nat. Nanotechnol.* **2011**, 6.

¹¹² S. Abe, M. Tsujimoto, K. Yoneda, M. Ohba, T. Hikage, M. Takano, S. Kitagawa, T. Ueno, *Small* **2012**, 8, 1314–1319.

¹¹³ H. Wei, S. House, J. Wu, J. Zhang, Z. Wang, Y. He, E. J. Gao, Y. Gao, H. Robinson, W. Li, J. Zuo, I. M. Robertson, Y. Lu, *Nano Res.* **2013**, 6.

¹¹⁴ R. Contreras-Montoya, G. Escolano, S. Roy, M. T. Lopez-Lopez, J. M. Delgado-López, J. M. Cuerva, J. J. Díaz-Mochón, N. Ashkenasy, J. A. Gavira, L. Álvarez de Cienfuegos, *Adv. Funct. Mater.* **2019**, 29, 1807351.

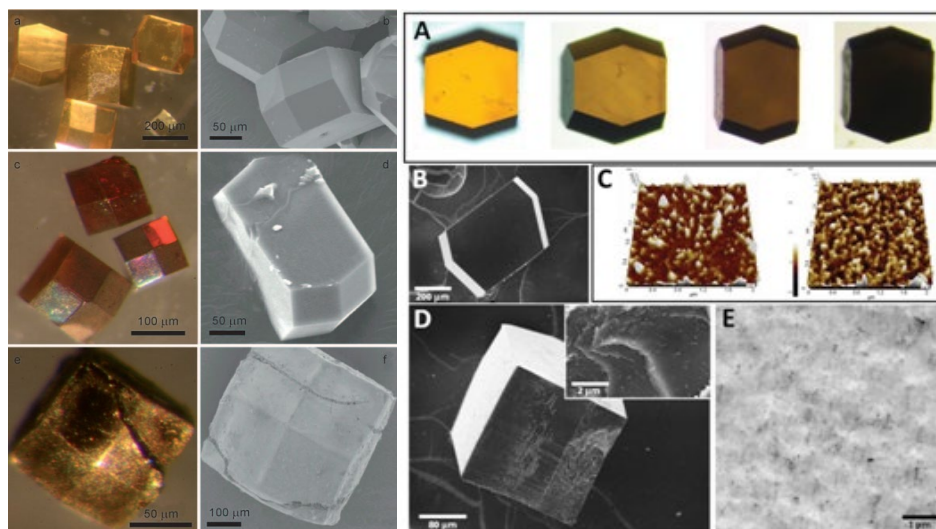


Figure 1.24. Composites based on lysozyme crystals. Left: for Au accumulation: a,b) control; c,d) with accumulated Au after UV irradiation; and e,f) after reaction of sodium borohydride with AuCl₄ ions. Reproduced with permission from Ref. 115. Copyright © 2010 WILEY-VCH Verlag GmbH & Co. KGaA, Weinheim. Right: Cross-linked protein crystals with composite hydrogels containing single-walled carbon nanotubes. Reproduced with permission from Ref. 114. Copyright © 2018 WILEY-VCH Verlag GmbH & Co. KGaA, Weinheim.

1.4.3. Nanoparticles of magnetite

Application & synthesis

Magnetite — FeO·Fe₂O₃ (mixed Fe²⁺/Fe³⁺ iron oxide) is a ferrimagnetic mineral and one of the main iron ores. Magnetite is the most magnetic of all the natural minerals on Earth (besides some extremely rare native iron deposits).¹¹⁶

Nanoparticles of magnetite have many applications as storage of information,¹¹⁷ in production of ferrofluids for centrifugal shock absorbers and lubricants in the aerospace industry.¹¹⁸ Furthermore, magnetite nanoparticles are used in

¹¹⁵ M. Guli, E. M. Lambert, M. Li and S. Mann, *Angew. Chem., Int. Ed.* **2010**, 49, 520–523.

¹¹⁶ R. J. Harrison, R. E. Dunin-Borkowski, A. Putnis, *Proc. Natl. Acad. Sci. U. S. A.* **2002**, 99, 16556–16561.

¹¹⁷ G. Reiss, A. Hütten, *Nature Materials* **2005**, 4.

¹¹⁸ L. Rodríguez-Arco, M. T. López-López, J. D. G. Durán, A. Zubarev, D. Chirikov, *J. Phys. Condens. Matter* **2011**, 23, 455101.

biomedicine for magnetic cell separation,¹¹⁹ DNA/RNA extraction,^{120,121} magnetic resonance,¹²² hyperthermia therapy^{123,124} as well as drug carriers in targeted chemotherapy treatment.¹²⁵

For most of these applications, one of the requirements is that magnetite nanoparticles were superparamagnetic at room and higher temperatures and have the capacity to be oriented and attracted by the applied magnetic field, allowing them to be guided through the organism to the target site, and behave as "non-magnetic" in the absence of external magnetic field to avoid aggregation. In magnetite nanoparticles, the efficiency of its response to an external magnetic field is determined by the magnetic moment per particle, which directly depends on the size (*Figure 1.25*). Superparamagnetism appears in very small particles (2–10 nm).¹²⁶

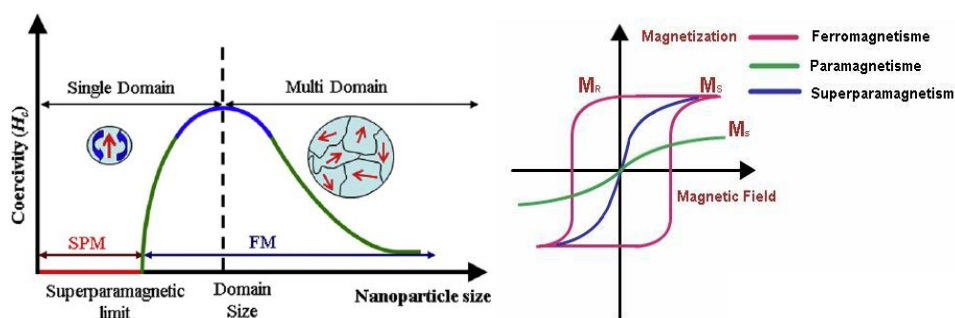


Figure 1.25. Left: The correlation between size and properties of magnetic particles. Right: The magnetization curves for paramagnetic, ferromagnetic, and superparamagnetic materials. Adapted with permission from Ref. 126. Copyright © 2011, IOP Publishing Ltd.

¹¹⁹ H. Haghighi, M. T. Khorasani, Z. Faghih, F. Farjadian, *Heliyon* **2020**, 6.

¹²⁰ C. Tang, Z. He, H. Liu, Y. Xu, H. Huang, G. Yang, Z. Xiao, S. Li, H. Liu, Y. Deng, Z. Chen, H. Chen, N. He, *Journal of Nanobiotechnology* **2020**, 18.

¹²¹ J. C. Chacón-Torres, C. Reinoso, D. G. Navas-León, S. Briceño, G. González, *Sci. Rep.* **2020**, 10.

¹²² A. Avasthi, C. Caro, E. Pozo-Torres, M. P. Leal, M. L. García-Martín, *Top. Curr. Chem.* **2020**, 378, 40.

¹²³ Y. Jabalera, A. Sola-Leyva, S. C. Gaglio, M. P. Carrasco-Jiménez, G. R. Iglesias, M. Perduca, C. Jimenez-Lopez, *Pharmaceutics* **2021**, 13.

¹²⁴ G. Iglesias, A. Delgado, M. Kujda, M. Ramos, *ColloidPolym. Sci.* **2016**, 294

¹²⁵ R. A. Revia, M. Zhang, *Mater. Today* **2016**, 19, 157–168.

¹²⁶ M. Mehrmohammadi, K. Y. Yoon, M. Qu, K. Johnston, S. Y. Emelianov, *Nanotechnology* **2011**, 22, 045502.

Thus, it is important that magnetite nanoparticles have an adequate size so that they can respond effectively to the external magnetic field and be able to direct them through a living organism. Size is also important in terms of its use in the treatment of hyperthermia since the heat releases per unit mass of the magnetic nanoparticles. To achieve the required temperature and to minimize the amount of nanoparticles introduced into the body it is important to control the nanoparticles size.¹²⁷

Routinely, magnetic nanoparticles are produced by thermal decomposition methods that require high temperature and organic solvents (*Figure 1.26*).

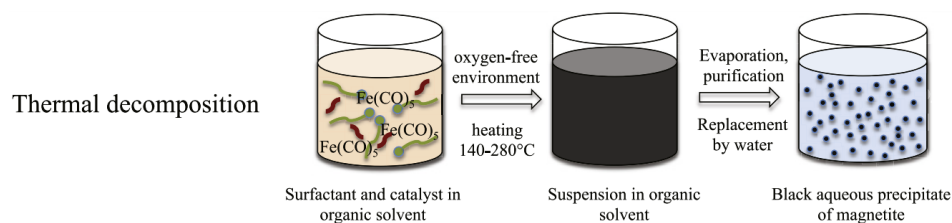


Figure 1.26. Thermal decomposition method of magnetite nanoparticles formation. Adapted with permission from Ref. 128. Copyright © 2013 IOP Publishing Ltd.

Magnetite nanoparticles can also be obtained by green methods using water as a reaction media and at room temperature. This method is called aqueous coprecipitation (*Figure 1.27*). It corresponds to the precipitation from ferrous and ferric iron in alkaline aqueous solution. It is quickly, not expensive, suitable for industrial applications and eco-friendly method. However, the design of the magnetite nanoparticles number and size, and therefore properties, are limited.¹²⁹

¹²⁷ A. J. Giustini, A. A. Petryk, S. M. Cassim, J. A. Tate, I. Baker, P. J. Hoopes, *Nano Life* **2010**, *1*.

¹²⁸ J. Gautier, E. Allard-Vannier, K. Hervé, M. Soucé, I. Chourpa, *Nanotechnology* **2013**, *24*, 432002.

¹²⁹ R. Contreras-Montoya, Y. Jabalera, V. Blanco, J. M. Cuerva, C. Jimenez-Lopez, L. Alvarez de Cienfuegos, *Cryst. Growth Des.* **2020**, *20*, 533–542.

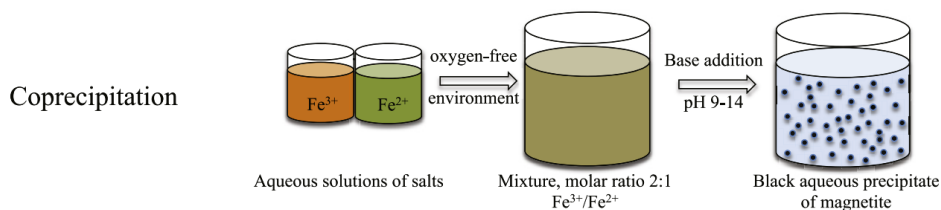


Figure 1.27. Magnetite nanoparticles synthesis by coprecipitation. Reproduced with permission from Ref. 128. Copyright © 2013 IOP Publishing Ltd.

Biom mineralization of magnetite in living organisms

Besides rocks, magnetite was found in living organisms that can mineralize it in their bodies. Homing pigeons produce magnetite for navigation in the magnetic field of the Earth; marine molluscs have magnetite on their teeth for being able to eat algae attached to rock, etc.¹³⁰

Nanoparticles of magnetite have been found in the human brain, discovered for the first time in 1992.¹³¹ It was hypothesised that magnetite were formed via *in situ* crystallisation, possibly within the 8-nm-diameter pores of ferritin (the iron storage protein).^{132,133} However, Maher et al. correlated the presence of magnetite nanoparticles with an external source. Their analysis showed high similarity of their properties with magnetite nanoparticles formed by combustion that is typical for industrial urban pollutants.¹³⁴

The most important organisms connected with magnetite formation are the magnetotactic bacteria as *Magnetospirillum* strains that are able to produce magnetite crystals inside their magnetosomes with an unusual morphologies,

¹³⁰ J. Baumgartner, G. Morin, N. Menguy, T. Perez Gonzalez, M. Widdrat, J. Cosmidis, D. Faivre, *Proc. Natl. Acad. Sci. U. S. A.* **2013**, *110*, 14883–14888.

¹³¹ J. L. Kirschvink, A. Kobayashi-Kirschvink, B. J. Woodford, *Proc. Natl. Acad. Sci. U. S. A.* **1992**, *89*, 7683–7687.

¹³² P. P. Schultheiss-Grassi, R. Wessiken, J. Dobson, *Biochim. Biophys. Acta* **1999**, *1426*, 212–216.

¹³³ C. Quintana, J. M. Cowley, C. Marhic, *J. Struct. Biol.* **2004**, *147*, 166–178.

¹³⁴ B. A. Maher, I. A. M. Ahmed, V. Karloukovski, D. A. MacLaren, P. G. Foulds, D. Allsop, D. M. A. Mann, R. Torres-Jardón, L. Calderon-Garciduenas, *Proc. Natl. Acad. Sci. U. S. A.* **2016**, *113*, 10797–10801.

homogeneous size and superparamagnetic properties (*Figure 1.28*). The chemical route of magnetite formation inside these organisms is still under investigation.¹³⁵

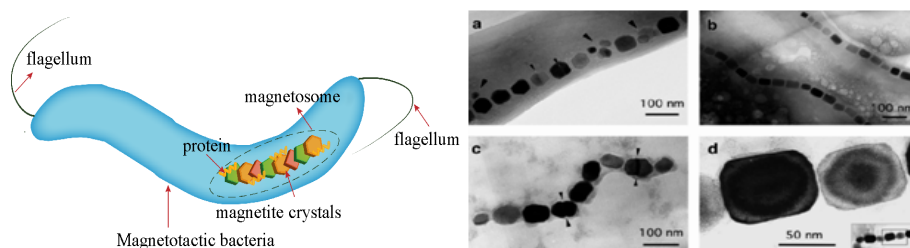


Figure 1.28. Left: The structure of Magnetospirillum bacteria. Reproduced with permission from Ref.136. Copyright © 2014, Springer Nature. Right: TEM of magnetite chains inside cells of magnetotactic bacteria. Reproduced with permission from Ref. 135. Copyright © 2000, ASM Press.

For understanding how this sophisticated synthesis occurs, it is important to take an integrated approach studying both the chemistry of iron and its transformations, and the biological (involvement of magnetosome proteins) and physical (confined space) environment in which this synthesis occurs.

Synthetic route of magnetite inside *Magnetospirillum* bacteria is discussed and ferrihydrite ($\text{Fe}_2\text{O}_3 \cdot x\text{H}_2\text{O}$),¹³⁷ hematite ($\alpha\text{-Fe}_2\text{O}_3$)¹³⁸ and maghemite ($\gamma\text{-Fe}_2\text{O}_3$),¹³⁹ are considered as precursors of magnetite (*Figure 1.29*). Some authors also include the transformation of many different iron (oxyhydr)oxide species.¹⁴⁰

In this sense Baumgartner et al.¹²⁸ proposed nanometric ferric (oxyhydr)oxides as a precursor of magnetite that forms from a highly disordered, phosphate-rich ferric hydroxide phase consistent with prokaryotic ferritins.

¹³⁵ D. A. Bazylinski, R. B. Frankel, in *Environmental Microbe-Metal Interactions*, **2000**, pp. 109–144.

¹³⁶ X. Wang, Y. Li, J. Zhao, H. Yao, S. Chu, Z. Song, Z. He, W. Zhang, *Front. Environ. Sci. Eng. China* **2020**, *14*.

¹³⁷ J. J. M. Lenders, C. L. Altan, P. H. H. Bomans, A. Arakaki, S. Bucak, G. de With, N. A. J. M. Sommerdijk, *Cryst. Growth Des.* **2014**, *14*, 5561–5568.

¹³⁸ M. L. Fdez-Gubieda, A. Muela, J. Alonso, A. García-Prieto, L. Olivi, R. Fernández-Pacheco, J. M. Barandiarán, *ACS Nano* **2013**, *7*, 3297–3305.

¹³⁹ D. Faivre, L. H. Böttger, B. F. Matzanke, D. Schüler, *Angew. Chem. Int. Ed Engl.* **2007**, *46*, 8495–8499.

¹⁴⁰ T. Ahn, J. H. Kim, H.-M. Yang, J. W. Lee, J.-D. Kim, *J. Phys. Chem. C* **2012**, *116*, 6069–6076.

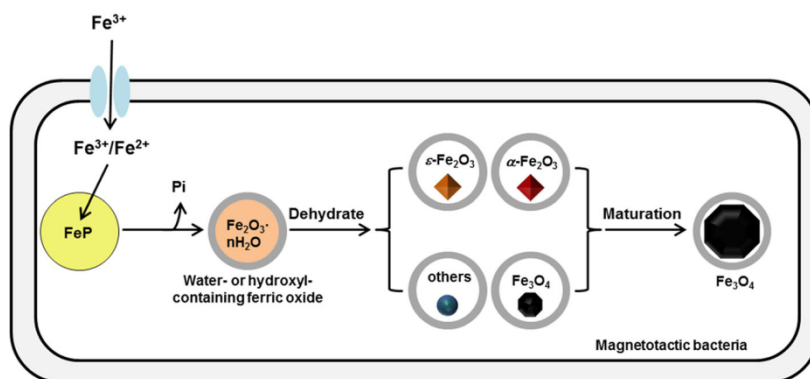


Figure 1.29. Illustration of synthetic route of magnetite with possible precursors inside *Magnetospirillum* bacteria. FeP — phosphate-rich ferric hydroxide phase (FeP) where the iron (Fe) is stored. Reproduced from Ref. 141.

Also, the biological basis of magnetite formation highlights the role of magnetosome proteins as iron oxidases that contribute to magnetite precursors formation. The process was studied by Siponen et al.,¹⁴² who proposed the mechanism where Fe^{2+} is oxidised by the protein MamPto ferrihydrite ($2\text{Fe}_2\text{O}_3 \cdot \text{H}_2\text{O}$) and then reduced MamP proteins contribute to evolution of ferrihydrite into magnetite with continuous addition of Fe^{2+} . MamP protein has four hemes on either side in which iron and porphyrin molecule serve as electron source during electron transfer or redox chemistry.

Biomimetic approaches of magnetite nanoparticles synthesis

This fascinating, “green”, but at the same time complex synthesis that bacteria make, have intrigued scientists to repeat it in a laboratory.

Lenders et al.¹³⁷ studied the *in situ* magnetite formation by slow coprecipitation of $\text{Fe}^{3+}/\text{Fe}^{2+}$ salts through NH_3 diffusion. Firstly, they obtained ferrihydrite at low pH values, which converted to magnetite at high pH values.

¹⁴¹ T. Wen, Y. Zhang, Y. Geng, J. Liu, A. Basit, J. Tian, L. Ying, J. Li, J. Ju, W. Jiang, *Biomaterials Research* **2019**, *23*,

¹⁴² M. I. Siponen, P. Legrand, M. Widdrat, S. R. Jones, W.-J. Zhang, M. C. Y. Chang, D. Faivre, P. Arnoux, D. Pignol, *Nature* **2013**, *502*, 681–684.

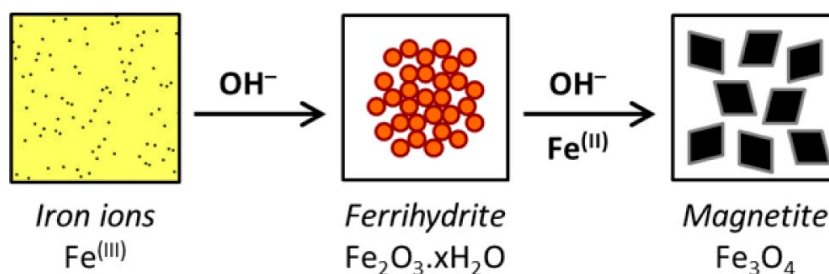


Figure 1.30. Magnetite formation from a ferrihydrate precursor. Reproduced with permission from Ref. 135. Copyright © 2014, American Chemical Society.

They also used M6A peptide (the active part of magnetosome protein Mms6) to control the nanoparticles formation and growth.

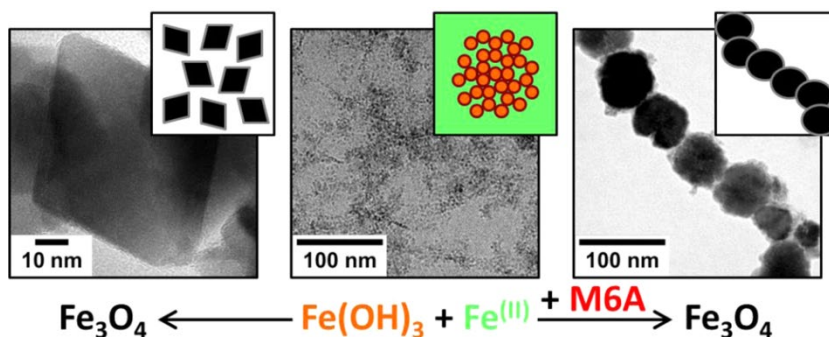


Figure 1.31. M6A peptide-associated synthesis of magnetite nanoparticles. Reproduced with permission from Ref. 135. Copyright © 2014, American Chemical Society.

Baumgartner et al.²⁴ tested nucleation theories on magnetite crystallization. In their study magnetite formation occurred without intermediate amorphous bulk precursor phase as it was proposed by non-classical nucleation passways.^{18,19} It goes via rapid agglomeration of nanometric primary particles (2 nm). With the study of magnetite crystallisation they established a conjunction between classical nucleation theory and non-classical pathway (see Section 1.1.3).

Also, different gels, gelatine ferrogels,¹⁴³ carrageenan gel¹⁴⁴ or chitosan hydrogel,¹⁴⁵ have been used to emulate live condition for the synthesis of

¹⁴³ S. Sturm, M. Sigleitmeier, D. Wolf, K. Vogel, M. Gratz, D. Faivre, A. Lubk, B. Büchner, E. V. Sturm (née Rosseeva), H. Cölfen, *Adv. Funct. Mater.* **2019**, 29, 1905996.

¹⁴⁴ A. L. Daniel-da-Silva, T. Trindade, B. J. Goodfellow, B. F. O. Costa, R. N. Correia, A. M. Gil, *Biomacromolecules* **2007**, 8, 2350–2357.

¹⁴⁵ Y. Wang, B. Li, Y. Zhou, D. Jia, *Nanoscale Res. Lett.* **2009**, 4, 1041.

magnetite nanoparticles. Particularly interesting is the work of Contreras-Montoya et al.¹²⁹ where it was proved that lysine, unlike other amino acids like arginine, is able to exert a control over the size of magnetite nanoparticles. The effect is supposed to be associated with lateral ammonium groups of lysine that could stabilise nuclei of nanoparticles and stimulate their growth.

To sum up, the biomineralization of magnetite in living organisms as well as biomimetic approach of magnetite formation *in situ* requires complex multidisciplinary study, involving physical, inorganic and biochemistry as well as crystallography.

***Lysozyme crystallisation in
hydrogel media under ultrasound
irradiation***

Rational approaches to obtain crystals with desirable properties, adequate size and quality, is still a major bottleneck. It is possible to “play” with supersaturation to stimulate crystallization, but it is difficult to control it. To control crystallization parameters scientists tried to use different external stimuli as electric^{146,147,148} and magnetic fields,¹⁴⁹ light,¹⁵⁰ audio¹⁵¹ and microwave.¹⁵²

Application of ultrasound, as a safety, waste preventive and eco-friendly alternative source of energy could help to modify production of protein crystals and to set desirable parameters.

Even though US effect on the crystallisation of substances in general has been studied for almost 100 years,⁷² the exact mechanism of the effect as well as its effect on protein crystallisation remains unclear. Although several studies have been conducted,⁹⁵⁻⁹⁹ they did not provide fundamental data or any general theory.

All the previous studies about an influence of ultrasound on crystallization in general, and in particular on protein crystallization, were performed in solution. To reveal the critical mechanism of ultrasonic wave’s impact on crystallization, our task was to explore the effect of ultrasound in the gel media that compartment the space and as the consequence removes sedimentation and convection,^{52,53} which in itself affects crystallization and interferes with an objective assessment of the result. Moreover, ultrasound could act as nucleation promoter by disaggregating critical nuclei and agarose may also amortize this impact.

As well, the purpose of this study was to think over and select all parameters: protein/precipitate concentration; time and duration of irradiation; observation time; ultrasound settings (source, power, time, direction and amplitude of the ultrasound waves), methods for assessing the impact of ultrasound. They could

¹⁴⁶ L. F. Alexander, N. Radacsi, *CrystEngComm* **2019**, *21*, 5014–5031.

¹⁴⁷ F. Li, R. Lakerveld, *Cryst. Growth Des.* **2018**, *18*, 2964–2971.

¹⁴⁸ E. Revalor, Z. Hammadi, J.-P. Astier, R. Grossier, E. Garcia, C. Hoff, K. Furuta, T. Okustu, R. Morin, S. Veessler, *J. Cryst. Growth* **2010**, *312*, 939–946.

¹⁴⁹ J. A. Gavira, J. M. García-Ruiz, *Cryst. Growth Des.* **2009**, *9*, 2610–2615.

¹⁵⁰ T. Okutsu, *J. Photochem. Photobiol. C: Photochem. Rev.* **2007**, *8*, 143–155.

¹⁵¹ C.-Y. Zhang, J. Liu, M.-Y. Wang, W.-J. Liu, N. Jia, C.-Q. Yang, M.-L. Hu, Y. Liu, X.-Y. Ye, R.-B. Zhou, D.-C. Yin, *Cryst. Growth Des.* **2019**, *19*, 258–267.

¹⁵² K. Mauge-Lewis, A. Mojibola, E. A. Toth, M. Mohammed, D. Seifu, K. Aslan, *Cryst. Growth Des.* **2015**, *15*, 3212–3219.

serve to deliver protocols and methods that make protein crystallization more efficient and reliable.

2.1. Objectives of the study

The main objective of this work is to study the potential use of ultrasound for controlling protein crystallization. Using the gel media suppose to objectivise the results by removing sedimentation and convection that could interfere the inrepretation of the results.

Objective 1. To study the influence of ultrasound on nucleation and growth of protein crystals in solution;

Objective 2. To study the influence of ultrasound on protein crystallization in agarose gel, and to characterize the impact of the gel on the process;

Objective 3. To study mechanical properties of agarose gels and to analyse the correlation between characteristics of the gels and influence of ultrasonic waves into the gels.

2.2. Materials and methods

2.2.1. Reagents and materials

All the reagents used in the study were obtained from commercial sources which will be specified throughout the text in italics.

The equipment used in the study was designed and produced in collaboration by engineers from the Ultrasonics lab at the University of Granada (Manuel Hurtado, Guillermo Rus and Juan Melchor). The rest of commercial equipment will be specified throughout the text by writing the model in italics.

2.2.2. Design & set-up of the ultrasound equipment

The bioreactor for conducting experiments on the effect of ultrasound on protein crystallisation (*Figure 2.1*) was developed in collaboration by engineers from the Ultrasonics lab at the University of Granada.

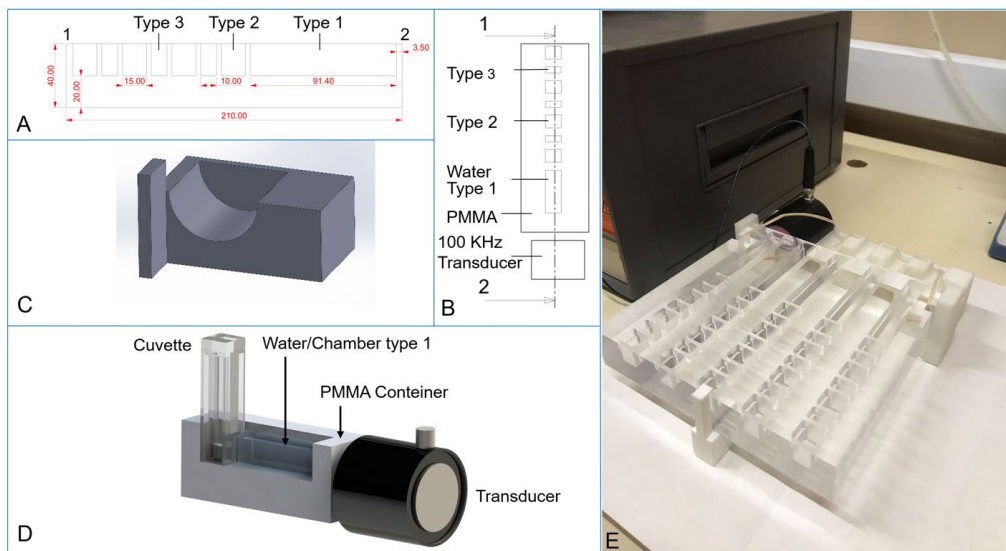


Figure 2.1. The bioreactor for conducting experiments on the effect of ultrasound on protein crystallisation: A and B – the lateral and top transversal section views of a bioreactor section shown in the photo E; C – 3D printed support to maintain the ultrasonic transducer in a correct position to ensure the alignment of the propagating waves. D – illustration of the US-bioreactor with the cuvette installed, ready for the experiment. Reproduced from Ref. 58.

This design solves several important problems:

First, location of samples in a distance from the US-emitter prevents the possibility of heterogeneous nucleation and disruption of the sample.

Avoiding direct contact with the transducer prevents samples heating (see Section 2.1.5).

Thirdly, this arrangement of cuvettes makes it possible to avoid the near field area (in this region the sound pressure levels vary considerably in terms of random positions of energy and it is difficult to control the sound pressure homogeneity).

The near field area was calculated with Equation 2.1:

$$N = \frac{D^2 f}{4c}$$

Equation 2.1

where (N) is the near field, (D) is the diameter of the transducer, (f) is the frequency of the US wave and (c) is the velocity of sound of the US wave.

$$N = \frac{4.5^2 \cdot 100}{4 \cdot 1525} = 3.32 \text{ cm}$$

Therefore, the testing samples were placed further than 3.32 cm far from the transducers.

The bioreactor was designed in *SolidWorks* software and 3D printed with polymethylmethacrylate (PMMA). This material was chosen due to its mechanical and low-density properties.

The support for the transducers (*Figure 2.1.C*) holds them in the appropriate position. For whole wave incidence into the chamber the transducer must be positioned perpendicular to the sample — propagation front of the ultrasonic waves is transmitted perpendicularly to the surface of the transducer.

The maximum resolution of the ultrasound beam sets along the the central axis of the transducer. Thus, to reach optimum intensity, the base of the cuvette must be placed along the central axis.

For tight contact between the transducer and the chamber, their surfaces were smeared with *Vaseline*. It also provides an optimal pressure of contact and no displacement during the irradiation experiments.

For the experiment we choose the contact piezo-electric transducers that meet the specifications to generate a monochromatic wave to be propagated in multilayer media and minimise the undesired noise.

They were connected to the wave generator *Agilent Technologies 33500B* и amplifier *AR 150A100D*.

At the beginning of the investigation, the ultrasound settings was screened: frequency (20-100 kHz), voltage (100-180 V), duty cycle (1-10%), time of irradiation (from immediately after samples preparation up to 7h after samples preparation) and its duration (10 sec-24 h). We have chosen the optimal settings: frequency 100 kHz, voltage 180 V, with a 5% duty cycle and 50 ms of burst period simulating a continuous propagation of the wave, because they gave clear results.

The time parameters in correlation with the crystallisation parameters were chosen: the optimal irradiation duration — 30 minutes: it is enough for observing an effect of the US influence (less than this time we did not observe the effect). As the time of irradiation we have chosen 2 points: 1 — immediately after sample preparation and 2 — 30 minutes after sample preparation, in order to

check where the irradiation would be more effective. We called it “Protocol US1” and “Protocol US2” respectively.

2.2.3. Characteristics of the materials

The necessary calculations were carried out to ensure the propagation and maximisation of the waves without loss of amplitude when passing from the emitter into the sample.

First of all, we calculated the impedance (resistance to the sound wave) of all materials and media through which the sound wave will pass: PMMA — the bioreactor material; water in which the cuvettes are placed; polystyrene (PS) — the cuvette material. Protein crystallisation experiments were carried out in aqueous protein solutions (crystallisation in solution) and in aqueous agarose solution (max concentration 0.200% — crystallisation in gel media). Since the solutions were not highly concentrated, we calculated their impedance as for water.

The impedance of materials was calculated using the formula:

$$Z = \rho \cdot c$$

Equation 2.2

where (Z) is the impedance, (ρ) is the density and (c) is the velocity of the wave through material.

Material	(ρ) Density Kg/m ³	(c) Velocity (m/s)	(Z) Impedance (Pa.s/m)
PMMA	1180	2765	3,263,183
Water (20°C)	993	1525	1,515,584
PS	612	2340	1,432,080

Table 2.1. Impedance of the media used in the experiment. Reproduced from Ref.58.

Based on these calculations, the transmission coefficient of the ultrasonic wave through each material was calculated:

$$D = \frac{4Z_1Z_2}{[Z_1 + Z_2]^2}$$

Equation 2.3

where (D) is the transmission coefficient, (Z_1) is the impedance of material 1 and (Z_2) is the impedance of material 2. The values are shown in *Table 2.2*.

D	PMMA	Water/gel	PS
PMMA	1	0,86	—
Water/gel	0,86	1	0,992
PS	—	0,9992	1

Table 2.2. Transmission coefficients between water, PMMA and PS. Reproduced from Ref. 58.

It means that from transducer into water enters 86% of acoustic pressure, from water through cuvette material goes 99% and into the sample penetrate 99% of the rest acoustic pressure (*Figure 2.2*).

The acoustic pressure in water in the unit where cuvette is placed, after passing from the transducer trough PMMA was measured with the needle hydrophone *Onda*. The pressure in the water was 618 Pa. Therefore with the transition of US waves from water to PS the pressure will be $P = 618 \text{ Pa} \cdot 0.99 = 611.82 \text{ Pa}$; from PS to sample: $P = 611.82 \text{ Pa} \cdot 0.99 = 605.7 \text{ Pa}$.

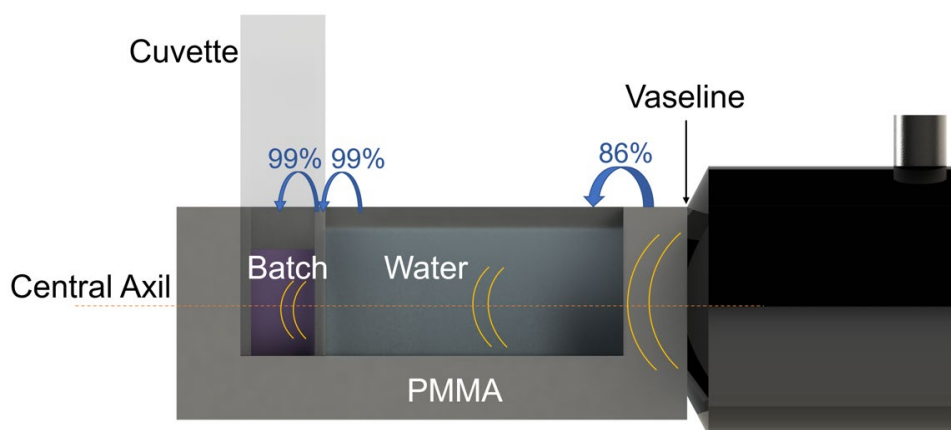


Figure 2.2. US-Bioreactor with the transmission coefficients of the media. Reproduced from Ref. 58.

2.2.4. Mechanical characterization of the gel media

Rheological methods were used to mechanically characterise the gel media in which we conducted the crystallisation experiments. All rheological studies were carried out using a *Bohlin CS10* controlled-stress rheometer. The selected geometry was concentric cylinders with grooved surfaces.

We were interested in characterising the mechanical properties of the medium in which the protein crystallisation occurred; how they changed through the time when we conducted an experiment in them (1 hour), how the kinetics of gel formation occurred; and whether ultrasound affected the mechanical properties.

Kinetics of gelation

According to the “Crystallisation in gel” protocol, agarose solution was mixed with the protein and precipitant solution, homogenised and irradiated with US during 30 min (Protocol US1) and kept 30 min and then irradiated during 30 min (Protocol US2). To know when exactly the gel formation took place, and how the mechanical properties of the media changed over the time, the gelation kinetics of the agarose solutions used for the crystallisation were measured. Gels were prepared directly inside the geometry of the rheometer. The measurement time was 1h (that includes the time applied for both Protocol US1 and Protocol US2), the parameters: oscillatory strain of 1 Hz of frequency and 1 Pa of the stress.

We measured gelation kinetics of the agarose solutions with a concentration of 0.050; 0.100; 0.200% (that includes the concentration area where the agarose transits from non-Newtonian fluid (0.100% w/v) to a regular gel (0.200% w/v)).⁵²

Three different samples were measured to ensure statistical significance of the results. The mean values and standard deviations of each magnitude are provided below.

Mechanical properties

In the same concentration range, the mechanical properties of agarose gels were studied. To see if the irradiation of ultrasound affected the mechanical properties, we measured frequency sweep (dependency of viscoelastic moduli in frequency on the non-destructive deformation range) before and after the irradiation of US (using both Protocol US1 and US2). Thus, we measured the storage (G') and loss (G'') moduli of the gels as functions of frequency (from 0.1 to 10 Hz) at a constant stress of 1 Pa. Gels before the irradiation of US were prepared directly inside the geometry of the rheometer; gels that were measured after the irradiation of US initially were irradiated by US (in the same way as the crystallisation samples) in a cuvette which has the parameters of the geometry, and then neatly without mechanical exposure were transferred into the geometry of the rheometer. As previously, three different samples were measured to ensure statistical significance of the results. The mean values and standard deviations of each magnitude are provided below.

2.2.5. Crystallisation set-up

The batch method was selected for the experiments, since it does not require any special consumables and it can be carried out in any container: in our case, it is micro spectrophotometer visible-cuvettes *Brand, GmbH, Co-KG*, which are suitable for parameters for the Type 1 unit (see *Figure 2.1*) of the bioreactor: they are wide and thin, which provides good irradiation of the contents and allows us to observe the sample in a microscope, without removing it from the cuvette.

In essence, the influence of US on crystallisation is primarily the influence on nucleation. Almost all the final parameters of the crystal depend on it. Therefore, it was necessary to 1) choose a system on which it would be possible and convenient to affect the nucleation; 2) to control the factors that can affect nucleation in addition to US.

The crystallisation conditions screening was carried out, to find a condition in which nucleation would have occurred within 1 h (no more: to be able to study many samples, and no less, because it would be difficult to evaluate the result). Another important requirement was the size and number of crystals formed in the conditions of crystallisation in control — it is much easier to evaluate any effect in small amount of big crystals.

Thus, a range of supersaturation values were tested by changing the lysozyme concentration, from 25 to 50 mg·mL⁻¹, NaCl concentration from 3.5% to 5.0% (w/v) (Table 2.3).



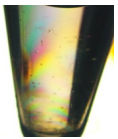
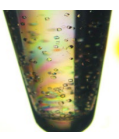
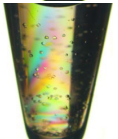
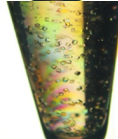
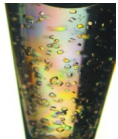
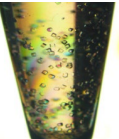
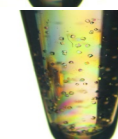
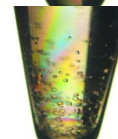
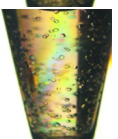
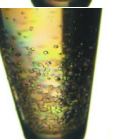

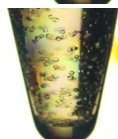

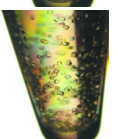
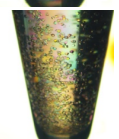




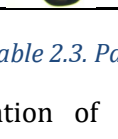
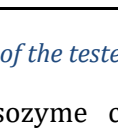
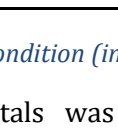
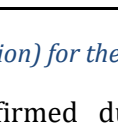
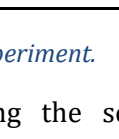
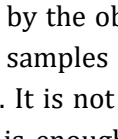
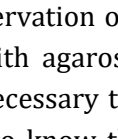
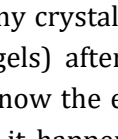
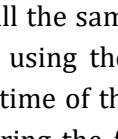
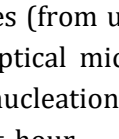
		Lysozyme, mg·mL ⁻¹				
		20	30	35	40	45
NaCl,%	c					
	3					
	3.3					
	3.5					
	3.7					
4						
4						

Table 2.3. Part of the tested condition (in solution) for the experiment.

The nucleation of lysozyme crystals was confirmed during the screening experiment by the observation of tiny crystals in all the samples (from un-gelled solution to samples with agarose gels) after 1 h using the optical microscope (Figure 2.3). It is not necessary to know the exact time of the nucleation, for our purpose it is enough to know that it happens during the first hour — selected time to study the irradiation effect.

This way it was determined that using 40 mg mL⁻¹ and NaCl 4.3% (w/v) for the experiments in un-gelled solution and 40 mg mL⁻¹ and NaCl 4.0% (w/v) for the experiment in agarose gels the nucleation induction time moved in the range of the initial 1h and therefore fitted our experimental requirements.

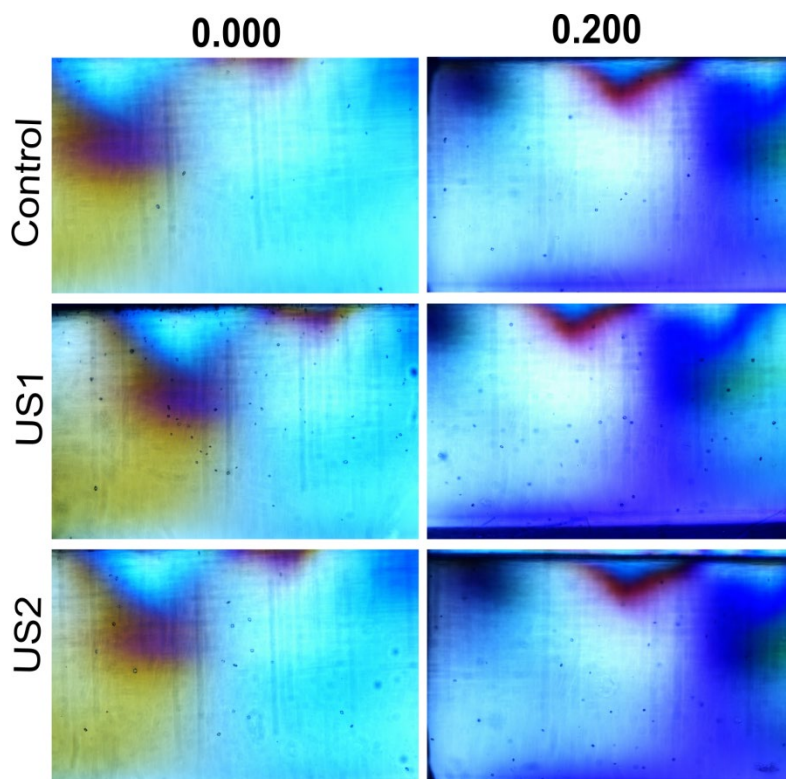


Figure 2.3. Lysozyme crystals observed 1h after the setting up the experiment in un-gelled solution (0.000) and with maximum agarose concentration (0.200%) used in the experiments under silent condition (Control) and ultrasonic irradiation for 30 minutes immediately after preparing the experiment (US1) and 30 minutes after preparation (US2) that indicated the nucleation occurred within 1h using $40 \text{ mg}\cdot\text{mL}^{-1}$ of lysozyme and 4.3% (w/v) of NaCl.

From *Equation 1.3*, the temperature is one of the parameters affecting nucleation and, as a consequence, crystallisation. It may determine if the crystallisation will occur at all and influence the final results. Therefore, the control of temperature was one of main focus in this work.

One of the essential conditions for planning the crystallization experiments is a temperature control.

The temperature at which our crystallisation conditions work ($40 \text{ mg}\cdot\text{mL}^{-1}$ of lysozyme and 4.3% (w/v) of NaCl) was required since it will ensure that nucleation will occur within 1 hour, as planned. Temperature must keep constant along the whole experiment in order to get comparable reproducible results.

Three requirements were fulfilled by performing the experiments with constant conditioning at 20 °C and monitoring the temperature throughout the experiment (24h). The temperature was measured with an electronic thermometer with accuracy of 0.01 °C. Since irradiation is known to increase the temperature we also measured the temperature in the nearest chambers to the ultrasonic transducer. In all cases the registered temperature was lower than < 0.01 °C, i.e., the heating effect is negligible with our configuration.

Also, during and after irradiation with US, before the observation, all samples were stored in water with strictly controlled temperature. The control was also kept in the same way.

It is worth to mention that the current design of the bioreactor, in which the sample is kept in a water bath far from the transducer, avoids heat transferred from the transducer to the cuvette.

2.2.6. The experiment set-up

The effect of US on the crystallisation of lysozyme was studied firstly in solution (*Figure 2.4 A1*), and then in agarose gel medium (*Figure 2.4 A2*) at 0.010%, 0.025%, 0.050%, 0.100% and 0.200% (w/v) concentrations.

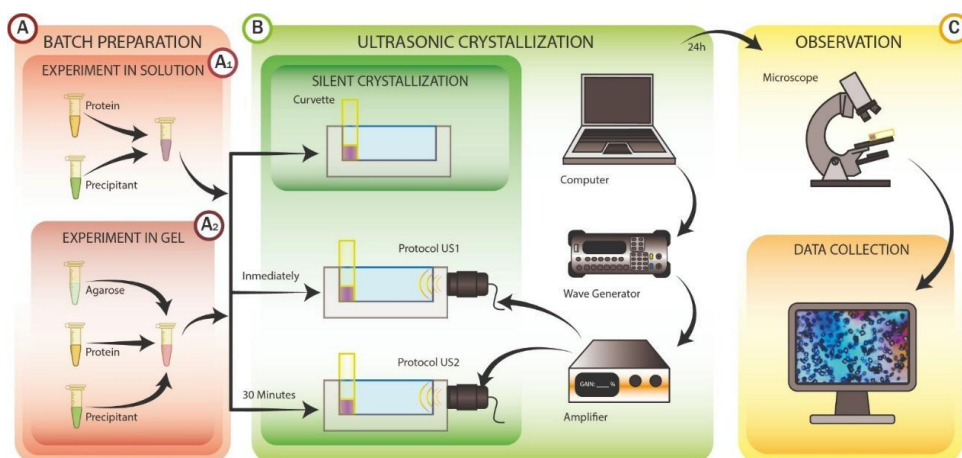


Figure 2.4. The experiment procedure: A) Batches preparation: A1 — experiments in solution; A2 — experiments in gel media. B) Crystallisation under ultrasound irradiation & control. C) Observations and data analysis. Reproduced with Ref. 58.

Lysozyme crystallization in solution under US

Preparation of the reagents

Lysozyme (HEWL, three-time crystallized powder) from *Sigma-Aldrich* was dissolved in 50mM AcONa from *Sigma-Aldrich* and dialysed during 24 h against 50 mM AcONa (pH 4.5) in a ratio 1:1000 at 4 °C. Then it concentrated by centrifugation at 4 °C ($g = *5000/25$ min) using 10-kDa cutoff Centricon concentrators *Amicon* to $\approx 150 \text{ mg}\cdot\text{mL}^{-1}$ determined spectrophotometrically at 280 nm using a theoretical value for the extinction coefficient of $2.56 \text{ mL}\cdot\text{mg}^{-1}\cdot\text{cm}^{-1}$. For additional purification, the solution was filtered through a 0.45 μm pore-size filter membrane system *Millipore*.

Sodium chloride from *Sigma-Aldrich* was prepared at 20% (w/v) in 50 mM AcONa (pH 4.5) and used as stock solution. Solutions of NaCl at desired concentration were prepared by diluting with 50 mM AcONa and filtered through a 0.45 μm pore-size filter membrane system *Millipore* prior using it.

Preparation of the samples

For the experiments in solution: lysozyme, NaCl and AcONa were mixed together in one Eppendorf tube, homogenised and divided in three aliquots of 100 μL using micro spectrophotometer visible-cuvettes *Brand, GMBH, CO-KG*.

The experiment

First sample was irradiated immediately after the preparation during 30 min (we called it "Protocol US1"); the second sample was kept and irradiated it after 30 min after the preparation, duration of the irradiation was the same – 30 min (we called it "Protocol US2"); the third sample was a control (without an irradiation).

Lysozyme crystallization in gel media under US

Preparation of the reagents

The protein/precipitant solutions for the experiments were prepared as in the previous section.

Agarose D5 with a melting point of 92 °C and gelling point of 37 °C was supplied by *Hispanagar*. Agarose sols with desirable concentration were obtained by dissolving agarose in 50 mM AcONa (pH 4.5) and heated at 90 °C to get a homogeneous transparent solution. Then the solution was cooled down to 50 °C

and kept at this temperature until finally mixed with the protein and precipitant solution.

Preparation of the samples

The agarose, protein and precipitant were mixed together in one Eppendorf tube, homogenised and divided in three aliquots of 100 μ L as in the experiments in solution.

The experiment

As well as with the experiments in solution, for the experiments in gel media Protocols US1 and US2 were tested. The third sample was a control (without an irradiation).

Observation & data collection

After the irradiation all the samples were kept at 20 °C in water. The evolution of the experiments was followed by standard optical microscopy (*Nikon AZ100*, zoom 2x2x0.6) observing the formation of tiny crystals in all the samples (un-gelled solution as well as in samples with agarose gels) after 1 h.

Number and size of crystals were evaluated after 24 h by optical microscopy using the *Image-Focus-Alpha* software of the *Nikon AZ100* microscope (zoom 2x2x0.6). Each image was divided in 25 equal regions (5 columns x 5 rows) avoiding zones near cuvettes borders where it was not possible to see the crystals clearly, and all the crystals were counted in all the regions. Crystals size were analysed by measuring a minimum of 100 crystals.

2.2.7. Statistical analysis

There are two interdependences parameter of crystals with which is possible to quantify the US influence on the crystallization — number and size of the crystals.

To characterize the simultaneous mean differences between the irradiated and not irradiated samples, as well as the difference between samples irradiated with Protocols US1 and US2 statistical tests were performed. The first step was to check the proof of normality *via* the Kolmogorov-Smirnov and Shapiro-Wilk tests. If the tests showed the distribution of the variables was parametric, a multiple

regression analysis via ANOVA was performed. In case the distribution was non-normal, Kruskal-Wallis test was performed. The p-value significances for the groups were obtained with Dunn's test. These p-values were compared with the significance level — 0.05 — the minimum accepted level indicates a difference between means. The notation that we have included hereafter is * $p < 0.05$, ** $p < 0.001$ and *** $p < 0.0001$ when the differences between means are statistically significant.

2.3. Results and discussion

2.3.1. Lysozyme crystallization in solution under US

The crystallization systems with fixed supersaturation were irradiated with “Protocol US1” and “Protocol US2” (US1 and US2 below)

Experiments in solution (0.000)

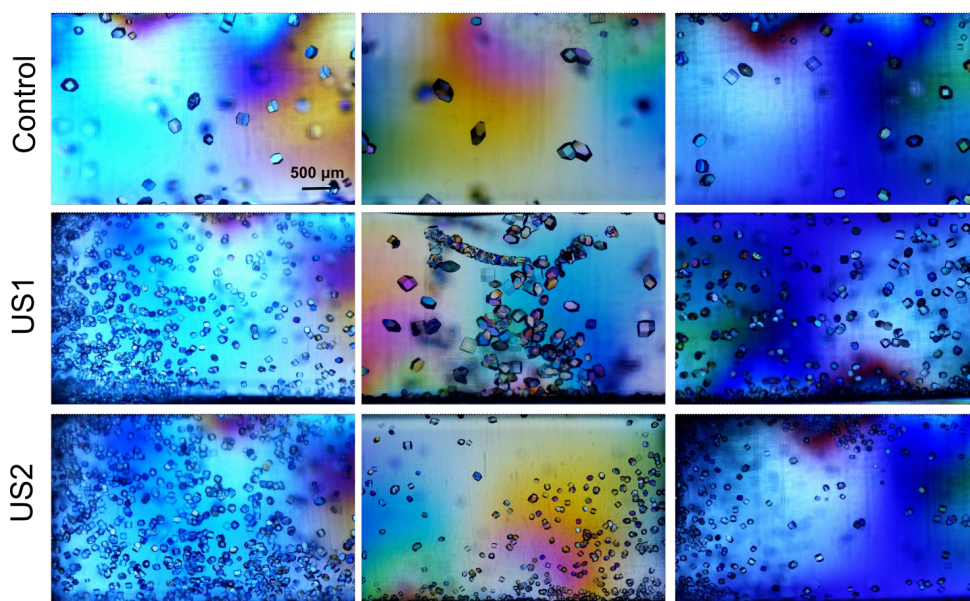


Figure 2.5. The lysozyme crystals obtained in solution with (US1 and US2) and without (Control) ultrasound irradiation. The black line in the bottom of some pictures — crystals sedimentation.

As was expected, the ultrasound irradiation activated the nucleation of the crystals: having the same supersaturation, the samples treated with “Protocol US1” and “Protocol US2” showed an increase of the number of crystals and decrease in their size (Figure 2.5). These changing are the visible and quantitative

consequences of increasing the nucleation rate: bigger amount of crystals is the evidence of higher nucleation rate, smaller size — the consequence of the higher nucleation rate (the protein was spent on many nucleus formations and could not been spent on crystals growth).

The analysis of the crystals size distribution showed that at the fixed chosen supersaturation after 24 h almost all the crystal in the control sample had the size around 200 μm . In the immediately US1 and US2 samples almost all the population of the crystals had around 100 μm .

Kruskal-Wallis test showed statistically significant difference in both crystals number and size between irradiated and non-irradiated samples. There is also statistically significant difference between crystals size in samples irradiated according to Protocol US1 and US2 (*Figure 2.6*).

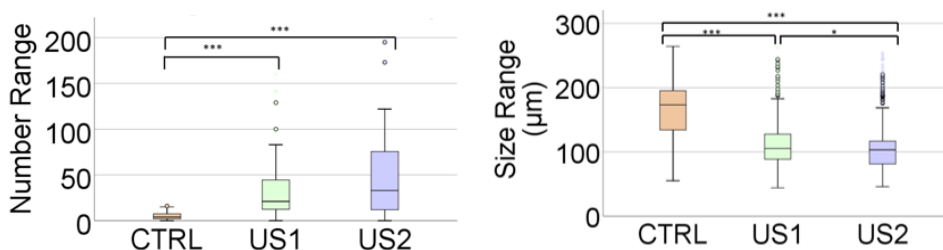


Figure 2.6. The statistical analysis of the number (left) and size (right) of the crystals obtained under silent condition (CTRL — control) and US irradiation for 30 min immediately after preparation of the experiment (US1) and 30 min after preparation (US2) in solution.

In addition, the size distribution in the irradiated samples was more homogeneous (*Figure 2.7*). That could be the result of narrowed nucleation time caused by US when majority of the nucleus appeared simultaneously and started to grow resulted in uniform size distribution. While in the non-irradiated samples happened not just one event of nucleation. The difference in time of nucleus formation resulted in the heterogeneity of the size distribution.

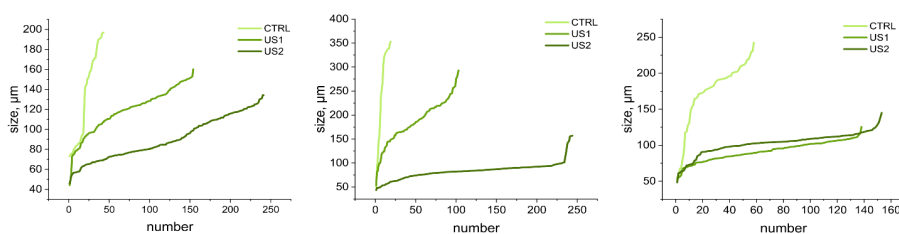


Figure 2.7. Distribution of lysozyme crystals size obtained in solution under silent (control) and ultrasonic (US1 & US2) crystallization conditions for the three experiments.

The results in solution approved the design of the bioreactor and the chosen parameters.

The experiments in solution show that ultrasound can be used as external stimuli for increasing nucleation, and as the result for controlling protein crystallization (for obtaining crystals with desirable parameters and homogeneous size). Ultrasound irradiation can be used for getting protein crystals in lower supersaturation than normally, due to enhancing nucleation. It means spending less substances and higher control over the crystallization process: if the system goes too quickly through the phase diagram (that could happen with high supersaturation), instead of crystalline material, an amorphous phase could precipitate (see *Figure 1.12*).

2.3.2. Lysozyme crystallization in gel media under US

Crystallization systems with fixed supersaturation and various agarose concentrations (0.010%, 0.025%, 0.050%, 0.100%, 0.200%) were irradiated with “Protocol US1” and “Protocol US2”.

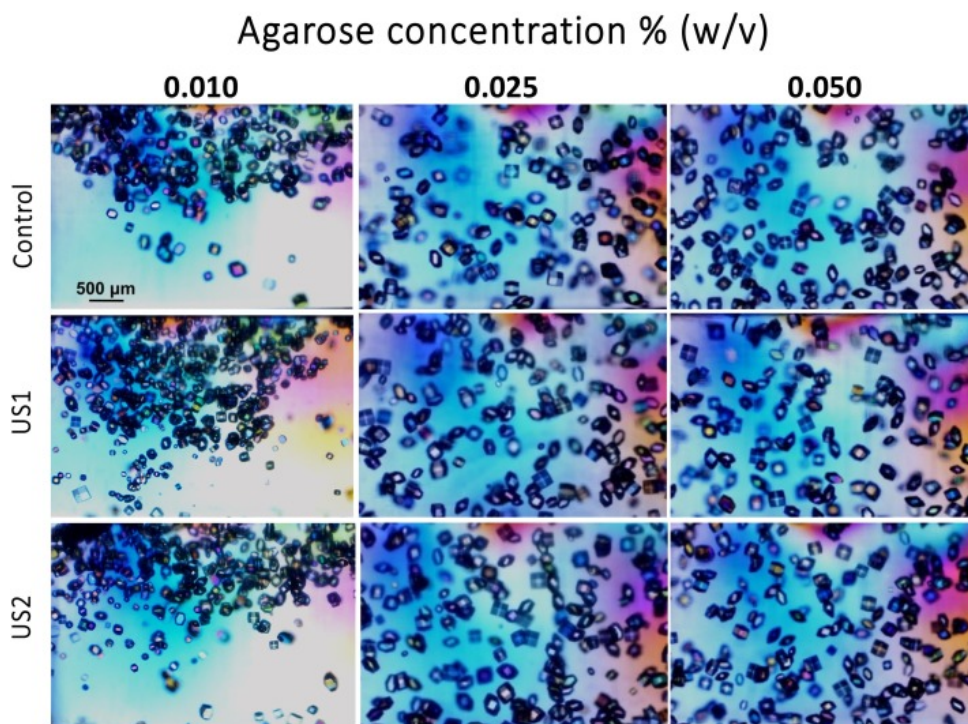


Figure 2.8. Lysozyme crystals obtained in gel media under silent condition (Control) and ultrasonic irradiation for 30 min immediately after preparing the experiment (US1) and 30 min after preparation, irradiated for 30 min (US2). From left to right it is shown the increasing concentration of agarose. The scale bar in the optical microscopy images is 500 μm in all the pictures. Reproduced from Ref. 58.

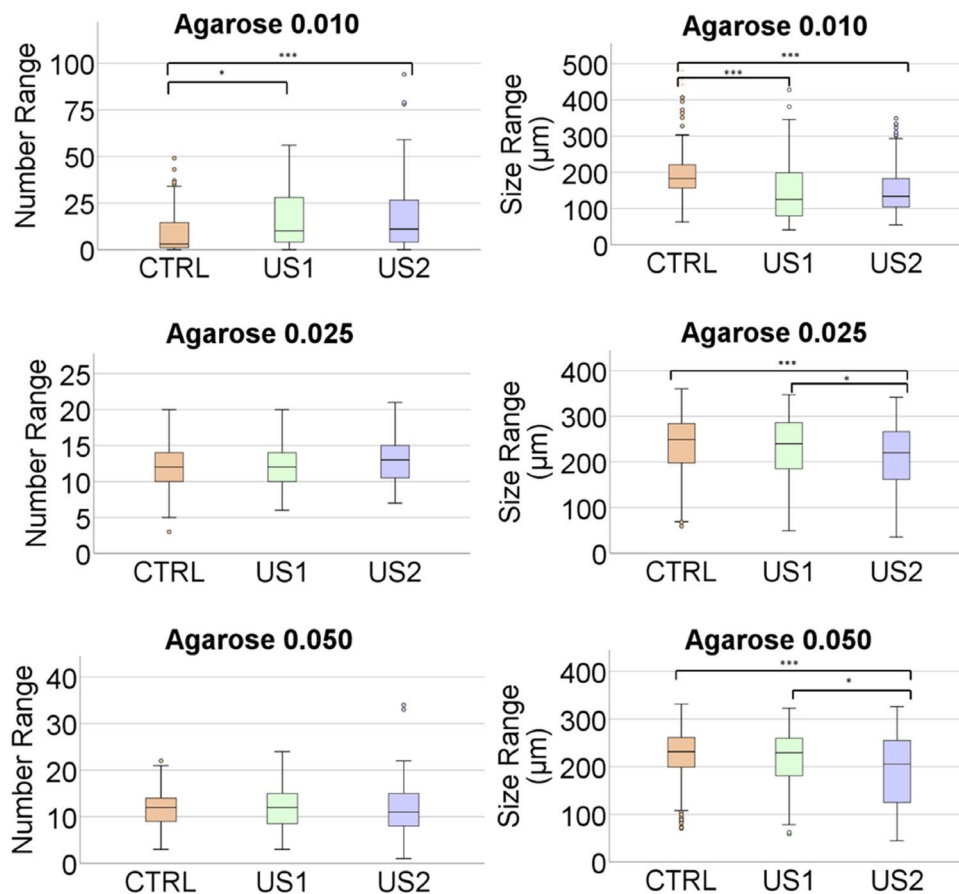


Figure 2.9. The statistical analysis of the number (left) and size (right) of the crystals obtained under silent condition (Control) and US irradiation for 30 min immediately after preparation of the experiment (US1) and 30 min after preparation (US2) in various agarose concentrations.

Until 0.100% of agarose, the irradiation with ultrasound resulted in statistically significant decreasing of crystals size and narrower size distribution in both used protocols (US1 and US2) compared to the control samples (Figures 2.8 and 2.9). The number of crystals in the system with low agarose concentration 0.010% was also significantly different in the irradiated samples compared to the control. In the rest of the tested systems the numbers of crystals were resembled in the irradiated and non-irradiated samples.

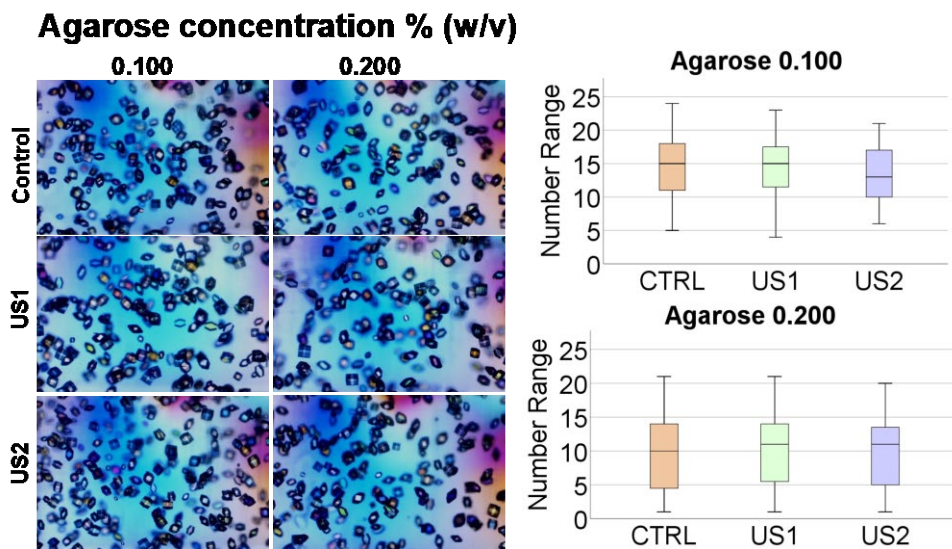


Figure 2.10. Lysozyme crystals obtained in agarose gels with the concentrations 0.100% and 0.200% under silent condition (Control) and ultrasonic irradiation for 30 minutes immediately after preparing the experiment (US1) and 30 minutes after preparation (US2). Reproduced from Ref. 58.

Started from 0.100% we have not observed statistically significant difference between irradiated and non-irradiated samples (Figure 2.10). At these concentrations agarose gels have strong mechanical characteristics (see Section 2.3.3) that may amortizes the ultrasound effect on the crystallization.

2.3.3. Mechanical properties of the gel media

The rheological properties of the agarose gels used for crystallization under US irradiation were studied. The system with concentrations under 0.100% demonstrated un-gelled behaviour: storage modulus (G') was always smaller than loss modulus (G'') regardless of the time or applied frequency.

The 0.100% and 0.200% agarose gels had the behaviour typical for gels (Figure 2.11). The gelation kinetics showed $G' > G''$ from the first minutes of the measurements for both conditions. With time in 0.100% gels G' and G'' increased, but did not reach the plateau, meaning that the gelation process was going on, but after 1h (time of the observation) the gels remained weak. G' and G'' in 0.200% agarose gels intensively increased at the beginning and stabilized with time.

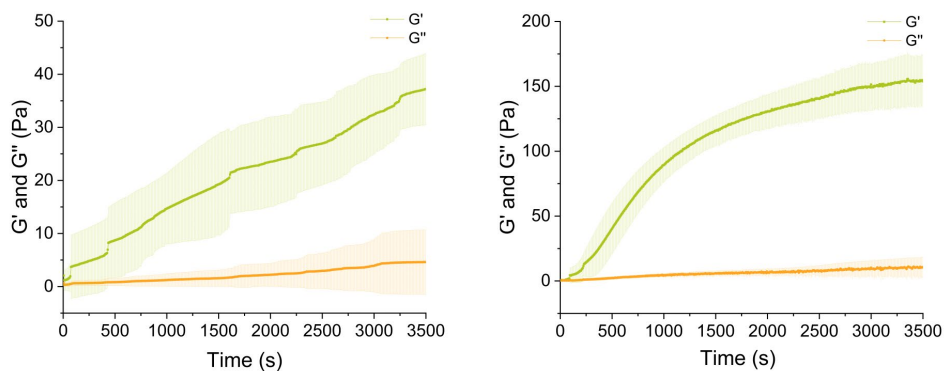


Figure 2.11. The gelation kinetics of 0.100% (left) and 0.200% (right) agarose solutions. Darker lines represent the mean values, whereas the lighter bands around them represent the standard deviations.

These results are supported by frequency sweep technique, were both conditions demonstrated $G' > G''$ in function of frequency (from 0.1 to 10 Hz) at a constant stress of 1 Pa. We studied if US irradiation affected the mechanical proprieties of the gel media. The storage (G') and loss (G'') moduli of irradiated (for both protocols) and non-irradiated gels were measured in function of frequency (Figure 2.12).

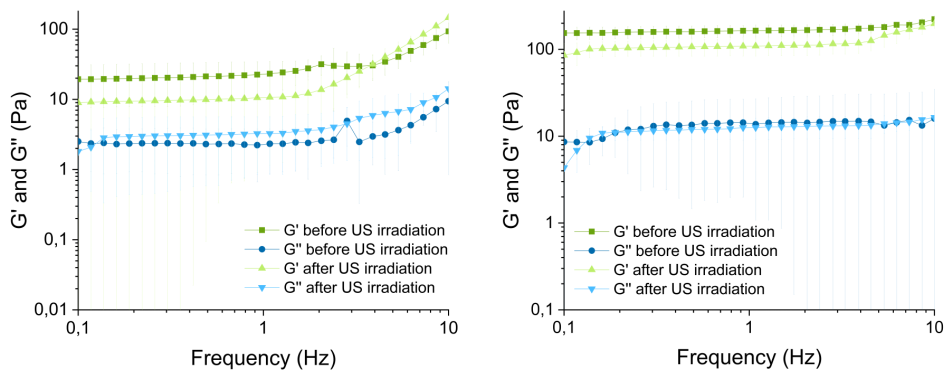


Figure 2.12. The viscoelastic moduli as a function of frequency at a constant stress of 1 Pa for 0.100 % (left), 0.200 % (right) agarose gels before and after applying the protocol US1. For each point (mean value) we represent the standard deviations. Note that the nonsymmetric appearance of standard deviations is due to the logarithmic scale.

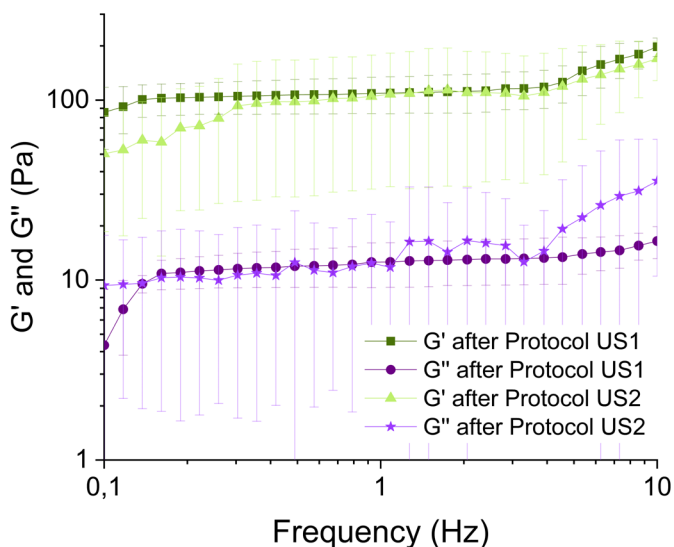


Figure 2.13. The viscoelastic moduli as a function of frequency at a constant stress of 1 Pa for 0.200% agarose gels after applying the protocol US1 and US2. For each point (mean value) we represent the standard deviations. Note that the nonsymmetric appearance of standard deviations is due to the logarithmic scale.

The study demonstrated the absence of an ultrasound effect on the mechanical properties of the gels for both protocols. The standard deviations of the mean values overlap in the graphics that is why the difference in the mean value of G' and G'' should not be considered as a difference in the mechanical properties of the gels.

2.4. Conclusions

In collaboration with the Ultrasonics lab at the University of Granada the US-bioreactor for protein crystallization was developed. Its design solves interferences such heating and near field area effects, but at the same time allows propagation and maximisation of the resolution of US waves into the samples.

The media where the crystallization experiments were carried out were characterised. The mechanical properties of the gel media were determined. Characteristics of the materials: impedance and transmissions coefficient prove that US waves penetrates into the samples without significant loses.

The lysozyme nucleation was induced by ultrasound irradiation resulting in an increase of crystals number, decreasing their mean size in almost twice while narrower size distribution.

The induction effect of US was observed also in agarose gel media at a concentration below 0.100%. Above this concentration the effect of US is hindered most probably due to the enhancement of the mechanical properties of the gels or mask by the nucleation induction effect of agarose.

***Magnetite crystallisation in confined
environments***

Crystallisation in confined spaces occurs in a different manner compared to crystallization in bulk. Reducing the volume of the system influences not only the nucleation density, but also the kinetic. If the environment also changes, it is possible to stabilize metastable polymorphs, to form crystals with preferred orientations, to modify morphologies, size and shape of crystals, etc.¹⁵

Many natural crystallization processes occur in confined environments, being the formation of magnetite nanoparticles inside magnetotactic bacteria one of the most intriguing phenomena. This type of bacteria forms magnetite crystal with unusual morphologies, homogeneous size and superparamagnetic properties considered the ideal magnetic nanoparticles.¹³⁵ The control of the magnetite nanoparticles formation could be explained by a combination of physical and chemical factors in which nucleation and growth of magnetite crystals is performed in confined vesicles (magnetosomes) modulated by the interaction with different proteins.¹⁵³

Scientists are trying to emulate this type of control over the precipitation/crystallization using porous membranes,^{154,155} porous glass,^{156,157} droplets,^{158,159} and even carbon nanotubes.^{160,161} In this sense we propose the use of protein crystals as templates for studying confinement crystallization. Protein crystals are biocompatible material with well-ordered and defined porous network of select diameters and inner surface of the order of zeolites. Besides it, protein crystals consist of charged aminoacids that are periodically aligned within pores that can influence the precipitation of magnetite by, for example, contributing to the accumulation of metal ions.¹⁰⁷ On the other hand

¹⁵³ A. Komeili, *FEMS Microbiol. Rev.* **2012**, *36*, 232–255.

¹⁵⁴ E. J. W. Crossland, N. Noel, V. Sivaram, T. Leijtens, J. A. Alexander-Webber, H. J. Snaith, *Nature* **2013**, *495*, 215–219.

¹⁵⁵ N. B. J. Hetherington, A. N. Kulak, Y.-Y. Kim, E. H. Noel, D. Snoswell, M. Butler, F. C. Meldrum, *Adv. Funct. Mater.* **2011**, *21*, 948–954.

¹⁵⁶ D. C. Steytler, J. C. Dore, C. J. Wright, *J. Phys. Chem.* **1983**, *87*, 2458–2459.

¹⁵⁷ K. Morishige, *J. Phys. Chem. C* **2018**, *122*, 5013

¹⁵⁸ D. Turnbull, *J. Chem. Phys.* **1952**, *20*, 411..

¹⁵⁹ D. Selzer, N. Tullmann, A. Kiselev, T. Leisner, M. Kind, *Cryst. Growth Des.* **2018**, *18*, 4896.

¹⁶⁰ J. Sloan, M. C. Novotny, S. R. Bailey, G. Brown, C. Xu, V. C. Williams, S. Friedrichs, E. Flahaut, R. L. Callender, A. P. E. York, K. S. Coleman, M. L. H. Green, R. E. Dunin-Borkowski, J. L. Hutchison, *Chem. Phys. Lett.* **2000**, *329*, 61

¹⁶¹ M. Wilson, *J. Chem. Phys.* **2002**, *116*, 3027.

protein crystals required a pre-stabilization, typically by chemical cross-linking to be able to manipulate them.¹⁶²

In this chapter we present our results on the precipitation of magnetite within protein crystals channels. Three protein models, lysozyme, glucose isomerase and lipase were selected, crystallized in the tetragonal $P4_32_12$, orthorhombic $I222$ and hexagonal $P6_1$, spaces groups, respectively (*Figure 3.1*). The packing of the three proteins in each space group generate pores in the range of the 2.0, 4.0 and 8.0 nm for lysozyme, glucose isomerase and lipase, respectively while the channels are decorated with different aminoacids expanding the potential influence of chemical interactions.

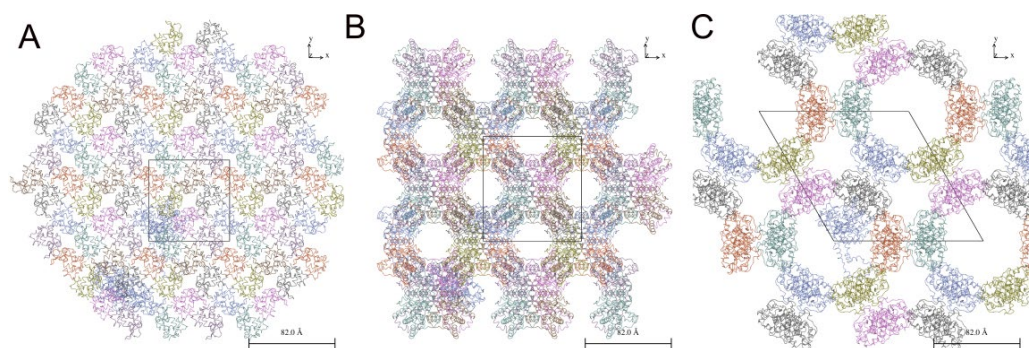


Figure 3.1. Crystal lattice structure of A — lysozyme, B — glucose isomerase, C — lipase.

3.1. Objectives of the study

The main objective of this work is to study the precipitation of magnetite into symmetrically well distributed and characterized protein crystals of different pore sizes. The chosen protein crystals have different amino acid decorations of the channel that may also have an influence of the precipitation of magnetite nanoparticles.

Objective 1. To study the compatibility of protein crystals to be use as templates for confinement precipitation of magnetite;

Objective 2. To develop a methodology for the biomineralization of magnetite inside pores of protein crystals;

Objective 3. To study and characterized the extension of the precipitation of iron oxides within the protein crystals as a function of the channel diameter;

¹⁶² C. P. Govardhan, *Curr. Opin. Biotechnol.* **1999**, *10*, 331–335.

Objective 4. To validate the use of protein crystals as tunable template material for the study of precipitation in confined environments.

3.2. Materials and methods

3.2.1. Reagents and materials

All the reagents and equipment used in the study were obtained from commercial sources which will be specified throughout the text in italics.

3.2.2. Preparation of cross-linked protein crystals

Preparation of the reagents

For lysozyme crystallisation

Lysozyme (HEWL, three-time crystallised powder) from *Sigma-Aldrich* was dissolved in 50mM AcONa from *Sigma-Aldrich* and dialysed during 24 h against 50 mM AcONa (pH 4.5) in a ratio 1:1000 at 4 °C. Then it was concentrated by centrifugation at 4 °C ($g = *5000/25$ min) using 10-kDa cutoff Centricon concentrators *Amicon* to ≈ 150 mg·mL⁻¹ and the concentration measured spectrophotometrically at 280 nm using a theoretical value for the extinction coefficient of 2.56 mL·mg⁻¹·cm⁻¹. The solution was filtered through a 0.45 µm pore-size filter membrane system *Millipore*.

Sodium chloride from *Sigma-Aldrich* was prepared at 20% (w/v) in 50 mM AcONa (pH 4.5) and used as a stock solution. Solutions of NaCl at desired concentration were prepared by diluting with 50 mM AcONa and filtered through a 0.45 µm pore-size filter membrane system *Millipore* prior using it.

For glucose isomerase crystallisation:

Glucose isomerase (D-xylose-ketol-isomerase) from *S. Rubiginosus* (*Hampton Research*) was dialysed for 24 h against HEPES 100 mM pH 7.0 at a ratio 1:1000 at 4 °C and concentrated by centrifugation at 4 °C ($g = *5000 / 1$ h) to ≈ 75 mg mL⁻¹ using a theoretical value for the extinction coefficient at 280 nm of 1.074 mL·mg⁻¹·cm⁻¹. Prior experimental set-up the protein solutions were filtered through a 0.45 µm pore-size filter membrane system *Millipore*.

Magnesium chloride from *Sigma-Aldrich* was prepared at 1M in 0.01 M HEPES pH 7.0 and used as a stock solution. Solutions of MgCl₂ at desired concentration were prepared by diluting with 0.01 M HEPES and filtered through a 0.45 µm pore-size filter membrane system *Millipore* prior using it.

For lipase crystallisation:

Lipase (*Aspergillus sp*, *Biolipasa-L*) from *Biocon* was dialysed for 24 h against Milli-Q water at a ratio 1:1000 at 4 °C and also concentrated by centrifugation at 4 °C (g = *5000 / 4 h) to ≈ 40 mg·mL⁻¹ using a theoretical value for the extinction coefficient at 280 nm of 1.2 mL·mg⁻¹cm⁻¹. Prior experimental set-up all the protein solutions were filtered through a 0.45 µm pore-size filter membrane system *Millipore*.

The mixture of monopotassium phosphate and monosodium phosphate from *Sigma Aldrich* was prepared at 1M (PO₄³⁻) in 0.1M TRIS pH 7 and used as a stock solution. Solutions of K/NaH₂PO₄ at desired concentration were prepared by diluting with Milli-Q water and filtered through a 0.45 µm pore-size filter membrane system *Millipore* prior using it.

Protein crystallisation

All the proteins were crystallised by batch method in the agarose gel media, because gels allow the slow incorporation of the cross-linker and a soft reaction avoiding any osmotic shock. The final composition of the crystallization cocktail is summarized in *Table 3.1*.

Agarose D5 with a melting point of 92 °C and gelling point of 37 °C was supplied by *Hispanagar*. Agarose sols with desirable concentration were obtained by dissolving agarose in Milli-Q water and heated at 90 °C to get a homogeneous transparent solution. Then the solution was cooled down to 50 °C and kept at this temperature until finally mixed with the protein and precipitant solution.

Protein	Precipitant	Buffer	Gel
30 mg/mL lysozyme	3% NaCl	50mM NaOAc	0.2% agarose
30 mg/mL glucose isomerase	0.2M MgCl ₂	0.01M HEPES	0.1% agarose

15 mg/mL lipase	0.3M K/NaH ₂ PO ₄	0.1M TRIS	0.2% agarose
-----------------	---	-----------	--------------

Table 3.1. The protein crystallisation condition. All the mentioned concentration — final concentrations. The crystallisation was performed at 20 °C.

Cross-linking of the protein crystals

Cross-linking of protein crystals firstly was demonstrated by Quioco et al.¹⁶³ in 1964. He used glutaraldehyde (GA) to obtaining carboxypeptidase-A with enhanced stability. From that time this technique is used for making protein crystals stable and insoluble in water.¹⁶⁴ Among the most used crosslinker are aldehyde and carbodiimide reagents. The mechanism of the cross-linking is based on the chemical interaction between the ionisable groups of amino acid side-chains, usually the target are primary amines, thiols or carboxylates, and the cross-linking agent. In the case of GA the reaction occurs between its formyl groups and the primary amines in a protein with a Schiff base formation shown in *Figure 3.2*.¹⁰⁷ However, it's not the only one mechanism of the glutaraldehyde action, Migneault et al.¹⁶⁵ proposed eight different reaction mechanisms to how GA can cross-link proteins.

¹⁶³ F. A. Quioco, F. M. Richards, *Proc. Natl. Acad. Sci. U. S. A.* **1964**, 52, 833-839

¹⁶⁴ E.-K. Yan, H.-L. Cao, C.-Y. Zhang, Q.-Q. Lu, Y.-J. Ye, J. He, L.-J. Huang, D.-C. Yin, *RSC Adv.* **2015**, 5, 26163–26174.

¹⁶⁵ I. Migneault, C. Dartiguenave, M. J. Bertrand, K. C. Waldron, *Biotechniques* **2004**, 37, 790–6, 798–802.

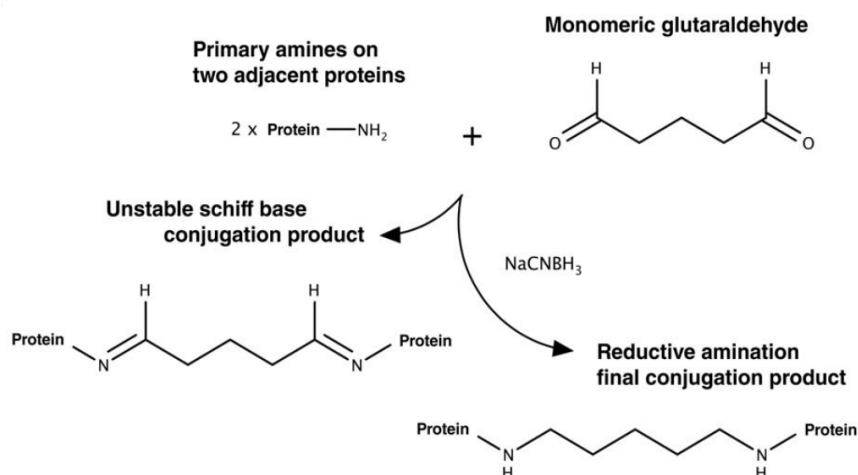


Figure 3.2. The cross-linked reaction between glutaraldehyde and a protein. Reproduced with permission from Ref. 107. Copyright © 2019, John Wiley & Sons, Inc.

After equilibration a mostly homogeneous crystal size distribution was obtained in the gel. For the cross-linking, glutaraldehyde solutions were prepared by diluting the commercial 25% solution with Milli-Q water. The amount of the cross-linking solution at 5% (v/v) identical to the amount of the batch was poured on top of the agarose gel containing protein crystals. Glutaraldehyde was allowed to diffused and cross-link the crystals for 24h at 20 °C. In case of glucose-isomerase and lipase crystals, they were additionally soaked in 10% glutaraldehyde solution for another 24 h to force the cross-linking. Cross-linked protein crystals (CLPCs) of lysozyme (CLLCs), glucose-isomerase (CLGICs) and lipase (CLLPCs) were obtained.

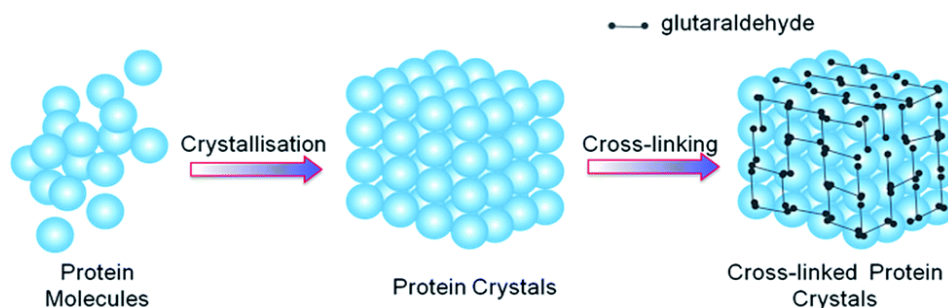


Figure 3.3. The process of cross-linking of a protein crystal. Reproduced Ref. 162.

3.2.3. *In situ* formation of magnetite

Preparation of the reagents

The stock solutions of 0.15M $\text{NaHCO}_3/\text{Na}_2\text{CO}_3$, 0.5 M $\text{Fe}(\text{ClO}_4)_2$, 1M FeCl_3 , and 1M NaOH were prepared from the corresponding reagent from *Sigma-Aldrich* with the deoxygenated water inside an anaerobic chamber *Coy Laboratory Products*, and filled with 4% H_2 in N_2 . The stock solutions were kept inside the chamber all the time until and while using.

The CLPCs (CLLCs, CLGICs, CLLPCs) were fished from the gel media with *CryoLoops* (0.06-0.7 mm) from *Hampton Research*, cleaned with *Micro-Tools Set* from *Hampton Research* and placed into a glass vial inside an anaerobic COY chamber.

Preliminary assays

To confirm that iron precipitation was possible within CLPCs some preliminary tests were performed. A 10 mL vials with the minimum 3 CLPCs of each type inside were fulfilled with oxygen free stock solutions to final concentration of $\text{NaHCO}_3/\text{Na}_2\text{CO}_3$ (3.5 mM/3.5 mM), $\text{Fe}(\text{ClO}_4)_2$ (2.78 mM), and FeCl_3 (5.56 mM). In this condition the crystals were incubated for 4 to 12 days to allow iron ions to penetrate inside crystals pores. Three replicas of each experiment including each protein were performed. After the incubation, NaOH was added to initiate the biomineralization by changing the pH from 8.0 to 12.5, pH value at which the solution turned black and precipitation occurred effectively (*Figure 3.4*). After adding NaOH , the solution stayed inside an anaerobic COY for 2 weeks to 6 months to allow the precipitation of iron oxide. The pH of the solutions was measured after each experiment.

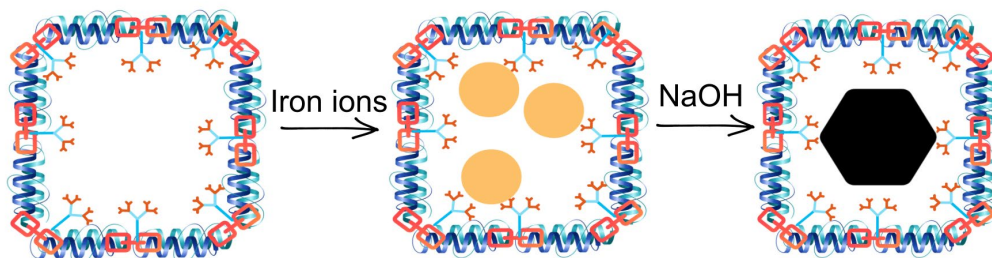


Figure 3.4. Magnetite biomineralization in protein crystals pores.

The biomineralization of magnetite within protein crystals

Research on magnetotactic bacteria showed that magnetite mineralization directly depends on the amount of iron in the media. *In vivo* experiments demonstrated the initiating of the magnetite formation from its precursors with the transfer of bacteria into Fe-containing media.¹³⁹ The conclusion drawn from these *in vitro* experiments on magnetite mineralization was that the formation of ferrihydrite precursor consumes almost all of the Fe^{3+} ions in solution, lowering the supersaturation and impeding the crystallization of magnetite. Therefore, it was suggested that for the crystallisation of magnetite it was necessary to replenish iron in the media by gradually increasing the amount of iron.¹³⁵

Based on this, and on our preliminary results, was decided to follow the evolution and growth of magnetite nanoparticles with periodically renewing of the iron solutions to ensure a continuous supply of the required reactant. For this, a 10 mL vials with the minimum of 100 CLPCs of each type inside were fulfilled with oxygen free stock solutions to final concentration of $\text{NaHCO}_3/\text{Na}_2\text{CO}_3$ (3.5 mM/3.5 mM), $\text{Fe}(\text{ClO}_4)_2$ (2.78 mM), and FeCl_3 (5.56 mM). In this condition the crystals were incubated for 4 days (the previous experiment showed that this time was enough for iron penetration inside crystals). After the incubation time, NaOH was added to initiate the biomineralization by changing the pH to 12.5 and the solution was left to precipitate inside an anaerobic COY for 10 days (Cycle 1). pH 12.5 was chosen from the previous experiments as the condition with the best results.

After the incubation during the cycles, minimum 2 crystals of each protein were taken out for TEM observation. The rest of the crystals were placed in a new vial with a freshly prepared reactant cocktail for biomineralization, initiating the new cycle. We have done 9 cycles for lysozyme and glucose isomerase crystals but in the case of lipase, crystals lost their integrity after two cycles. We have not investigated further the instability of CLLPCs versus increasing number of cycles but everything points to the high pH value as the source of it.

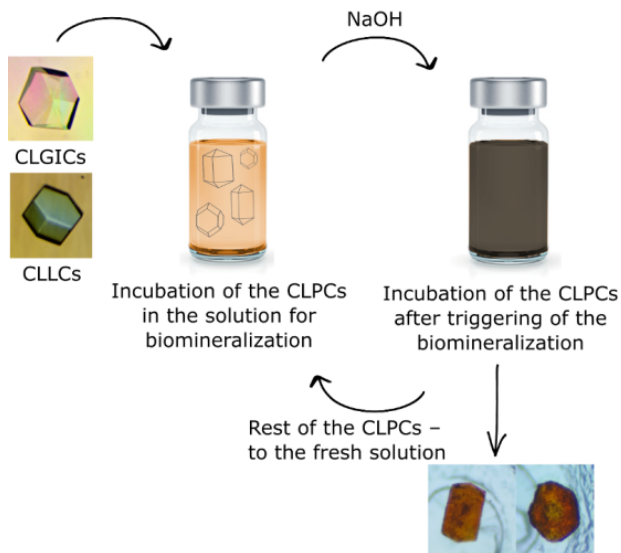


Figure 3.5. The experimental scheme. The cycles: (1) incubation of the CLPCs in the master solution for 4 days; (2) initiating the biomineralization by changing the pH to 12.5, (3) incubation for 10 days; (4) fishing out 2 crystals for TEM analyses and keeping the rest for subsequent cycles.

The control experiment: magnetite precipitation in solution

To evaluate the magnetite mineralization inside of protein crystals properly, we carried out a series of control experiments in absence of protein crystals. For this purpose we followed the same procedure described in previous section. A 100 mL vial was filled with oxygen free stock solutions to final concentration of $\text{NaHCO}_3/\text{Na}_2\text{CO}_3$ (3.5 mM/3.5 mM), $\text{Fe}(\text{ClO}_4)_2$ (2.78 mM), and FeCl_3 (5.56 mM). In this condition the solution was incubated for 4 days. Then NaOH was added to increase the pH of the master solution to 12.5. After adding NaOH, the sample was homogenised and aliquoted in 10 different bottles. After a full cycle (14 days) a sample was collected out of the chamber for evaluation with TEM.

3.2.4. Characterization of the nanoparticles

Preparation of ultrafine cuts of the crystals and controls

To prepare the samples for TEM analysis, after fishing the crystals out of the biomineralizing solution, CLPCs were dehydrated with ethanol and embedded in Epoxy Resin: EMBED-812 from *Electron Microscopy Sciences* and let it solidified.

Ultrathin sections of 50–70 nm were cut using a *Reichert Ultracut S microtome*. Then the thin slides were deposited onto G300 Mesh Square Copper from *Agar Scientific* support.

In the case of the magnetite nanoparticles from the control samples crystals were deposited onto CF200-Cu Carbon Film Mesh 200 Copper grids from *Electron Microscopy Sciences*.

Electron microscopy

The distribution, size and growth of formed magnetite nanoparticles inside the pores of CLPCs and in the control samples were analysed with TEM *LIBRA 120 PLUS*.

The elemental analysis and diffraction patterns of the magnetite nanoparticles formed inside and outside the pores of CLPCs were analysed making use of the high-resolution TEM (HR-TEM) *FEI TITAN G2*.

Diffraction patterns were analysed with *ImageJ 1.53e* software from SAED pictures to determine the d-spacing used to compared with known values for the magnetite d-spacing.^{166,167}

3.2.5. Statistical analysis

The size, number, distribution and diffraction patterns of the nanoparticles were analyzed with *ImageJ 1.53e* software. Above 100 nanoparticles per sample were measured to calculate size distribution. For nanoparticles distribution near and far from the border TEM micrographs were divided in 100 zones of equal area (182.5 nm²). 3 random zones in the centre and 3 random zones near the border of the crystal were chosen for counting and measuring all the particles. The statistical analyses were done with *OriginPro 2021*.

To characterize the simultaneous mean differences of the nanoparticles near the border and in the centre statistical tests were performed. The first step was to check the proof of normality via the Kolmogorov-Smirnov and Shapiro-Wilk tests. If the tests showed that the distribution of the variables was parametric, a

¹⁶⁶ B. A. Wechsler, D.H. Lindsley, C.T. Prewitt *American Mineralogist* **1984**, 69, 754-770.

¹⁶⁷ C. Haavik, S. Stolen, H. Fjellvag, M. Hanfland, D. Hausermann *American Mineralogist* **2000**, 85, 514-523.

multiple regression analysis *via* ANOVA was performed. In case the distribution was non-normal, Kruskal-Wallis test was performed. The p-value significances for the groups were obtained with Dunn's test. These p-values have been compared with the significance level — 0.05 — the minimum accepted level that indicates a difference between means. The notation that we have included hereafter is * $p < 0.05$, ** $p < 0.001$ and *** $p < 0.0001$ when the differences between means are statistically significant.

The nanoparticles distribution from the border to the centre of a CLLC along a crystal section was also evaluated (*Figure 3.6*). For this, we firstly convert the TEM image in a black & white image, and divided the length of the crystal in eight sections of 135 nm. Then using the image analysis software *ImageJ 1.53e* we calculate the black/white ratio for which the value "0" (black) was indicative of the presence of iron particles and the value "255" (white) corresponded to the absence of nanoparticles. The distribution based on this analysis is presented in *Figure 3.19*.

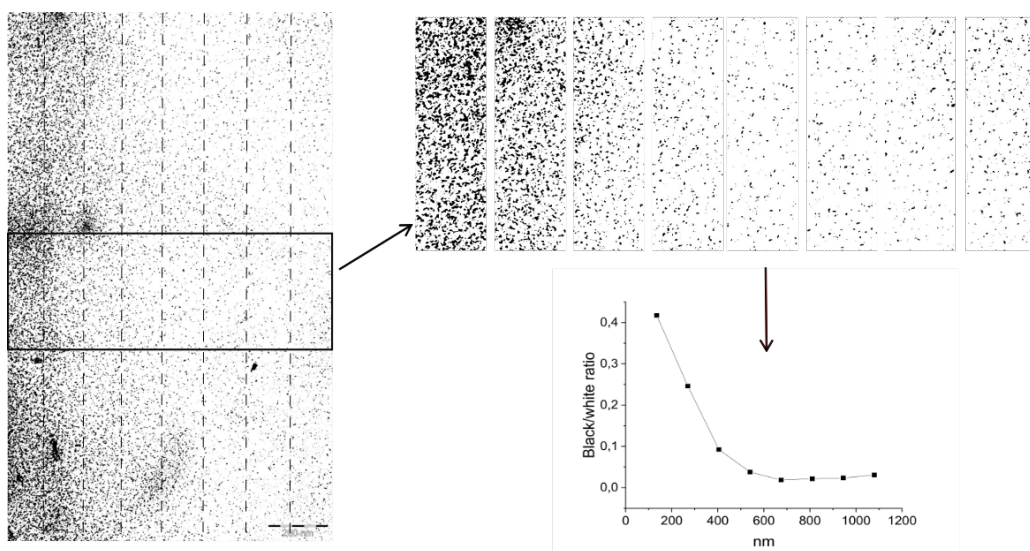


Figure 3.6. The evaluation of the nanoparticles distribution from the border to the center of the crystal.

3.3. Results and discussion

3.3.1. Precipitation of iron particles inside CLPCs

The CLPCs were used as a template to study the precipitation behaviour of magnetite in well characterized confined environments. The TEM observation of cut CLPCs showed the clear difference in nanoparticles formation in the bulk and inside CLPCs (*Figure 3.7*). While outside of the protein-crystals the formed nanoparticles had sizes range from 3 nm to 20 nm, inside the protein channels the average size was around 2 nm.

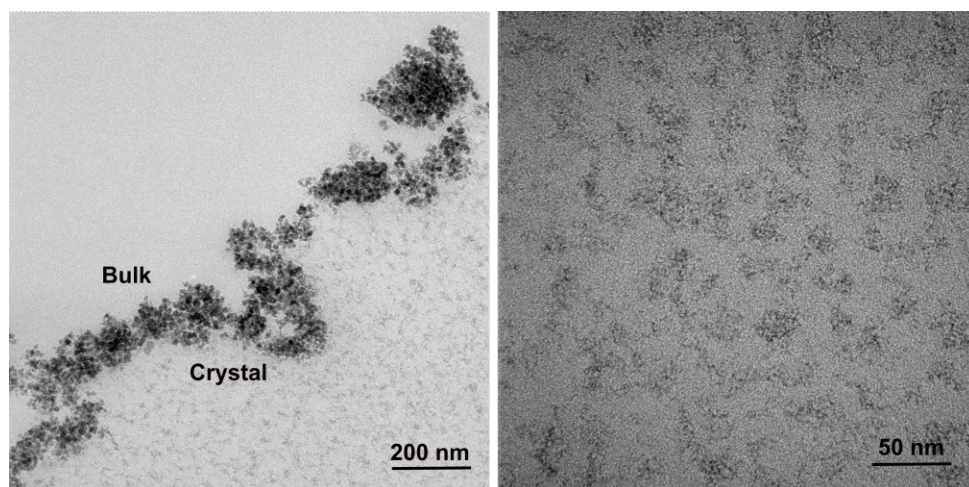


Figure 3.7. TEM images of iron nanoparticles grown in bulk and inside CLPC (left) and inside of CLPC (right).

To identify the nanoparticles HR-TEM was used. The particles formed outside of the CLPCs in bulk demonstrated (111), (100) and (311) crystal faces identical to magnetite (*Figure 3.8.B*). The EELS analysis and X-ray spectrum of the particles formed inside the CLPCs confirm that the nanoparticles are Fe-rich aggregates (*Figure 3.8.E*) but the absence of diffraction peaks point to the amorphous character of the nanoparticles (*Figure 3.8.D*).

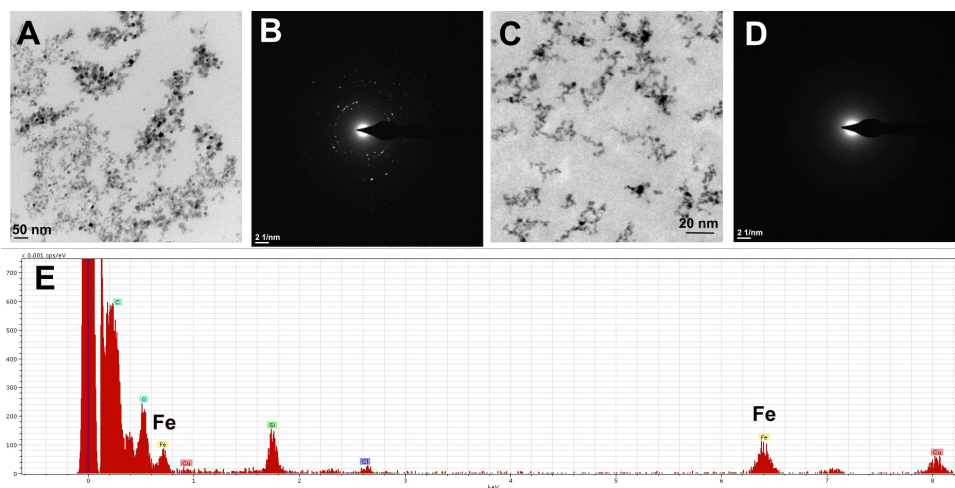


Figure 3.8. (A) TEM image of magnetite outside of the CLLCs. (B) The diffraction pattern of magnetite outside of the crystal. (C) HR-TEM image of lysozyme crystals with particles inside. (D) diffraction image of the particles inside the lysozyme crystals. (E) Energy Dispersive X-ray spectrum of the particles inside the lysozyme crystals.

However, after an extended incubation time of 6 month, none nanoparticles were detected inside the CLLCs. The lower stabilisation energy of the amorphous aggregates versus the magnetite crystals form at the interface and bulk solution drives the dissolution of the amorphous following the Ostward ripening rule. After this observation the clicling procedure to renew the iron solution in the system was adopted.

Never the less the formation of small homogenous Fe-rich nanoparticles was observed in all the CLPCs: lysozyme, glucose isomersase and lipase incubated from 2 weeks up to 3 months. In all the cases we observed that clear magnetite particles were formed at the interface between the crystal and the solution and that nanoparticles were distributed through all the crystals volume (*Figure 3.9*).

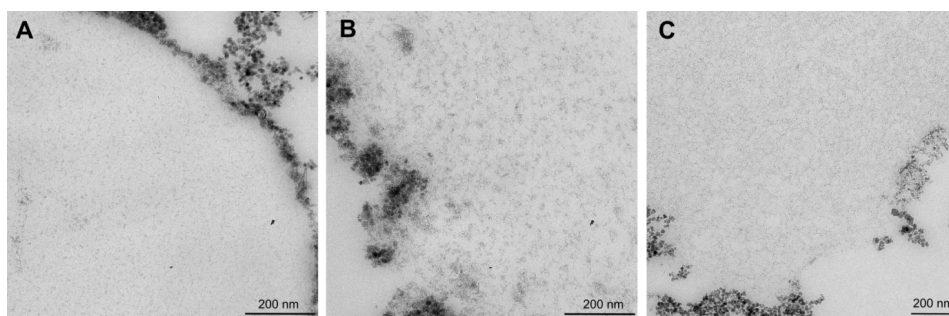


Figure 3.9. TEM images of (A) lysozyme, (B) glucose isomerase, and (C) lipase crystals with iron nanoparticles inside.

Interestingly despite these proteins systems have different pores diameters: lysozyme (2.0 nm), glucose isomerase (4.0 nm), and lipase (8.0 nm), the mean size of the formed nanoparticles was 2 nm in all the crystals with dispersion of approximately 1.0, 0.5 and 1.0 nm for lysozyme, glucose isomerase and lipase, respectively (Figure 3.10).

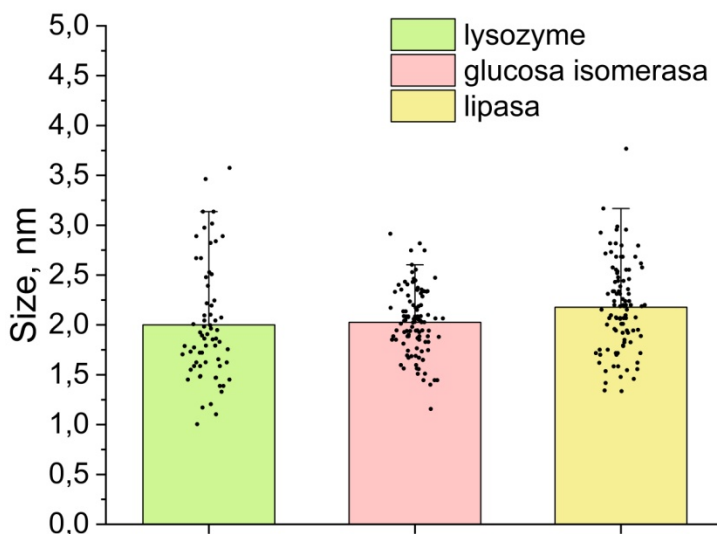


Figure 3.10. The average nanoparticles size for the three proteins.

However, after the extended incubation time — 6 month, inside of the CLPCs were not observed nanoparticles. It could be explained by depletion of reserves of Fe. With the depletion the intermediates particles have not matured into magnetite, but their Fe were spent of magnetite nanoparticles formation and growth in bulk (outside of the crystals).

3.3.2. Evolution of magnetite nanoparticles inside CLPCs

To evaluate the evolution and growth of the nanoparticles, CLPCs were placed succesively into new iron solutions to feed the system with Fe ions avoiding its depletion inside the channels. A total of 9 cycles were performed with lysozyme

and glucose isomerase crystals. Lipase crystals collapsed after 2 cycles even with enhanced cross-linking treatment (see the protocol in *Section 3.2.2*).

We observed that the formation of magnetite nanoparticles in the bulk started from the 1st cycle while the nanoparticles inside the CLPCs could appear at the first or second second cycle.

The observations with TEM were done after each cycle. The observations with HR-TEM with EDX and diffraction analysis were performed after the 2nd, 4th, 6th, 8th and 9th cycles to study the nature and evolution of the particles inside the CLPCs.

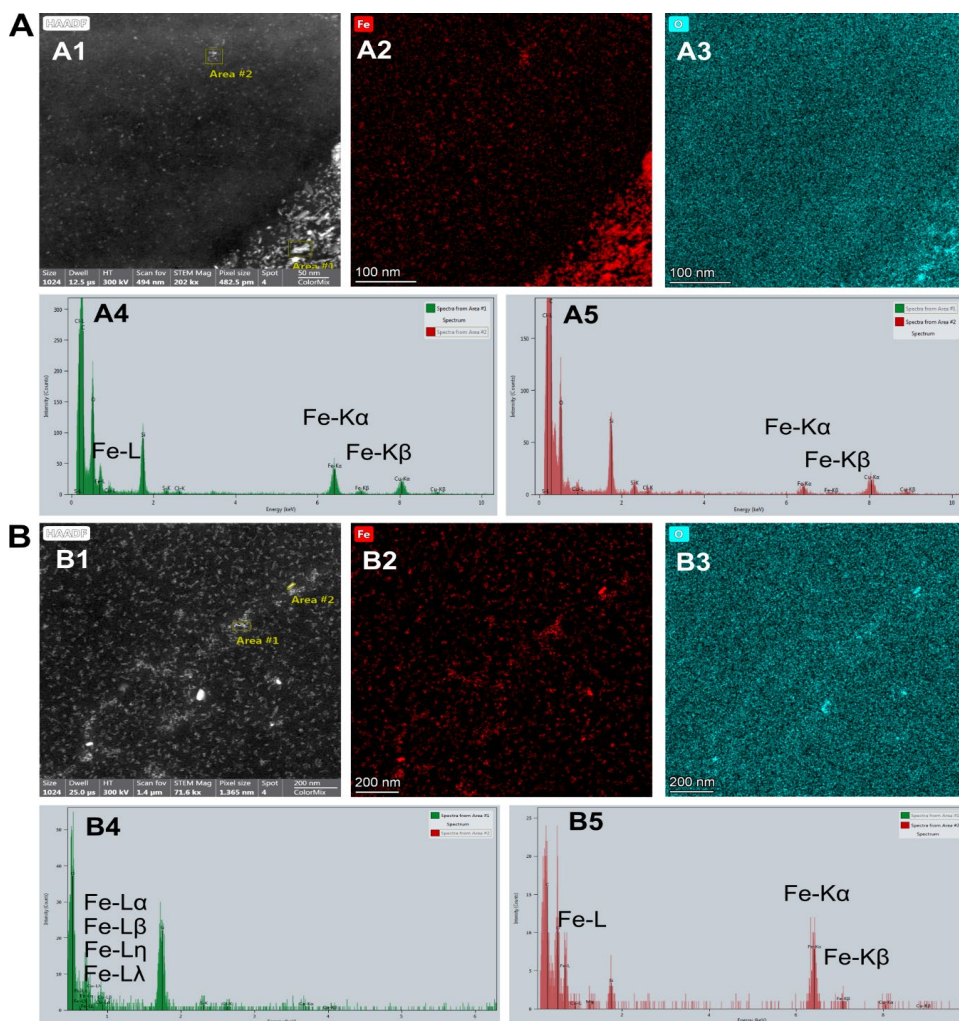


Figure 3.11. Elemental analysis of CLPCs in the initial (A) and last cycles (B)
 A1 — HR-TEM image of CLPC with definition of the areas for elemental analysis; A2 — elemental analysis of iron distribution inside the CLPC; A3 — elemental analysis of oxygen

distribution inside the CLPC; A4 — the spectrum from the area 1 in A1; A5 — the spectrum from the area 2 in A1; B1 — HR-TEM image of CLPC with definition of the areas for elemental analysis; B2 — EDX analysis of iron distribution inside the CLPC; B3 — elemental analysis of oxygen distribution inside the CLPC; B4 — the spectrum from the area 1 in B1; B5 — the spectrum from the area 2 in B1.

As observed in *Figure 3.11* from the initial cycle to the last, the amount of Fe inside the crystals increases, although we have not quantitatively determined this amount.

The transport of Fe from the bulk into the crystal induced a gradient in the Fe concentration from a higher concentration near the border of the crystal to a lower concentration farther from the border (*Figure 3.12*). In each case diffraction analysis was performed to identify the iron phase.

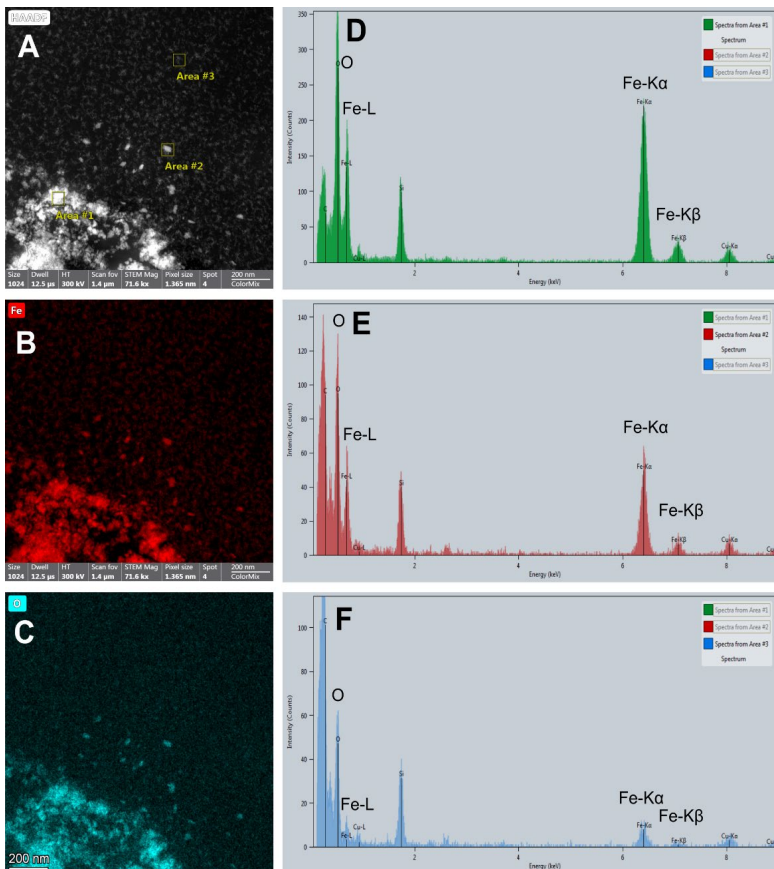


Figure 3.12. EDX analysis of CLPCs in the middle of the experiment (6st cycle).

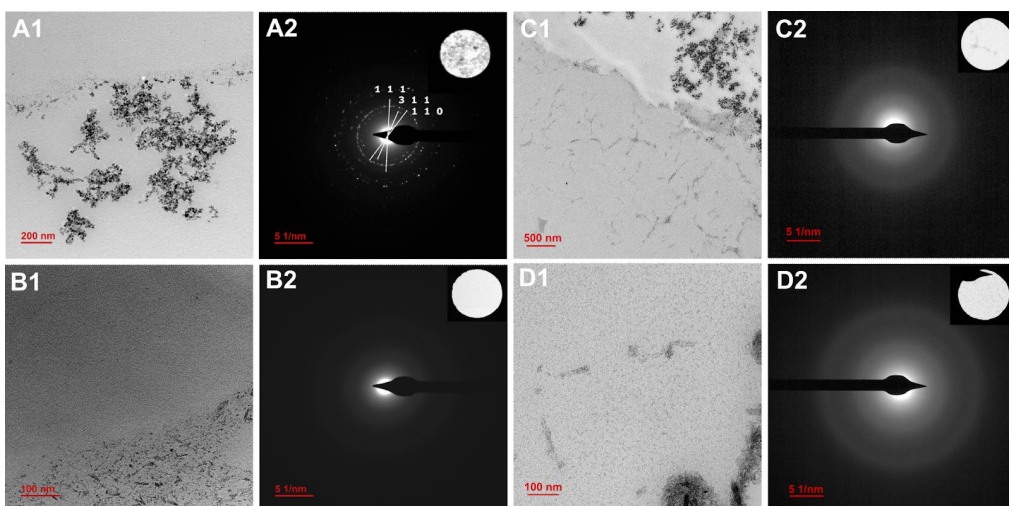


Figure 3.13. HR-TEM images of magnetite particles grown outside (A1) and inside (B1, C1 & D1) CLLCs after cycle number 2 (A1 & B1), 4 (C1) and 8 (D1). By side SAED diffraction images of showed regions (inserts in A2, B2, C2 and D2).

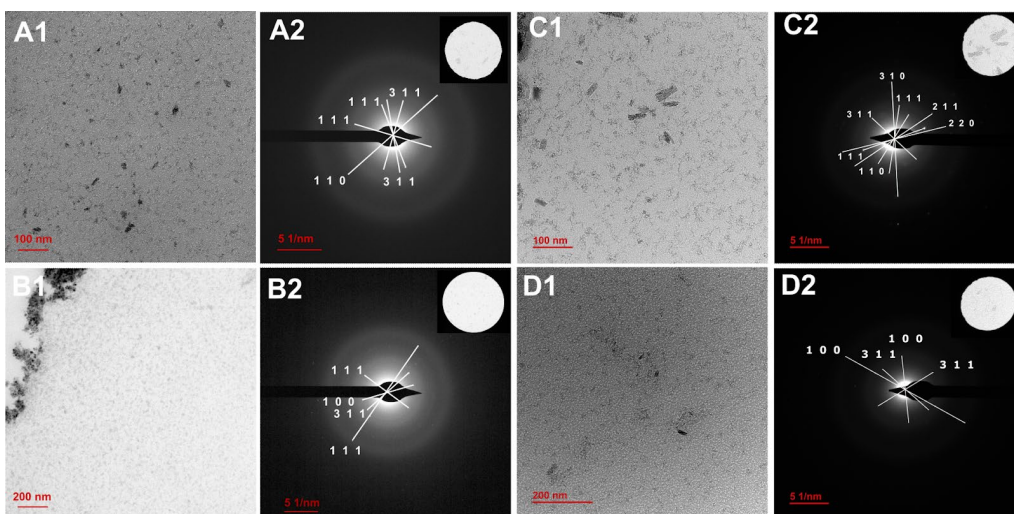


Figure 3.14. HR-TEM images of magnetite particles grown inside CLGICs after cycle number 2 (A1), 4 (B1), 6 (C1) and 8 (D1) and the corresponding SAED diffraction images of selected regions (inserts in A2, B2, C2 and D2).

Only nanoparticles formed outside of the lysozyme crystals (A1 Figure 3.13) showed diffraction pattern of magnetite. The nanoparticles formed inside of lysozyme crystals from initial, middle and the final cycle did not diffracted X-ray, showing its amorphous character. On the other hand, all the nanoparticles samples analyzed from glucose isomerase crystals showed typical magnetite pattern from the initial cycle (Figure 3.14). It means that recharging with Fe in

case of lysozyme did not promote the formation of magnetite, even though the particles are of similar size, but prevent the dissolution of the amorphous phases. The amorphous nanoparticles of approximately 2 nm size were observed in all the CLLCs.

The maintaining of amorphous state in case of nanoparticles grown inside lysozyme crystals could be explained by their pore size that is almost equal to the primary nanoparticles size, 2 nm.²⁴ In this case, the steric hindrance to increase the size may be the main reason to hinder the transformation of this phase to magnetite. Also the role of amino acids side chains nearby the nanoparticle and most probably in contact with them may play also an important role on the inhibition of the magnetite nanoparticle formation. None the less, other effects such as the blocked of the confined pores avoiding the replenishing of Fe, essential for crystalline magnetite formation,¹³⁵ may also have an influence. In the case of glucose isomerase, the formation of 2 nm particles does not obstruct the crystals pores, they have 4.0 nm pore diameter, thus, Fe transport into glucose isomerase crystals was maintained.

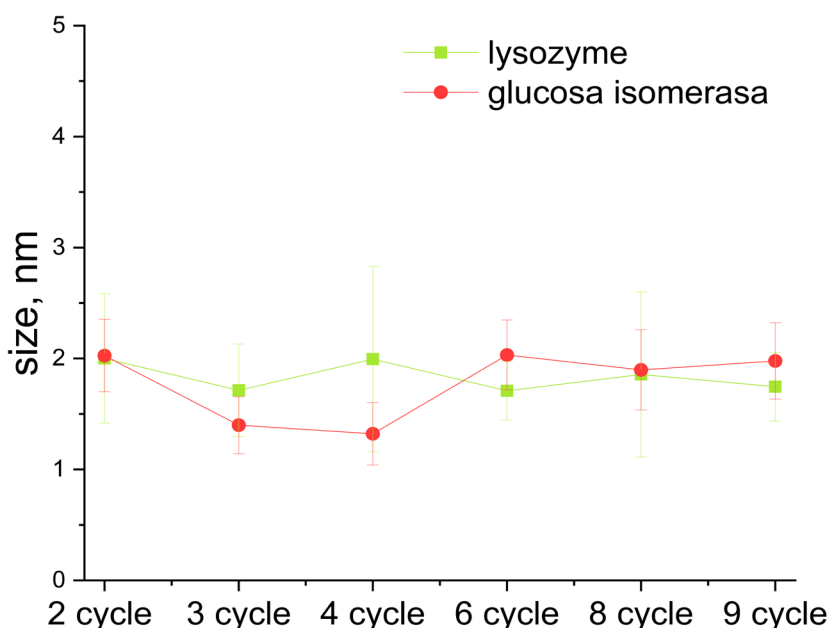


Figure 3.15. Mean size of magnetite nanoparticles formed inside pores of CLPCs during the cycles. Darker lines represent the mean values, whereas the lighter bands around them represent the standard deviations.

On the other hand, it was observed that nanoparticles maintained the same homogeneous size distribution of approximately 2 nm from the initial cycle until the last cycle regardless of the crystal's pores size. Remarkably, this size is correlated with the metastable primary particles size as reported in hiswork Baumgartner et al.²⁴ They studied the crystallization of magnetite in bulk solution by the same method — coprecipitation of Fe^{2+} and Fe^{3+} ions. In 2 min, after the initialisation of the biomineralization, the authors observed monodisperse 2 nm amorphous intermediates of iron (hydr)oxide — magnetite precursor, by means of HR cryo-TEM. The size of the primary particles corresponded to well-defined minimum ΔG of the particles. These primary particles grown to 5–15 nm nanoparticles in the next 4 min and further converted into magnetite.

In our research the nanoparticles size remained constant at 2 nm during the whole experimentation time (more than 100 days). Meanwhile control nanoparticles formed without presence of CLPCs in bulk continued growing (Figures 3.16 and 3.17).

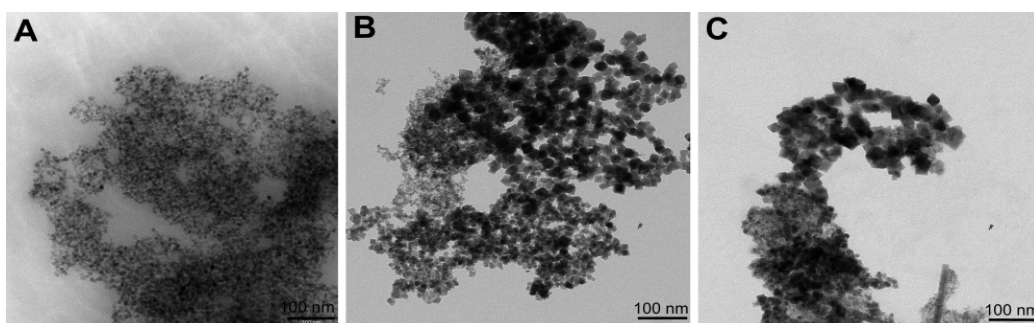


Figure 3.16. TEM images of magnetite nanoparticles formed without a presence of protein crystals (Control) after the incubation in the beginning (A), middle (B) and the end of (C) the experiment.

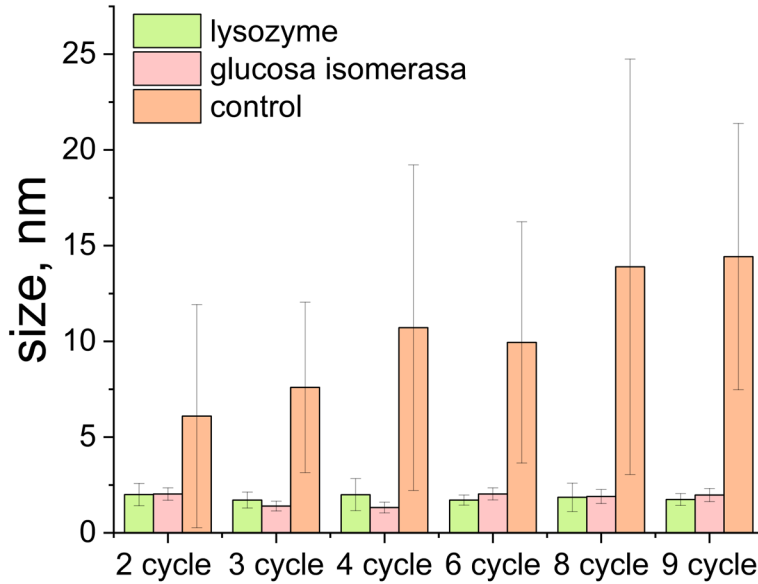


Figure 3.17. Mean size of magnetite nanoparticles formed inside pores of CLPCs and in bulk without a presence of protein crystals (control), big SD in the controls appears because of heterogeneous size of the particles in case of mineralization in bulk.

On the other hand, while the particles size stays stable with cycles, the number of particles inside the CLPCs increases (*Figure 3.18*) demonstrating that there is not clog of iron diffusion within the lysozyme crystals.

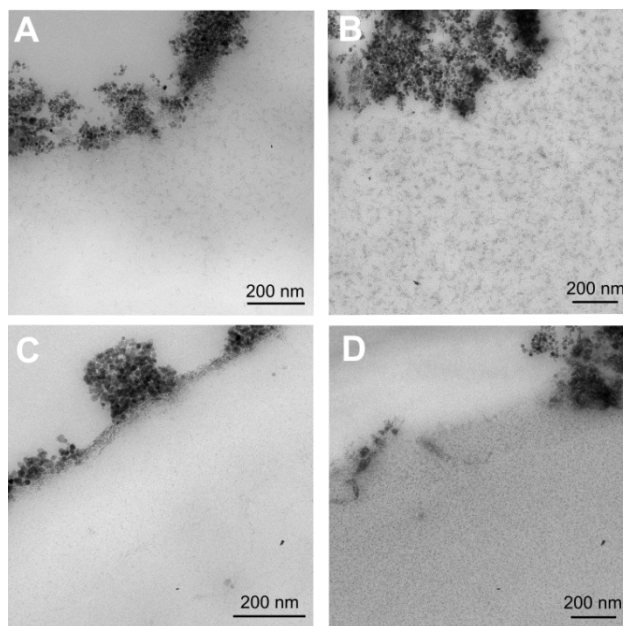


Figure 3.18. TEM images of CLPCs with magnetite nanoparticles formed inside of their pores: A and B — CLGICs after the initial and the last cycle in accordance; C and D — CLLCs after the initial and the last cycle in accordance.

Figure 3.19 shows the distribution of nanoparticles along a section of the protein crystal. Flow of Fe created different supersaturation conditions near the border and in the centre of the crystals. As a result, nanoparticles are dispersing along the protein crystal section following a non-homogeneous distribution. There is a concentration of nanoparticles near borders which is three times bigger than farther from the border. This particle gradient is kept along the different cycles (*Figure 3.20*) and in both CLLCs (*Figure 3.19*) and CLGICs (*Figure 3.21*).

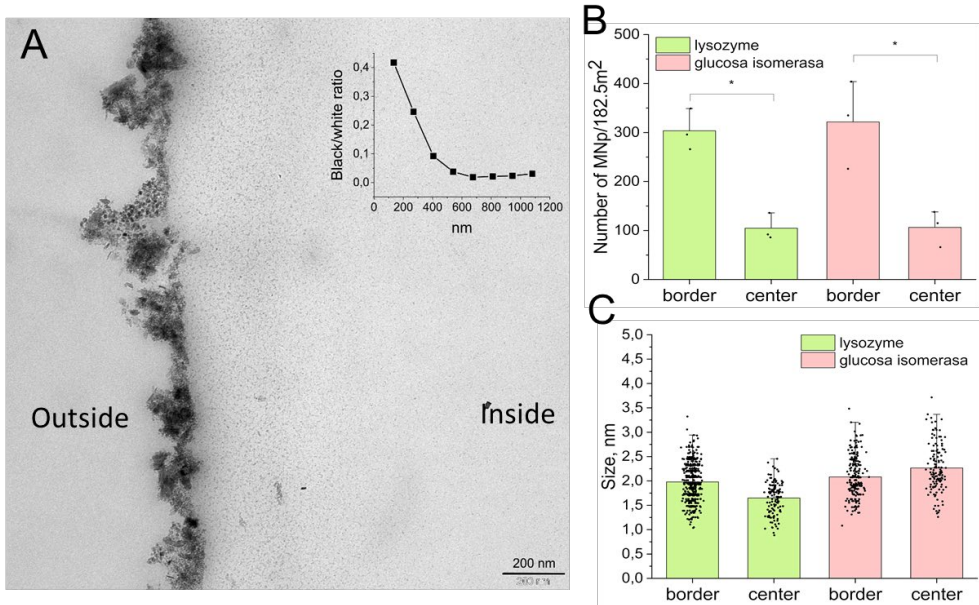


Figure 3.19. A) TEM image of CLGICs after 8th cycles which illustrates the distribution of magnetite nanoparticles and the black/white ratio of each 135 nm from the border to the centre of the crystal. B) number and C) size of the magnetite nanoparticles formed near and far from the border of the CLPCs, based on TEM images from the 9th cycle.

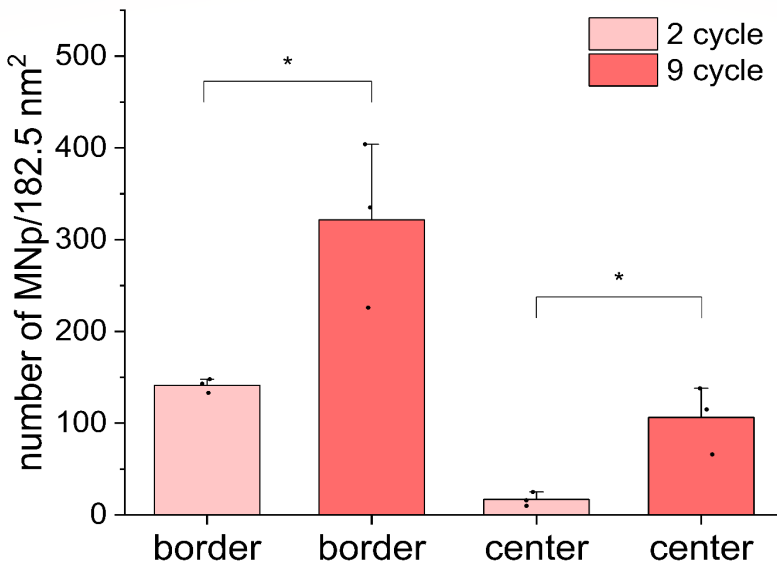


Figure 3.20. Number of the magnetite nanoparticles formed near the border and in the centre of CLGICs in the initial and the last cycle.

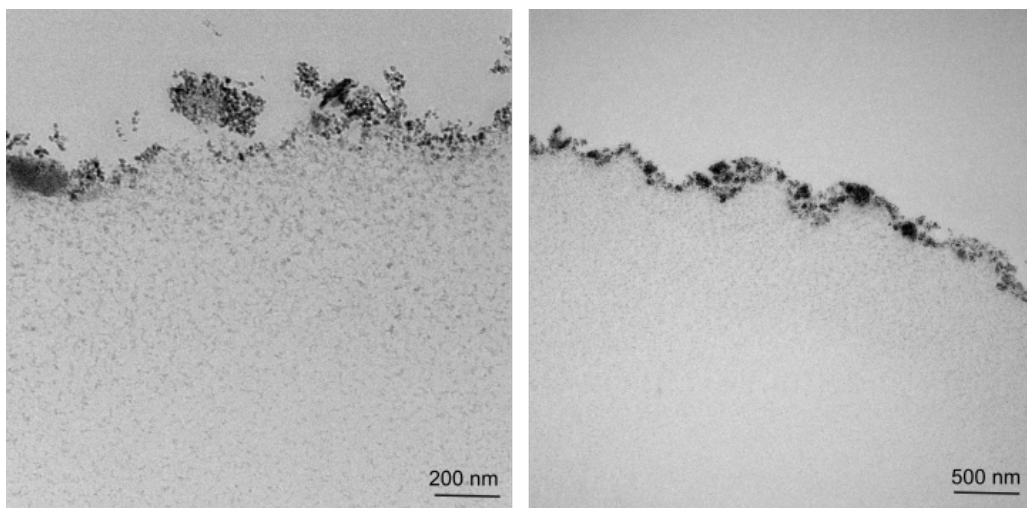


Figure 3.21. The gradients of the magnetite nanoparticles distribution formed inside of CLGICs in different cycles.

3.4. Conclusions

For understanding magnetite formation in confined spaces, proteins with various pores diameters: lysozyme (2.0 nm), glucose isomerase (4nm) and lipase (8 nm) were crystallized and cross-linked to enhance their stability.

Our preliminary experiments showed us that the pre-formed Fe-nanoparticles inside protein channels could disappear: particle dissolved to feed bulk magnetite crystals. This observation imposed a constant supplied of iron to the systems to avoid Ostward ripening behaviour.

With constant repletion of iron ions, a gradient distribution of nanoparticles with a narrow size distribution of around 2 nm independently of the channel diameter size of the CLPCs used was obtained. Interestingly while in the case of CLGICs the nanoparticles can be identified as magnetite, inside CLLCs the iron nanoparticles remained as amorphous phase. It is very interesting to note that this average size, 2 nm is also the maximum dimension of CLLCs pore diameter, seems to be critical in the process of magnetite formation being the metastable nuclei size from which bigger crystals can be obtained. How these size-constrains may affect the formation of magnetite nanoparticle scape from our understanding.

At the same time when the pore size of the system was big enough, such as the case of CLGICs (4 nm), homogeneous and narrowed size distribution of magnetite nanocrystals of 2 nm in average were obtained in all the cycles. Interestingly the

maximum average size of the nanoparticle was also 2 nm independently of the number of the cycles and the location within the CLGCs. This interesting behaviour requires further investigation.

Annex

LIST OF THE PUBLICATIONS

The results presented in the thesis have been published:

- M. Savchenko, M. Hurtado, M. T. Lopez-Lopez, G. Rus, L. Álvarez de Cienfuegos, J. Melchor, J. A. Gavira, *Ultrason. Sonochem.* **2022**, *88*, 106096.

- M. Savchenko, V. Sebastian, M. T. Lopez-Lopez, H. Cölfen, C. Jimenez-Lopez, L. Álvarez de Cienfuegos, J. A. Gavira Manuscript in preparation.